ผลเฉลยของตัวกลางยืดหยุ่นที่มีผลกระทบจากหน่วยแรงที่ผิว

นายพงศ์อินทร์ อินทฤทธิ์

วิทยานิพนธ์นี้เป็นส่วนหนึ่งของการศึกษาตามหลักสูตรปริญญาวิศวกรรมศาสตรดุษฎีบัณฑิต
สาขาวิชาวิศวกรรมโยธา ภาควิชาวิศวกรรมโยธา
คณะวิศวกรรมศาสตร์ จุฬาลงกรณ์มหาวิทยาลัย
ปีการศึกษา 2555

ลิขสิทธิ์ของจุฬาลงกรณ์มหาวิทยาลัย
บทคัดย่อและแฟ้มข้อมูลฉบับเต็มของวิทยานิพนธ์ตั้งแต่ปีการศึกษา 2554 ที่ให้บริการในคลังปัญญาจุฬาฯ (CUIR)
เป็นแฟ้มข้อมูลของนิสิตเจ้าของวิทยานิพนธ์ที่ส่งผ่านทางบัณฑิตวิทยาลัย
The abstract and full text of theses from the academic year 2011 in Chulalongkorn University Intellectual Repository(CUIR)
are the thesis authors' files submitted through the Graduate School.

SOLUTIONS OF ELASTIC MEDIUM WITH SURFACE STRESS EFFECTS

Mr.Pong-in Intarit

A Dissertation Submitted in Partial Fulfillment of the Requirements

for the Degree of Doctor of Philosophy Program in Civil Engineering

Department of Civil Engineering

Faculty of Engineering

Chulalongkorn University

Academic Year 2012

Copyright of Chulalongkorn University

Thesis Title	SOLUTIONS OF ELASTIC MEDIUM WITH SURFACE STRESS EFFECTS
By	Mr.Pong-in Intarit
Field of Study	Civil Engineering
Thesis Advisor	Professor Teerapong Senjuntichai, Ph.D.
Thesis Co-advisor	Associate Professor Jaroon Rungamornrat, Ph.D.

Accepted by the Faculty of Engineering, Chulalongkorn University in Partial Fulfillment of the Requirements for the Doctoral Degree

.....Dean of the Faculty of Engineering
(Associate Professor Boonsom Lerdhirunwong, Dr.Ing.)

THESIS COMMITTEE

.....Chairman
(Professor Thaksin Thepchatri, Ph.D.)

..... Thesis Advisor
(Professor Teerapong Senjuntichai, Ph.D.)

.....Thesis Co-advisor
(Associate Professor Jaroon Rungamornrat, Ph.D.)

.....Examiner
(Associate Professor Akhrawat Lenwari, Ph.D.)

.....Examiner
(Assistant Professor Watanachai Smittakorn, Ph.D.)

.....External Examiner
(Associate Professor Pruettha Nanakorn, D.Eng.)

พงศ์อินทร์ อินทฤทธิ์ : ผลเฉลยของตัวกลางยืดหยุ่นที่มีผลกระทบจากหน่วยแรงที่ผิว. (SOLUTIONS OF ELASTIC MEDIUM WITH SURFACE STRESS EFFECTS) อ.ที่ปรึกษาวิทยานิพนธ์หลัก : ศ.ดร.ธีรพงศ์ เสนจันทร์ฒิไชย, อ.ที่ปรึกษาวิทยานิพนธ์ร่วม : รศ.ดร.จรูญ รุ่งอมรรัตน์, 98 หน้า.

วิทยานิพนธ์ฉบับนี้นำเสนอการศึกษาผลกระทบจากหน่วยแรงที่ผิวต่อพฤติกรรมเชิงกลของวัสดุยืดหยุ่นโดยใช้สมการของเกอร์ตินและเมอร์ดอครูปแบบสมบูรณ์ในการจำลองพฤติกรรมของหน่วยแรงที่ผิว ในการศึกษานี้ได้นำเสนอผลเฉลยมูลฐานของวัสดุชั้นยืดหยุ่นภายใต้แรงกระทำต่างๆ และผลเฉลยของปัญหาที่มีความไม่ต่อเนื่องของการเคลื่อนที่และรอยแตกร้าวเกิดขึ้นในตัวกลางยืดหยุ่นโดยใช้วิธีการแปลงฟูเรียร์และการแปลงแฮงเคลในการแก้ปัญหาค่าขอบเขตที่เกี่ยวข้องเมื่อพิจารณาผลกระทบจากหน่วยแรงที่ผิว ผลเฉลยเชิงวิเคราะห์ของปัญหามูลฐานต่างๆ สามารถแสดงอยู่ในรูปของปริพันธ์กึ่งอนันต์และสามารถคำนวณหาคำตอบที่ถูกต้องแม่นยำโดยการใช้ระเบียบวิธีเชิงตัวเลขที่เหมาะสม ผลเฉลยเชิงตัวเลขได้ถูกนำเสนอเพื่อแสดงถึงอิทธิผลของหน่วยแรงที่ผิวที่มีผลต่อคำตอบของสนามยืดหยุ่น และพบว่าหน่วยแรงที่ผิวมีอิทธิพลต่อสนามยืดหยุ่นของชั้นวัสดุยืดหยุ่นอย่างมีนัยสำคัญโดยเฉพาะบริเวณใกล้เคียงพื้นผิว นอกจากนี้หน่วยแรงที่ผิวจะส่งผลให้พฤติกรรมของวัสดุขึ้นอยู่กับขนาดของวัสดุซึ่งตรงข้ามกับผลเฉลยในปัญหาดั้งเดิม จากการศึกษาในครั้งนี้สามารถสรุปได้ว่าหน่วยแรงที่ผิวมีอิทธิพลสำคัญต่อพฤติกรรมเชิงกลของวัสดุในระดับนาโนและวัสดุยืดหยุ่นอ่อน โดยผลเฉลยมูลฐานที่เสนอในการศึกษานี้สามารถนำไปใช้ในการพัฒนาระเบียบวิธีเชิงตัวเลขเพื่อใช้วิเคราะห์ปัญหาค่าขอบเขตที่มีความซับซ้อนที่เกี่ยวข้องกับโครงสร้างระดับนาโนและวัสดุยืดหยุ่นอ่อนได้

ภาควิชา วิศวกรรมโยธา ลายมือชื่อนิสิต .....

สาขาวิชา วิศวกรรมโยธา ลายมือชื่ออ.ที่ปรึกษาวิทยานิพนธ์หลัก .....

ปีการศึกษา 2555 ลายมือชื่ออ.ที่ปรึกษาวิทยานิพนธ์ร่วม .....

4971856521 : MAJOR CIVIL ENGINEERING

KEYWORDS : SURFACE STRESSES / ELASTIC LAYER / ELASTIC MEDIUM / CONTINUUM MECHANICS / SIZE DEPENDENT

PONG-IN INTARIT : SOLUTIONS OF ELASTIC MEDIUM WITH SURFACE STRESS EFFECTS. ADVISOR : TEERAPONG SENJUNTICHAI, Ph.D., CO-ADVISOR : JAROON RUNGAMORNRAT, Ph.D., 98 pp.

This dissertation presents a theoretical study of an isotropic elastic material with the consideration of surface stress effects by adopting complete Gurtin-Murdoch continuum theory of elastic material surfaces. The fundamental solutions of an isotropic elastic layer under different loading cases, and an elastic medium with dislocations and crack are presented. Fourier and Hankel integral transforms are used to solve appropriate boundary value problems involving non-classical boundary conditions associated with the surface stresses. The analytical solutions are expressed in terms of semi-infinite integrals that can be accurately computed by employing numerical quadrature scheme. Selected numerical results are presented to portray the influence of surface stresses on the bulk elastic field. It is found that surface stresses show a significant influence on elastic fields of an isotropic elastic material especially in the vicinity of the surface. In contrast to classical elasticity, extensive parametric studies observed in numerical results indicate that the response of the bulk material becomes size-dependent with the consideration of surface stresses. Numerical results presented in this study confirm the fact that the influence of surface stresses is significant in the analysis of problems involving nanoscale systems and soft elastic materials where the surface energy effects are not negligible. The fundamental solutions presented in this study can be used in the development of boundary integral equation and other methods to analyze complicated boundary value problems associated with nanoscale structures and soft elastic solids.

Department : CIVIL ENGINEERING Student's Signature : .....

Field of Study : CIVIL ENGINEERING Advisor's Signature : .....

Academic Year : 2012 Co-advisor's signature : .....

ACKNOWLEDGEMENTS

This research work was supported by the Thailand Research Fund (TRF) under the Royal Golden Jubilee Ph.D. (RGJ-Ph.D.) scholarship. Their supports are gratefully acknowledged.

The author wishes to express his sincere appreciation to his advisor, Professor Dr.Teerapong Senjuntichai, and his co-advisor, Associate Professor Dr.Jaroon Rungamornrat, for their kind guidance and long-term support throughout this work. He also wishes to express his gratitude to Professor Dr.Nimal Rajapakse at the Simon Fraser University, Canada, for his kindness and invaluable advice on the research work and very warm welcome during the visits at SFU in 2010 and 2012. Grateful acknowledgements are due to Professor Dr.Thaksin Thepchatri, Associate Professor Dr.Pruettha Nanakorn, Associate Professor Dr. Akhrawat Lenwari and Assistant Professor Dr.Watanachai Smittakorn for their helpful comments and serving in the thesis committee.

Special thanks are also due to everyone who has helped directly and indirectly in the preparation of this thesis. Finally, the author would like to express his gratitude to his parents for their support and love.

CONTENTS

page

Abstract (Thai) iv

Abstract (English) v

Acknowledgements vi

Contents vii

List of Figures ix

List of Abbreviations xiv

Chapter I Introduction 1

1.1 General 1

1.2 Objectives and Scopes Present Study 3

Chapter II Literature Reviews 4

2.1 General 4

2.2 Surface Elasticity Model 5

2.3 Fundamental Problems with Surface Stresses 7

2.4 Dislocation and Crack Problems with Surface Stresses 8

Chapter III Basic Equations and General Solutions 11

3.1 Basic Equations of Continuum with Surface Stresses 11

3.1.1 Basic Equations for Plane Problems 13

3.1.2 Basic Equations for Axisymmetric Problems 14

3.2 General Solutions for Bulk Materials 15

3.2.1 General Solutions for Plane Problems 15

3.2.2 General Solutions for Axisymmetric Problems 16

Chapter IV Internally Loaded Elastic Layer 18

4.1 Fundamental Solutions for Plane Problems 18

4.1.1 Surface Loading on Finite Thickness Layer 21

4.1.2 Internal Loading in Semi-Infinite Medium 23

4.2 Fundamental Solutions for Axisymmetric Problems 24

4.3 Numerical Results 29

page

4.3.1 Plane Problems 29
4.3.2 Axisymmetric Problems 32
4.4 Conclusion 34
Chapter V Dislocations and Crack in Elastic Medium 45
5.1 Dislocations in Semi-Infinite Elastic Medium 45
5.1.1 Shear Dislocation 47
5.1.2 Opening Dislocation 47
5.1.3 Numerical Results 48
5.2 Penny-Shaped Crack in Infinite Elastic Medium 51
5.2.1 Formulation of Dual Integral Equations 51
5.2.2 Numerical Results 54
5.3 Conclusion 56
Chapter VI Rigid-Indentation on Elastic Layer 70
6.1 Axisymmetric Green Functions for Elastic Layer 70
6.2 Axisymmetric Rigid Punch Problems 71
6.2.1 Rigid Frictionless Punch Problems 72
6.2.2 Rigid Fully Bonded Punch Problems 72
6.2.3 Rigid Rough Punch Problems 73
6.3 Rigid Frictionless Flat-Ended Cylindrical Punch 73
6.4 Numerical Results 74
6.5 Conclusion 75
Chapter VII Conclusions 84
7.1 Summary 84
7.2 Suggestions for Further Work 85
References 86
Appendix 92
Appendix A 93
Biography 98

LIST OF FIGURES

page

Figure 4.1 An isotropic elastic layer subjected to internal vertical and tangential loading: (a) plane strain case (b) axisymmetric case.. 35

Figure 4.2 Non-dimensional stress profiles of a half-plane under vertical surface load: (a) Vertical stress (b) Horizontal stress (c) Shear stress... 36

Figure 4.3 Non-dimensional stress profiles of a half-plane under horizontal surface load: (a) Vertical stress (b) Horizontal stress (c) Shear stress 37

Figure 4.4 Non-dimensional stress profiles of a half-plane at z_0 = 0.1 under vertical surface load for different surface material constants (Λ): (a) Vertical stress (b) Horizontal stress (c) Shear stress... 38

Figure 4.5 Non-dimensional stress profiles of a half-plane at z_0 = 0.1 under vertical surface load for different residual surface stresses (τ^s): (a) Vertical stress (b) Horizontal stress (c) Shear stress.. 39

Figure 4.6 Non-dimensional stress profiles along the z -axis of a half-plane under internal vertical load: (a) Vertical stress (b) Horizontal stress.. 40

Figure 4.7 Non-dimensional shear stress profiles along the z -axis of a half-plane under internal horizontal load... 40

page

Figure 4.8 Non-dimensional stress profiles along the z -axis of a finite thickness layer under vertical surface load: (a) Vertical stress (b) Horizontal stress.... 41

Figure 4.9 Non-dimensional shear stress along the z -axis of a finite thickness layer under horizontal surface load.... 41

Figure 4.10 Normalized displacement profiles at r_0/a_0 = 0.5 of a layer with finite thickness t_0/a_0 = 5 under parabolic vertical load at the surface: (a) Vertical displacement (b) Radial displacement..... 42

Figure 4.11 Normalized displacement profiles at r_0/a_0 = 0.5 of a layer with finite thickness t_0/a_0 = 5 under parabolic tangential load at the surface: (a) Vertical displacement (b) Radial displacement.. 42

Figure 4.12 Normalized displacement profiles at r_0/a_0 = 0.5 of a layer with finite thickness t_0/a_0 = 5 under uniformly distributed vertical load at the surface: (a) Vertical displacement (b) Radial displacement.... 43

Figure 4.13 Normalized vertical displacement at r_0 = 0 of a layer with finite thickness t_0/a_0 = 5 under parabolic vertical load at the surface..... 43

Figure 4.14 Non-dimensional stress profiles of a layer with finite thickness t_0/a_0 = 5 under parabolic vertical load at the surface: (a) Vertical stress (b) Radial stress (c) Shear stress..... 44

page

Figure 5.1 Dislocations in a semi-infinite elastic medium at a depth h below the surface.. 58

Figure 5.2 Non-dimensional stress profiles under shear dislocation at h_0 = 1.0: (a) Vertical stress (b) Horizontal stress (c) Shear stress.. 59

Figure 5.3 Non-dimensional stress profiles under opening dislocation at h_0 = 1.0: (a) Vertical stress (b) Horizontal stress (c) Shear stress.. 60

Figure 5.4 Non-dimensional stress profiles under opening dislocation for different depths of dislocation plane (z_0 = 1.0): (a) Vertical stress (b) Horizontal stress (c) Shear stress.. 61

Figure 5.5 Non-dimensional stress profiles under opening dislocation for different material constants (h_0 = 1.0 and z_0 = 0.1): (a) Vertical stress (b) Horizontal stress (c) Shear stress.. 62

Figure 5.6 Non-dimensional stress profiles under opening dislocation for different residual surface stresses (h_0 = 1.0 and z_0 = 0.1): (a) Vertical stress (b) Horizontal stress (c) Shear stress.. 63

Figure 5.7 A penny-shaped crack in an infinite elastic medium subjected to applied internal pressure.. 64

Figure 5.8 Convergence of non-dimensional vertical stress in the vicinity of crack tip.. 65

page

Figure 5.9 Comparison of classical numerical solutions with exact solutions: (a) Vertical stress (b) Crack opening displacement.. 66

Figure 5.10 Non-dimensional vertical stress profile in the vicinity of crack tip for different residual surface stresses (τ^s)..... 67

Figure 5.11 Non-dimensional crack opening displacement for different residual surface stresses (τ^s)..... 68

Figure 5.12 Non-dimensional vertical stress profiles in the vicinity of crack tip for different size of crack (a_0).. 69

Figure 6.1 An isotropic elastic layer under axisymmetric rigid punch..... 78

Figure 6.2 An isotropic elastic layer under rigid frictionless flat-ended cylindrical punch of a radius a 78

Figure 6.3 Convergence of normalized contact pressure of a half space ($t_0 \to \infty$) under flat-ended cylindrical punch with contact radius a_0 = 0.5..... 79

Figure 6.4 Comparison of numerical vertical displacement with benchmark solutions.. 80

Figure 6.5 Distribution of normalized contact pressure under flat-ended cylindrical punch with various contact radii... 81

page

Figure 6.6 Normalized vertical displacement of the surface layer under flat-ended cylindrical punch with various contact radii.. 81

Figure 6.7 Normalized displacement profiles of a layer with finite thickness t_0/a_0 = 5 under flat-ended cylindrical punch with contact radius a_0 = 0.5: (a) Vertical displacement (b) Radial displacement..... 82

Figure 6.8 Normalized stress profiles of a layer with finite thickness t_0/a_0 = 5 under flat-ended cylindrical punch with contact radius a_0 = 0.5: (a) Vertical stress (b) Radial stress (c) Shear stress..... 83

LIST OF ABBREVIATIONS

b_i	the components of the Burger's vector in the i–direction;
H	Heaviside step function;
J_n	Bessel functions of the first kind of order n;
n_i	unit normal vector in the i-direction;
p	an applied normal traction;
q	an applied tangential traction;
r	radial coordinate;
t	thickness of an elastic layer;
t_i^0	prescribed traction on the surface in the i-direction;
u_i	displacement in the i–direction;
x	horizontal coordinate;
z	vertical coordinate;
μ , λ	Lamé constants of the bulk material;
μ^s , λ^s	Lamé constants of the surface material;
κ^s	surface material constant;
τ^s	residual surface stress under unstrained condition;
σ_{ij}	stress components;
ε_{ij}	strain components;
δ_{ij}	Kronecker delta;

ξ integral transform parameter;

Λ, $\bar{\Lambda}$ material characteristic length;

χ Airy stress function;

Φ Love's strain potential;

∇_1^2 Laplacian operator in a Cartesian coordinate;

∇^2 Laplacian operator in a cylindrical coordinate.

CHAPTER I

INTRODUCTION

1.1 General

Nanotechnology has important applications in various disciplines such as biology, chemistry, physics, medicines and engineering. After the discovery of carbon nanotube (CNT) in 1991 by Iijima (1991), a number of advanced researches have been studied to improve performance of various devices by utilizing superior mechanical, electronic and optical properties of nanoscale materials. For example, computer memory storage device called Nano-RAM, which is faster and denser than common RAM, has been developed based on the position of carbon nanotubes deposited on a chip-like substrate.

There are generally two basic approaches to study the mechanical behavior of nanoscale systems, which are experimental methods and theoretical simulations. Several experiments have been performed to investigate mechanical responses of nanoscale materials in the literature. For example, Wong et al. (1997) determined the mechanical properties, i.e. Young's modulus, strength and toughness of isolated silicon carbide (SiC) nanorods (NRs) and multi-wall carbon nanotubes (MWNTs) by using atomic force microscopy. Mao et al. (2003) utilized the same method to determine the hardness of ZnO and SnO2 nano-belts. Although actual behavior of a material can be obtained by performing an experiment, the results based on this approach nevertheless highly depend on experimental environments. Moreover, the cost of experimental study is very expensive due to their requirement of high-precision testing instruments and procedures. Theoretical simulations based upon mathematical modeling are therefore attractive options, which have been widely used to analyze the mechanical behavior of nanoscale systems. Two major models have been commonly employed in the

analysis of nanoscale systems, i.e. atomistic simulation and continuum based approach. Although atomistic simulations are considered very accurate for nanoscale systems, the associated computational resources are significantly huge since the billions of atom need to be modeled when applied at a device/system level. Extending continuum mechanics concepts to the nanoscale level is thus an attractive option that is very efficient in obtaining first-approximation to nanoscale systems.

From atomistic study, it is found that the energy associated with atoms at or near a free surface or interface is different from that of atoms in the bulk material (Miller and Shenoy, 2000; Shenoy, 2005). The excess energy associated with the surface/interface atoms is called the surface free energy, which is generally neglected in the context of microscale systems or larger. However, for nanoscale structures, the surface to volume ratio is much higher and the surface energy effects can no longer be ignored. Modified continuum methods that account for surface energy effects and size-dependency are then developed to examine the mechanical behavior of the materials in nanoscale level. A rigorous theory based on continuum mechanics concepts incorporating the surface energy effects was proposed by Gurtin and Murdoch (1975, 1978), and Gurtin et al. (1998). In the past decade, Gurtin-Murdoch formulation has been extensively used to investigate a variety of problems such as nano-inhomogeneities, nano-plates, cracks etc.

This dissertation is concerned with the development of fundamental solutions for an isotropic elastic material in nanoscale system based upon continuum mechanics incorporating surface energy effects by employing Gurtin-Murdoch theory of surface elasticity. The analytical solutions are derived for fundamental problems to provide a fundamental understanding on mechanical behavior of nanoscale structures and materials. The solutions for more complex problems can also be obtained using the application of the derived fundamental solutions. In this study, analytical solutions of an isotropic elastic material involving different loading cases and defects, i.e. dislocations and crack, are presented for the case of plane strain and

axisymmetric problems by employing Fourier and Hankel integral transform techniques respectively. Numerical results are presented for various boundary value problems to portray the influence of surface stresses on the elastic field of the bulk material.

1.2 Objectives and Scopes of Present Study

The main objectives and scopes of the present study are given as follows:

1) To develop analytical solutions of isotropic elastic material with the consideration of surface stresses by adopting complete Gurtin-Murdoch continuum theory of elastic material surfaces for various boundary value problems that are fundamental in the area of solid mechanics.

2) To investigate size-dependent and nanoscale influence on elastic fields of various fundamental problems.

CHAPTER II

LITERATURE REVIEWS

2.1 General

Research on nanomechanics has remarkably received increasing attentions in recent years. It concerns with the study of fundamental mechanical behavior, i.e. elastic, thermal and kinetic properties, of physical systems at the nanometer scale. Since the prefix 'nano' means a billionth, one nanometer (abbreviated as 1 nm) is therefore 1/1,000,000,000 of a meter. Nanostructures and nanomaterials refer to structures and materials that have at least one of the overall dimensions in the nanoscale level (approximately 1 nm to 100 nm). Existing experimental studies of materials at nanoscale level reveal that their mechanical properties show size-dependent behaviors that are completely different from those in macroscopic structures, where their mechanical properties are independent of their size. Classical continuum mechanics is therefore not applicable at the nanoscale level due to surface energy, related size-dependency and quantum effects. Behavior of nanoscale systems can be accurately predicted by using first-principle quantum mechanical simulations (Sun and Zhang, 2002; Liang et al., 2005; Ji and Gao, 2004). Such simulations are computationally prohibitive (often practically unrealistic) when applied at a device/system level. Extending continuum mechanics concepts to the nanoscale is therefore an attractive option. Modified continuum methods that account for surface energy effects and size-dependency are considered very efficient in obtaining first-approximation to nanoscale systems.

2.2 Surface Elasticity Model

The concepts of surface energy and surface stress were first formulated by Gibbs (1906). In the formulation of the thermodynamics of surfaces, Gibbs defined the surface free energy (γ) as the reversible work per unit area needed to create a new surface. For the surface of solids, Gibbs introduced another surface quantity, called surface stress that represents the reversible work per unit area needed to elastically stretch a pre-existing surface. From the thermodynamics of solid surfaces, Shuttlleworth (1950) and Cammarata (1994) derived the relationship between the surface stress and the surface free energy. They interpreted surface stress in a term of variation of the surface free energy with respect to surface strain. It should be noted that surface free energy is a scalar quantity, while the surface stress is a second order tensor in the tangent plane of the surface, and the strain normal to the surface is excluded. Cammarata (1994) also expressed the surface stress in Lagrangian coordinate system that greatly simplifies the analysis in several problems.

The influence of surface energy effect is generally neglected when a microscopic system and larger is considered. In a nanoscale system, however, the surface energy effects could have significant influence on their behavior. The ratio of surface free energy γ (J/m^2), and Young's modulus E (J/m^3), γ/E, is a parameter with a dimension of length (Yakobson, 2003). This intrinsic length scale is usually small, in the nanometer range or even smaller, for metallic materials. When a structure of a material has at least one characteristic length comparable to this intrinsic scale, the influence of surface energy effects becomes important, and thus the mechanical properties of this system become size-dependent. In the case of a soft elastic solid, such as polymer gels and biological materials, its elastic modulus is much smaller than that of a conventional solid. Consequently, the corresponding intrinsic length scale of a soft solid is much larger and becomes comparable to material dimensions in practical situations and thus

the surface energy effects can play an important role on its mechanical properties (He and Lim, 2006).

Several theoretical frameworks based on continuum model are developed incorporating surface energy effects (Miller and Shenoy, 2000; Park et al., 2006; Slattery et al., 2004). For a linearly isotropic elastic material, a rigorous theory based on continuum mechanics concepts that incorporate the effects of surface energy is presented by Gurtin and Murdoch (1975, 1978), and Gurtin et al. (1998). In their model, the surface is considered as a mathematical layer of zero thickness perfectly bonded to an underlying bulk. Miller and Shenoy (2000) performed atomistic simulations of nano-scale plates and bars subjected to uni-axial loading and pure bending and found that their results were in excellent agreement with those based on the Gurtin-Murdoch model.

The surface stresses are, in general, anisotropic and depend on the crystallographic direction of the surface (Gurtin et al., 1998; Shenoy, 2005). However, it would take an enormous effort in order to analyze problems with fully surface stresses. Moreover, the assumption of isotropic surface stresses is considered acceptable and sufficient in the study of surface energy effects to depict the fundamental understanding of its importance in the analysis of nanoscale system (Weissmuller and Cahn, 1997). Based on Gurtin-Murdoch continuum theory of surface elasticity, the surface stress effects are incorporated in a non-classical boundary condition on the surface/interface, in which the traction across the surface/interface is discontinuous. This boundary condition and the surface stress-strain relation together with the classical elasticity equations constitute a coupled system of field equations. Over the past decade, Gurtin-Murdoch surface elasticity model has been extensively employed by several researchers to investigate various problems with the presence of surface stress effects.

2.3 Fundamental Problems with Surface Stresses

A variety of problems have been successfully investigated in nanoscale level with the consideration of surface energy effects by employing Gurtin-Murdoch theory of surface elasticity. For example, several researchers have examined the problems involving nano-inclusions and nano-inhomogeneities (Sharma et al., 2003; Duan et al., 2005; Tian and Rajapakse, 2007; Mogilevskaya et al., 2008), ultra-thin elastic film (He et al., 2004; Huang, 2008), thin plate (Lu et al., 2006), nano-indentation problems (Zhao, 2009; Pinyochotiwong, 2010) and crack problems (Wang et al., 2008; Kim et al., 2010, 2011).

The fundamental study of an elastic layer under surface and internal loading is important to diverse engineering applications in the context of classical continuum mechanics. The classical solution of a finite thickness elastic layer subjected to surface loads was given by Pickett (1938), which have been widely used for applications in tribology, geomechanics, biomechanics, etc. In addition, the classical solution of a half-plane subjected to internal loading was derived by Melan (1932). For the problems in nanoscale level, those classical solutions are not applicable and the influence of surface stresses need to be considered. He and Lim (2006) derived the surface Green's function for a soft incompressible isotropic elastic half-space by assuming that the surface elastic properties are the same as bulk properties. The elastic field of a half-plane subjected to surface loading in the presence of surface stresses was considered by Wang and Feng (2007). Zhao and Rajapakse (2009) studied the plane-strain and axisymmetric response of an isotropic elastic layer bonded to a rigid base under vertical and horizontal surface loads.

In the above studies, the surface stress tensor is considered as a two-dimensional quantity and its out-of-plane components are excluded. A recent study by Wang et al. (2010), who formulated the surface elasticity theory in the Lagrangian and Eulerian frameworks, indicated that the deformed and

undeformed configurations should be discriminated even in the case of small deformations. The out-of-plane terms of the surface displacement gradient could be significant particularly for curved and rotated surfaces. Povstenko (1993) studied the influence of residual surface stress gradient on the elastic field of a half-space that has a jump in residual surface stress over a circular area. The fundamental solutions of an elastic layer under surface and buried applied loads with the complete surface stresses have important application in various problems, such as nano-coatings and nanoscale surface layers used in electronic devices, advanced materials, communication devices, etc. In addition, the soft elastic layer can be found in micro-fluidic devices. Moreover, these fundamental solutions can be employed in the development of boundary element method (BEM) formulation for more complicated problems involving nanoscale structures and soft elastic solids.

2.4 Dislocation and Crack Problems with Surface Stresses

The studies of defects such as cracks and dislocations in elastic materials are important to various engineering applications and have been extensively studied in the context of classical continuum mechanics (Perez, 2004). For dislocations and cracks in nanoscale system, the influence of surface energy effects could become significant on their behavior such as near-tip fields, the energy release rate and their propagation behavior. By employing atomistic model, Hoagland et al. (1991) investigated the stress and displacement fields near a tip of a brittle crack and found that the solutions are in good agreement with the prediction of linear elastic fracture mechanics except at the vicinity of the crack tip where the effects of surface energy should be accounted for. From literature survey, however, few studies have been focused on the dislocation and crack problems with the consideration of surface energy effects although the concept of surface elasticity was established several decades ago.

For the crack problems, a few researchers have considered the influence of surface stresses on mechanics of single crack in an elastic solid.

For example, Wu (1999) and Wu and Wang (2000, 2001) investigated the influence of surface tension on two-dimensional crack problems and proposed that surface tension induced a pair of point loads at the crack tip. The singularity of the crack-tip stress fields then becomes r^{-1} instead of being $r^{-1/2}$ as a result of those point loads. With the assumption of blunt crack-tip, Wang et al. (2008) examined the effects of surface stress on the elastic fields near a crack tip for mode-I (opening) and mode-III (tearing) cracks with finite root radius based on Gurtin-Murdoch theory of surface elasticity and found that the surface stresses have a significant influence on the stress and displacement fields in the vicinity of blunt crack tip, especially when the curvature radius of the crack tip is in nanometer level. By performing finite element analysis, Fu et al. (2008) investigated a blunt mode-II (sliding) cracks with the consideration of surface stress effects and proposed that, when the curvature radius of the crack tip reduces to nanometers, surface stress effects have a considerable influence on both the magnitude and positions of the maximum stresses.

The fundamental problem of mode-I crack was also investigated by Oh et al. (2006) based upon an extension of continuum mechanics incorporating the effects of nanoscale through the long-range intermolecular force obtained from atomistic simulations. In their study, they summarized that the crack tip should be sharp rather than blunt and more importantly, the stress singularity at the crack tip is eliminated when considered at nanoscale level. The assumption of finite stress at crack tip was also found in the analysis of mode-I, II and III cracks by Kim et al. (2010, 2011) by employing Gurtin-Murdoch surface elasticity. Recently, Sendova and Walton (2010) examined mode-I crack in an infinite elastic medium with different models of surface energy effects such as constant surface tension model and curvature dependent surface tension model. For the case of constant surface tension, they proposed that the stress singularity at the crack tip is reduced to logarithmic singular, whereas, the finite stress at the crack tip is observed for the case of curvature dependent surface tension. In addition, the logarithmic stress

singularity was also perceived in the analysis of crack problems based upon Gurtin-Murdoch theory of surface elasticity by Kim et al. (2012). A review of literature indicates that the influence of surface energy effects on the elastic field in crack problem is still unclear especially in the vicinity of crack tip, moreover, all existing studies related to crack problems with the consideration of surface stresses are concerned with the analysis of plane problems. Therefore a rigorous analysis of three dimensional crack with the presence of surface energy effects could provide fundamental understanding of fracture mechanics in nanoscale systems.

Study on dislocations in an elastic solid has also received wide attentions among mechanics researches. The presence of dislocations strongly affects mechanical properties of materials. However, papers on dislocation problems with the consideration of surface energy effects are very limited in the literature. For example, the mechanics of dislocation problem was investigated for screw dislocations in Molybdenum and Tantalum by performing atomistic simulation (Woodward and Rao, 2001). Recently, Shodja et al. (2010) examined the behavior of a screw dislocation inside a nanotube with the consideration surface energy effects based on Gurtin-Murdoch theory of surface elasticity. The solutions of dislocation have important application in various problems such as fracture mechanics (Bilby and Eshelby, 1968). Gross (1982) developed the displacement discontinuity method (DDM), which is an indirect boundary element method based on the solutions for distributed dislocations (Crouch and Starfield, 1983). Such techniques can be adopted to investigate fracture problems involving complicated geometry and boundary conditions. Based on literature survey, the fundamental solutions for shear and opening dislocations in an elastic half-plane with the consideration of surface stresses, which can be employed in the DDM formulation to analyze the special problem of cracks in an elastic half-plane, do not exist.

CHAPTER III

BASIC EQUATIONS AND GENERAL SOLUTIONS

In this chapter, the basic equations of classical continuum mechanics with considering surface stress effects based on Gurtin-Murdoch continuum theory of surface elasticity are presented. The general solutions for plane strain and axisymmetric problems are then obtained by solving the governing equations through the applications of Fourier and Hankel integral transforms respectively. These general solutions will be employed to derive the fundamental solutions of an isotropic elastic layer under internal or surface loading, as well as dislocation and crack problems in the subsequent chapters.

3.1 Basic Equations of Continuum with Surface Stresses

According to Gurtin-Murdoch continuum model of surface elasticity, for an isotropic elastic material, the surface stress effects are accounted for by considering the surface of a solid as a thin layer with negligibly thickness adhering to the underlying bulk material without slipping. The material constants of the surface are different from those of the bulk material. The surface stress effects are displayed in the set of non-classical boundary conditions. These boundary conditions and the surface stress-strain relation together with the classical elasticity equations form a coupled system of field equations. In the bulk, the governing equations are the same as those in classical elasticity. In addition, on the surface (or interface), the generalized Young-Laplace equation (Povstenko ,1993) and a set of constitutive relations have to be satisfied. The basic equations for small displacements and infinitesimal strains of a continuum with surface stress effects can then be established based on the Gurtin-Murdoch model.

In the absence of body forces, the equilibrium equation, constitutive relation, and strain-displacement relationship of the bulk material are given respectively by

$$\sigma_{ij,j} = 0 \tag{3.1a}$$

$$\sigma_{ij} = 2\mu\varepsilon_{ij} + \lambda\delta_{ij}\varepsilon_{kk} \tag{3.1b}$$

$$\varepsilon_{ij} = \frac{1}{2}\left(u_{i,j} + u_{j,i}\right) \tag{3.1c}$$

where σ_{ij}, ε_{ij} and u_i denote the components of stress, strain and displacement tensors respectively. In addition, μ and λ are Lamé constants of the bulk material.

On the surface, the generalized Young-Laplace equation (Povstenko, 1993), surface constitutive relations and strain-displacement relationship can be expressed as (Gurtin and Murdoch, 1975; Gurtin and Murdoch, 1978; Gurtin et al., 1998),

$$\sigma^s_{i\alpha,\alpha} + \sigma_{ij}n_j + t^0_i = 0 \tag{3.2a}$$

$$\sigma^s_{\beta\alpha} = \tau^s\delta_{\beta\alpha} + 2\left(\mu^s - \tau^s\right)\varepsilon_{\beta\alpha} + \left(\lambda^s + \tau^s\right)\varepsilon_{\gamma\gamma}\delta_{\beta\alpha} + \tau^s u^s_{\beta,\alpha};\ \sigma^s_{3\alpha} = \tau^s u^s{}_{3,\alpha} \tag{3.2b}$$

$$\varepsilon^s_{\alpha\beta} = \frac{1}{2}\left(u^s_{\alpha,\beta} + u^s_{\beta,\alpha}\right) \tag{3.2c}$$

where the superscript 's' is used to denote the quantities corresponding to the surface; μ^s and λ^s are surface Lamé constants; τ^s is the residual surface stress (or surface tension) under unstrained condition; n_i denotes the components of the unit normal vector of the surface and t^0_i denotes the prescribed traction on the surface. It is noted that the value of τ^s is constant for a given surface orientation of a pure metal/semiconductor at a specific temperature (Zhao and Rajapakse 2009).

In the above equations, Greek subscripts denote the field quantities associated with the surface and take the value of 1 or 2, while the Latin subscripts adopt values from 1 to 3. A majority of existing studies based on the Gurtin-Murdoch theory has formulated the problems in undeformed configuration due to the assumption of infinitesimal deformations thus the out-of-plane component of surface stresses given by the second equation in Eq. (3.2b) is

normally ignored. The term $\tau^s u_{3,\alpha}$ can simply be viewed as the out-of-plane component of the pre-existing surface tension τ^s in the deformed configuration whereas the surface gradient of the displacement $u_{3,\alpha}$ act as the out-of-plane component of the unit vector tangent to the surface in the deformed state. While the component $\tau^s u_{3,\alpha}$ has physical meaning only in the deformed state and identically vanishes in the undeformed configuration, its contribution to the constitutive equation, Eq. (3.2b), is of the same order as other terms. As recently pointed out by Wang et al. (2010), these out-of-plane terms could become significant even in the case of small deformations.

In this study, the fundamental problems are considered for the case of plane strain and axisymmetric problems. The equilibrium equations, constitutive law and strain-displacement relations for the bulk and the surface material can be specialized for each case as follows:

3.1.1 Basic Equations for Plane Problems

In the case that the deformations under consideration are assumed as plane strain in the xz-plane, i.e. $\varepsilon_{xy} = \varepsilon_{yy} = \varepsilon_{yz} = 0$, basic equations of the bulk material in Eqs. (3.1a) to (3.1c) can be expressed in a Cartesian coordinate as

$$\frac{\partial \sigma_{xx}}{\partial x} + \frac{\partial \sigma_{xz}}{\partial z} = 0 \tag{3.3a}$$

$$\frac{\partial \sigma_{zx}}{\partial x} + \frac{\partial \sigma_{zz}}{\partial z} = 0 \tag{3.3b}$$

$$\sigma_{xx} = (\lambda + 2\mu)\varepsilon_{xx} + \lambda \varepsilon_{zz} \tag{3.3c}$$

$$\sigma_{zz} = (\lambda + 2\mu)\varepsilon_{zz} + \lambda \varepsilon_{xx} \tag{3.3d}$$

$$\sigma_{xz} = \sigma_{zx} = 2\mu \varepsilon_{xz} \tag{3.3e}$$

$$\varepsilon_{xx} = \frac{\partial u_x}{\partial x} \tag{3.3f}$$

$$\varepsilon_{zz} = \frac{\partial u_z}{\partial z} \tag{3.3g}$$

$$\varepsilon_{xz} = \varepsilon_{zx} = \frac{1}{2}\left(\frac{\partial u_z}{\partial x} + \frac{\partial u_x}{\partial z} \right) \tag{3.3h}$$

On the surface, the basic equations in Eqs. (3.2a) to (3.2c) for the case of flat surface are given by

$$\frac{\partial \sigma^s_{xx}}{\partial x} + \sigma_{xz}\Big|_{z=0} + t^0_x = 0 \tag{3.4a}$$

$$\frac{\partial \sigma^s_{zx}}{\partial x} + \sigma_{zz}\Big|_{z=0} + t^0_z = 0 \tag{3.4b}$$

$$\sigma^s_{xx} = \tau^s + \kappa^s \varepsilon^s_{xx} \tag{3.4c}$$

$$\sigma^s_{zx} = \tau^s \frac{du^s_z}{dx} \tag{3.4d}$$

$$\varepsilon^s_{xx} = \frac{du^s_x}{dx} \tag{3.4e}$$

where $\kappa^s = 2\mu^s + \lambda^s$

3.1.2 Basic Equations for Axisymmetric Problems

In the case that the deformations under consideration are rotationally symmetric about the z-axis, the corresponding elastic fields are described in a cylindrical coordinate (r, θ, z). It is noted that the responses of the elastic solid are independent of θ, i.e. $\varepsilon_{r\theta}$ = $\varepsilon_{z\theta}$ = 0. For the bulk material, basic equations in Eqs. (3.1a) to (3.1c) can be expressed in a cylindrical coordinate as

$$\frac{\partial \sigma_{rr}}{\partial r} + \frac{\partial \sigma_{rz}}{\partial z} + \frac{\sigma_{rr} - \sigma_{\theta\theta}}{r} = 0 \tag{3.5a}$$

$$\frac{\partial \sigma_{rz}}{\partial r} + \frac{\partial \sigma_{zz}}{\partial z} + \frac{\sigma_{rz}}{r} = 0 \tag{3.5b}$$

$$\sigma_{rr} = (\lambda + 2\mu)\varepsilon_{rr} + \lambda\varepsilon_{\theta\theta} + \lambda\varepsilon_{zz} \tag{3.5c}$$

$$\sigma_{\theta\theta} = \lambda\varepsilon_{rr} + (\lambda + 2\mu)\varepsilon_{\theta\theta} + \lambda\varepsilon_{zz} \tag{3.5d}$$

$$\sigma_{zz} = \lambda\varepsilon_{rr} + \lambda\varepsilon_{\theta\theta} + (\lambda + 2\mu)\varepsilon_{zz} \tag{3.5e}$$

$$\sigma_{rz} = \sigma_{zr} = 2\mu\varepsilon_{rz} \tag{3.5f}$$

$$\varepsilon_{rr} = \frac{\partial u_r}{\partial r} \tag{3.5g}$$

$$\varepsilon_{\theta\theta} = \frac{u_r}{r} \tag{3.5h}$$

$$\varepsilon_{zz} = \frac{\partial u_z}{\partial z} \tag{3.5i}$$

$$\varepsilon_{rz} = \varepsilon_{zr} = \frac{1}{2}\left(\frac{\partial u_r}{\partial z} + \frac{\partial u_z}{\partial r}\right) \tag{3.5j}$$

On the surface, the basic equations in Eqs. (3.2a) to (3.2c) for the case of flat surface are given by

$$\frac{d\sigma_{rr}^s}{dr} + \frac{\sigma_{rr}^s - \sigma_{\theta\theta}^s}{r} + \sigma_{zr}\big|_{z=0} + t_r^0 = 0 \tag{3.6a}$$

$$\frac{d\sigma_{zr}^s}{dr} + \frac{\sigma_{zr}^s}{r} + \sigma_{zz}\big|_{z=0} + t_z^0 = 0 \tag{3.6b}$$

$$\sigma_{rr}^s = \tau^s + (2\mu^s + \lambda^s)\varepsilon_{rr}^s + (\lambda^s + \tau^s)\varepsilon_{\theta\theta}^s \tag{3.6c}$$

$$\sigma_{\theta\theta}^s = \tau^s + (2\mu^s + \lambda^s)\varepsilon_{\theta\theta}^s + (\lambda^s + \tau^s)\varepsilon_{rr}^s \tag{3.6d}$$

$$\sigma_{zr}^s = \tau^s \frac{du_z^s}{dr} \tag{3.6e}$$

$$\varepsilon_{rr}^s = \frac{du_r^s}{dr} \tag{3.6f}$$

$$\varepsilon_{\theta\theta}^s = \frac{u_r^s}{r} \tag{3.6g}$$

3.2 General Solutions for Bulk Materials

3.2.1 General Solutions for Plane Problems

For the plane strain case, the solution for the bulk material can be obtained by solving the two-dimensional biharmonic equation,

$$\nabla_1^2 \nabla_1^2 \chi = 0 \tag{3.7}$$

where ∇_1^2 denotes the two-dimensional Laplacian operator, $\nabla_1^2 = \frac{\partial^2}{\partial x^2} + \frac{\partial^2}{\partial y^2}$; and χ denotes Airy stress function.

By applying Fourier integral transform into Eq. (3.7), we then obtain

$$\int_{-\infty}^{+\infty} \nabla_1^2 \nabla_1^2 \chi e^{i\xi x} dx = \left(\frac{d^2}{dz^2} - \xi^2 \right)^2 \Omega(\xi, z) = 0 \tag{3.8}$$

where $\Omega(\xi, z) = \int_{-\infty}^{+\infty} \chi e^{i\xi x} dx$. The general solution of above equation may be written in the following form

$$\Omega(\xi, z) = (A + Bz)e^{-|\xi|z} + (C + Dz)e^{|\xi|z} \tag{3.9}$$

where A, B, C and D are arbitrary functions that can be determined from the boundary conditions.

Therefore, the general solutions for the bulk stresses and displacements of a two-dimensional elastic solid can be expressed with respect to a Cartesian coordinate system as (Sneddon 1951),

$$\sigma_{zz} = -\frac{1}{2\pi} \int_{-\infty}^{+\infty} \xi^2 \Omega e^{-i\xi x} d\xi \tag{3.10a}$$

$$\sigma_{xx} = \frac{1}{2\pi} \int_{-\infty}^{+\infty} \frac{d^2\Omega}{dz^2} e^{-i\xi x} d\xi \tag{3.10b}$$

$$\sigma_{xz} = \frac{1}{2\pi} \int_{-\infty}^{+\infty} i\xi \frac{d\Omega}{dz} e^{-i\xi x} d\xi \tag{3.10c}$$

$$u_z = \frac{1}{8\pi\mu(\lambda + \mu)} \int_{-\infty}^{+\infty} \left[(\lambda + 2\mu) \frac{d^3\Omega}{dz^3} - (3\lambda + 4\mu)\xi^2 \frac{d\Omega}{dz} \right] e^{-i\xi x} \frac{d\xi}{\xi^2} \tag{3.10d}$$

$$u_x = \frac{1}{8\pi\mu(\lambda + \mu)} \int_{-\infty}^{+\infty} \left[(\lambda + 2\mu) \frac{d^2\Omega}{dz^2} + \lambda\xi^2 \Omega \right] i e^{-i\xi x} \frac{d\xi}{\xi} \tag{3.10e}$$

3.2.2 General Solutions for Axisymmetric Problems

For the axisymmetric case, the solution for the bulk material can be obtained by solving the following biharmonic equation in a cylindrical coordinate system.

$$\nabla^2 \nabla^2 \Phi = 0 \tag{3.11}$$

where ∇^2 denotes the Laplacian operator in a cylindrical coordinate, $\nabla^2 = \frac{\partial^2}{\partial r^2} + \frac{1}{r}\frac{\partial}{\partial r} + \frac{\partial^2}{\partial z^2}$; and Φ is Love's strain potential.

By applying Hankel integral transform into Eq. (3.11), we obtain,

$$\int_0^\infty r\nabla^2\nabla^2\Phi J_0(\xi r)\,dr = \left(\frac{d^2}{dz^2} - \xi^2\right)^2 \Omega'(\xi, z) = 0 \tag{3.12}$$

where $\Omega'(\xi, z) = \int_0^\infty r\Phi J_0(\xi r)\,dr$ and $J_n(\xi)$ denotes the Bessel functions of the first kind of order n. The general solution of above equation may be written in the form

$$\Omega'(\xi, z) = (A' + B'z)e^{-\xi z} + (C' + D'z)e^{\xi z} \tag{3.13}$$

where A', B', C' and D' are arbitrary functions that can be determined from the boundary conditions.

Therefore, the general solutions for bulk stresses and displacements of an elastic solid can be expressed with respect to a cylindrical coordinate system as (Sneddon, 1951; Selvadurai, 2000)

$$\sigma_{rr} = \int_0^\infty \xi\left[\lambda\frac{d^3\Omega'}{dz^3} + (\lambda + 2\mu)\xi^2\frac{d\Omega'}{dz}\right]J_0(\xi r)\,d\xi - \frac{2(\lambda+\mu)}{r}\int_0^\infty \xi^2\frac{d\Omega'}{dz}J_1(\xi r)\,d\xi \tag{3.14a}$$

$$\sigma_{\theta\theta} = \lambda\int_0^\infty \xi\left[\frac{d^3\Omega'}{dz^3} - \xi^2\frac{d\Omega'}{dz}\right]J_0(\xi r)\,d\xi + \frac{2(\lambda+\mu)}{r}\int_0^\infty \xi^2\frac{d\Omega'}{dz}J_1(\xi r)\,d\xi \tag{3.14b}$$

$$\sigma_{zz} = \int_0^\infty \xi\left[(\lambda + 2\mu)\frac{d^3\Omega'}{dz^3} - (3\lambda + 4\mu)\xi^2\frac{d\Omega'}{dz}\right]J_0(\xi r)\,d\xi \tag{3.14c}$$

$$\sigma_{rz} = \int_0^\infty \xi^2\left[\lambda\frac{d^2\Omega'}{dz^2} + (\lambda + 2\mu)\xi^2\Omega'\right]J_1(\xi r)\,d\xi \tag{3.14d}$$

$$u_r = \frac{\lambda+\mu}{\mu}\int_0^\infty \xi^2\frac{d\Omega'}{dz}J_1(\xi r)\,d\xi \tag{3.14e}$$

$$u_z = \int_0^\infty \xi\left[\frac{d^2\Omega'}{dz^2} - \frac{\lambda+2\mu}{\mu}\xi^2\Omega'\right]J_0(\xi r)\,d\xi \tag{3.14f}$$

CHAPTER IV

INTERNALLY LOADED ELASTIC LAYER

In this chapter, the fundamental solutions of an isotropic elastic layer of finite thickness bonded to a rigid material base is derived with the consideration of surface stresses by employing Gurtin-Murdoch continuum theory of elastic material surfaces. The boundary value problems corresponding to buried vertical and horizontal loads with non-classical boundary conditions due to surface stresses are solved by using Fourier integral transform technique for the case of plane problems. In addition, the fundamental solutions corresponding to axisymmetric surface vertical and horizontal loads are determined by the application of Hankel integral transform technique. Selected numerical results are presented to portray the influence of surface stresses on the elastic field.

4.1 Fundamental Solutions for Plane Problems

Consider a two-dimensional elastic layer of finite thickness t bonded to a rigid base, and subjected to vertical and horizontal loading at a depth h below the free surface as shown in Figure 4.1(a). The solutions for the problem shown in Figure 4.1(a) can be derived by dividing the elastic layer into two sub-domains. The sub-domain '1' corresponds to the region where $0 \le z \le h$ and the sub-domain '2' corresponds to the region where $h \le z \le t$. The general solutions of the sub-domain '1' are given by Eqs. (3.10a) to (3.10e) whereas the general solutions of the sub-domain '2' are also given by Eqs. (3.10a) to (3.10e) with the arbitrary functions A to D being replaced by E to H respectively. A superscript 'i' ($i = 1, 2$) is used hereafter to denote quantities associated with each sub-domain. The arbitrary functions A to H corresponding to each sub-domain can be obtained by solving the following boundary value problem.

$$\sigma_{zz}^{(1)}\Big|_{z=0}+\left(\frac{d\tau^s}{dx}\frac{du_z^{(1)}}{dx}+\tau^s\frac{d^2u_z^{(1)}}{dx^2}\right)_{z=0}=0 \tag{4.1a}$$

$$\sigma_{zx}^{(1)}\Big|_{z=0}+\left(\frac{d\tau^s}{dx}+\kappa^s\frac{d^2u_x^{(1)}}{dx^2}\right)_{z=0}=0 \tag{4.1b}$$

$$\sigma_{zz}^{(1)}\Big|_{z=h^-}-\sigma_{zz}^{(2)}\Big|_{z=h^+}=p(x) \tag{4.1c}$$

$$\sigma_{zx}^{(1)}\Big|_{z=h^-}-\sigma_{zx}^{(2)}\Big|_{z=h^+}=q(x) \tag{4.1d}$$

$$u_z^{(1)}\Big|_{z=h^-}=u_z^{(2)}\Big|_{z=h^+} \tag{4.1e}$$

$$u_x^{(1)}\Big|_{z=h^-}=u_x^{(2)}\Big|_{z=h^+} \tag{4.1f}$$

$$u_z^{(2)}\Big|_{z=t}=0 \tag{4.1g}$$

$$u_x^{(2)}\Big|_{z=t}=0 \tag{4.1h}$$

where $\kappa^s=\lambda^s+2\mu^s$ is a surface material constant; $p(x)$ and $q(x)$ denote the jump of the normal traction and shear traction across the plane $z=h$ due to the applied internal vertical and horizontal loads respectively (see Figure 4.1(a)).

It should be noted that both Eqs. (4.1a) and (4.1b) are non-classical boundary conditions obtained from Eqs. (3.4a) and (3.4b). In addition, Eq. (4.1a) contains the out-of-plane component of surface stresses associated with residual surface stress, which has generally been ignored in previous studies. For a flat surface, it can be seen from Eqs. (4.1a) and (4.1b) that the influence of residual surface stress τ^s will be neglected if the out-of-plane component of surface stresses is disregarded (the second term on the left-hand side of Eq. (4.1a) vanishes) and the residual surface stress is assumed to be constant. In view of Eqs. (3.10a) to (3.10e), the following set of linear simultaneous equations for determining the arbitrary functions can be constituted by applying Fourier integral transform to Eqs. (4.1a) to (4.1h) together with the assumption that the residual surface stress is constant.

$$\left(1+\frac{|\xi|}{2\mu}\tau^s\right)A+\frac{\tau^s}{2(\lambda+\mu)}(B+D)+\left(1-\frac{|\xi|}{2\mu}\tau^s\right)C=0 \tag{4.2a}$$

$$\left(1+\frac{|\xi|}{2\mu}\kappa^s\right)|\xi|A-\left(1+\frac{(\lambda+2\mu)}{2\mu(\lambda+\mu)}|\xi|\kappa^s\right)B-\left(1-\frac{|\xi|}{2\mu}\kappa^s\right)|\xi|C-\left(1-\frac{(\lambda+2\mu)}{2\mu(\lambda+\mu)}|\xi|\kappa^s\right)D=0 \quad (4.2b)$$

$$(A-E)e^{-|\xi|h}+(B-F)he^{-|\xi|h}+(C-G)e^{|\xi|h}+(D-H)he^{|\xi|h}=-\frac{\overline{p}(\xi)}{\xi^2} \quad (4.2c)$$

$$|\xi|(A-E)e^{-|\xi|h}-(1-|\xi|h)(B-F)e^{-|\xi|h}-|\xi|(C-G)e^{|\xi|h}-(1+|\xi|h)(D-H)e^{|\xi|h}=\frac{i\overline{q}(\xi)}{\xi} \quad (4.2d)$$

$$|\xi|(A-E)e^{-|\xi|h}+\left(|\xi|h+\frac{\mu}{\lambda+\mu}\right)(B-F)e^{-|\xi|h}-|\xi|(C-G)e^{|\xi|h}-\left(|\xi|h-\frac{\mu}{\lambda+\mu}\right)(D-H)e^{|\xi|h}=0 \quad (4.2e)$$

$$|\xi|(A-E)e^{-|\xi|h}+\left(|\xi|h-\frac{\lambda+2\mu}{\lambda+\mu}\right)(B-F)e^{-|\xi|h}+|\xi|(C-G)e^{|\xi|h}+\left(|\xi|h+\frac{\lambda+2\mu}{\lambda+\mu}\right)(D-H)e^{|\xi|h}=0 \quad (4.2f)$$

$$|\xi|Ee^{-|\xi|t}+\left(|\xi|t+\frac{\mu}{\lambda+\mu}\right)Fe^{-|\xi|t}-|\xi|Ge^{|\xi|t}-\left(|\xi|t-\frac{\mu}{\lambda+\mu}\right)He^{|\xi|t}=0 \quad (4.2g)$$

$$|\xi|Ee^{-|\xi|t}+\left(|\xi|t-\frac{\lambda+2\mu}{\lambda+\mu}\right)Fe^{-|\xi|t}+|\xi|Ge^{|\xi|t}+\left(|\xi|t+\frac{\lambda+2\mu}{\lambda+\mu}\right)He^{|\xi|t}=0 \quad (4.2h)$$

where $\overline{p}(\xi)$ and $\overline{q}(\xi)$ are the Fourier transforms of $p(x)$ and $q(x)$ respectively and are given by

$$\overline{p}(\xi)=\int_{-\infty}^{+\infty}p(x)e^{i\xi x}dx \quad (4.3a)$$

$$\overline{q}(\xi)=\int_{-\infty}^{+\infty}q(x)e^{i\xi x}dx \quad (4.3b)$$

By solving the set of linear simultaneous equations displayed in Eqs. (4.2a) to (4.2h), the following solutions are obtained for the arbitrary functions A to H.

$$A=\frac{(A_p+iA_q)}{I};\ B=\frac{(B_p+iB_q)}{I} \quad (4.4a)$$

$$C=\frac{(C_p+iC_q)}{I};D=\frac{(D_p+iD_q)}{I} \quad (4.4b)$$

$$E=\frac{(E_p+iE_q)}{I};F=\frac{(F_p+iF_q)}{I} \quad (4.4c)$$

$$G=\frac{(G_p+iG_q)}{I};H=\frac{(H_p+iH_q)}{I} \quad (4.4d)$$

where the explicit expressions of A_p, A_q, B_p, B_q, C_p, C_q, D_p, D_q, E_p, E_q, F_p, F_q, G_p, G_q, H_p, H_q and I are given in the Appendix.

In the following subsections, the explicit expressions of the arbitrary functions for the special cases of surface loading ($h \to 0$) and a semi-infinite medium ($t \to \infty$) are presented.

4.1.1 Surface Loading on Finite Thickness Layer

The surface loading of a nanoscale layer has many practical applications. The elastic field corresponding to this case can be obtained by taking the limit of $h \to 0$ in Eqs. (4.4a) to (4.4d). The corresponding arbitrary functions are given by Eqs. (4.4a) and (4.4b) with A_i to D_i ($i = p, q$) defined as follows:

$$A_p = \frac{\bar{p}(\xi)}{2\xi^2}\left\{(\lambda+3\mu)\left[\left(1+\Lambda|\xi|\right)e^{2|\xi|t} - \Lambda|\xi|\right] + 2(\lambda+\mu)t|\xi|\left((\Lambda+t)|\xi|-1\right) - \frac{2(\lambda+\mu)^2}{(\lambda+2\mu)}\Lambda t^2|\xi|^3 + \frac{\lambda^2+4\lambda\mu+5\mu^2}{\lambda+\mu}\right\} \quad (4.5a)$$

$$B_p = \frac{\bar{p}(\xi)}{2|\xi|}\left\{(\lambda+3\mu)\left[\left(1+\frac{\lambda+\mu}{\lambda+2\mu}\Lambda|\xi|\right)e^{2|\xi|t} - \frac{\lambda+\mu}{\lambda+2\mu}\Lambda|\xi|\right] + \frac{2(\lambda+\mu)^2}{\lambda+2\mu}\Lambda t\xi^2 + (\lambda+\mu)\left(1-2t|\xi|\right)\right\} \quad (4.5b)$$

$$C_p = \frac{\bar{p}(\xi)}{2\xi^2}\left\{(\lambda+3\mu)\left[\left(1-\Lambda|\xi|\right)e^{-2|\xi|t} + \Lambda|\xi|\right] + 2(\lambda+\mu)t|\xi|\left((\Lambda+t)|\xi|+1\right) + \frac{2(\lambda+\mu)^2}{(\lambda+2\mu)}\Lambda t^2|\xi|^3 + \frac{\lambda^2+4\lambda\mu+5\mu^2}{\lambda+\mu}\right\} \quad (4.5c)$$

$$D_p = -\frac{\bar{p}(\xi)}{2|\xi|}\left\{(\lambda+3\mu)\left[\left(1-\frac{\lambda+\mu}{\lambda+2\mu}\Lambda|\xi|\right)e^{-2|\xi|t} + \frac{\lambda+\mu}{\lambda+2\mu}\Lambda|\xi|\right] + \frac{2(\lambda+\mu)^2}{\lambda+2\mu}\Lambda t\xi^2 + (\lambda+\mu)\left(1+2t|\xi|\right)\right\} \quad (4.5d)$$

$$A_q = -\frac{\bar{q}(\xi)}{|\xi|\xi}\left\{(\lambda+3\mu)\left[\frac{\tau^s|\xi|}{4(\lambda+\mu)}e^{2|\xi|t} - \frac{\tau^s|\xi|}{4(\lambda+\mu)}\right] + \frac{\mu(\lambda+2\mu)}{\lambda+\mu} + (\lambda+\mu)t^2\xi^2 - \frac{\tau^s t\xi^2}{2} - \frac{(\lambda+\mu)}{2\mu}\tau^s t^2|\xi|^3\right\} \quad (4.5e)$$

$$B_q = \frac{\bar{q}(\xi)}{2\xi}\left\{(\lambda+3\mu)\left[\left(1+\frac{\tau^s|\xi|}{2\mu}\right)e^{2|\xi|t} - \frac{\tau^s|\xi|}{2\mu}\right] + (\lambda+\mu)\left(1+2t|\xi|\right) - \frac{(\lambda+\mu)}{\mu}\tau^s t\xi^2\right\} \quad (4.5f)$$

$$C_q = \frac{\bar{q}(\xi)}{|\xi|\xi}\left\{(\lambda+3\mu)\left[-\frac{\tau^s|\xi|}{4(\lambda+\mu)}e^{-2|\xi|t} + \frac{\tau^s|\xi|}{4(\lambda+\mu)}\right] + \frac{\mu(\lambda+2\mu)}{\lambda+\mu} + (\lambda+\mu)t^2\xi^2 - \frac{\tau^s t\xi^2}{2} + \frac{(\lambda+\mu)}{2\mu}\tau^s t^2|\xi|^3\right\} \quad (4.5g)$$

$$D_q = \frac{\bar{q}(\xi)}{2\xi}\left\{(\lambda+3\mu)\left[\left(1-\frac{\tau^s|\xi|}{2\mu}\right)e^{-2|\xi|t} + \frac{\tau^s|\xi|}{2\mu}\right] + (\lambda+\mu)\left(1-2t|\xi|\right) - \frac{(\lambda+\mu)}{\mu}\tau^s t\xi^2\right\} \quad (4.5h)$$

The fundamental solutions corresponding to an elastic layer subjected to a vertical line load P_0 and a horizontal line load Q_0 can be obtained by substituting $\bar{p}(\xi) = P_0$ and $\bar{q}(\xi) = Q_0$ in the above solutions.

For the cases of vertical strip load of constant magnitude p_0 and horizontal strip load of constant magnitude q_0 over the region $-a \le x \le a$,

$$\bar{p}(\xi) = \frac{2\sin(\xi a)}{\xi} p_0 \tag{4.6a}$$

$$\bar{q}(\xi) = \frac{2\sin(\xi a)}{\xi} q_0 \tag{4.6b}$$

Note that $\Lambda = \kappa^s(\lambda + 2\mu)/2\mu(\lambda + \mu)$ is a parameter with a dimension of length. This parameter can be viewed as a material characteristic length that represents the influence of surface stress. It is clear from the above solutions that the influence of surface stresses does not only come from the surface material constant κ^s (or Λ) but also from the residual surface stress τ^s. In the absence of surface stress effects, Λ and τ^s vanish and the above solutions reduce to the classical elasticity solutions (Pickett, 1938).

The elastic field of a semi-infinite medium under surface loading can readily be obtained from the solutions in Eqs. (4.4a) and (4.4b), with A_i to D_i ($i = p, q$) given by Eqs. (4.5a) to (4.5h), by taking the limit of $t \to \infty$. Note that the arbitrary functions C and $D \equiv 0$ to ensure the regularity of the solutions at infinity. In the case of the vertical load, the arbitrary functions A and B take the form,

$$A = \frac{\bar{p}(\xi)}{\eta\xi^2}\left(1 + \Lambda|\xi|\right) \tag{4.7a}$$

$$B = \frac{\bar{p}(\xi)}{\eta|\xi|}\left[1 + \frac{(\lambda + \mu)}{(\lambda + 2\mu)}\Lambda|\xi|\right] \tag{4.7b}$$

where

$$\eta = \left(1+\Lambda|\xi|\right)+\frac{\tau^s}{2\mu}|\xi|\left[\frac{\lambda+2\mu}{\lambda+\mu}+\frac{\lambda+3\mu}{\lambda+2\mu}\Lambda|\xi|\right] \tag{4.8}$$

In the case of the horizontal loading,

$$A = -i\frac{\overline{q}(\xi)}{\eta\xi}\left[\frac{\tau^s}{2(\lambda+\mu)}\right] \tag{4.9a}$$

$$B = i\frac{\overline{q}(\xi)}{\eta\xi}\left(1+\frac{\tau^s|\xi|}{2\mu}\right) \tag{4.9b}$$

4.1.2 Internal Loading in Semi-infinite Medium

The stress and displacement fields of a semi-infinite medium under vertical and horizontal loads applied at a depth h below free surface can also be obtained from the solutions in Eqs. (4.4a) to (4.4d) by taking the limit of $t \to \infty$. Note that the arbitrary functions G and $H \equiv 0$ to ensure the regularity of the solutions at infinity. The corresponding arbitrary functions A to F can be specialized to the case of a half-plane subjected to internal vertical load as follows:

$$A=\frac{\overline{p}(\xi)e^{-|\xi|h}}{2\eta\xi^2}\left\{\left(1+\Lambda|\xi|\right)\left(1+\frac{\lambda+\mu}{\lambda+2\mu}h|\xi|\right)-\frac{\tau^s}{2\mu}|\xi|\left[\frac{\lambda+2\mu}{\lambda+\mu}+h|\xi|+\frac{\lambda+3\mu}{\lambda+2\mu}\Lambda|\xi|+\frac{(\lambda+\mu)^2}{(\lambda+2\mu)^2}\Lambda h\xi^2\right]\right\} \tag{4.10a}$$

$$B=\frac{\overline{p}(\xi)e^{-|\xi|h}}{2(\lambda+2\mu)\eta|\xi|}\left\{\lambda+3\mu+(\lambda+\mu)(\Lambda+2h)|\xi|-\frac{\tau^s}{2\mu}|\xi|\left[\lambda+2\mu+\frac{(\lambda+\mu)(\lambda+3\mu)}{\lambda+2\mu}\Lambda|\xi|+\frac{2(\lambda+\mu)^2}{\lambda+2\mu}\Lambda h\xi^2\right]\right\} \tag{4.10b}$$

$$C=-\frac{\overline{p}(\xi)e^{-|\xi|h}}{2\xi^2}\left[1+\frac{\lambda+\mu}{\lambda+2\mu}h|\xi|\right] \tag{4.10c}$$

$$D=\frac{\overline{p}(\xi)e^{-|\xi|h}(\lambda+\mu)}{2|\xi|(\lambda+2\mu)} \tag{4.10d}$$

$$E=\frac{\overline{p}(\xi)}{2\eta\xi^2}\left\{\begin{array}{l} e^{|\xi|h}\left\{\left(1+\Lambda|\xi|\right)\left(1-\frac{\lambda+\mu}{\lambda+2\mu}h|\xi|\right)+\frac{\tau^s}{2\mu}|\xi|\left[\frac{\lambda+2\mu}{\lambda+\mu}-h|\xi|+\frac{\lambda+3\mu}{\lambda+2\mu}\Lambda|\xi|-\frac{(\lambda+\mu)(\lambda+3\mu)}{(\lambda+2\mu)^2}\Lambda h\xi^2\right]\right\} \\ +e^{-|\xi|h}\left\{\left(1+\Lambda|\xi|\right)\left(1+\frac{\lambda+\mu}{\lambda+2\mu}h|\xi|\right)-\frac{\tau^s}{2\mu}|\xi|\left[\frac{\lambda+2\mu}{\lambda+\mu}+h|\xi|+\frac{\lambda+3\mu}{\lambda+2\mu}\Lambda|\xi|+\frac{(\lambda+\mu)^2}{(\lambda+2\mu)^2}\Lambda h\xi^2\right]\right\} \end{array}\right\} \tag{4.10e}$$

$$F=\frac{\overline{p}(\xi)}{2(\lambda+2\mu)\eta|\xi|}\left\{\begin{array}{l} e^{|\xi|h}\left\{(\lambda+\mu)(1+\Lambda|\xi|)+\frac{\tau^s}{2\mu}|\xi|\left[\lambda+2\mu+\frac{(\lambda+\mu)(\lambda+3\mu)}{\lambda+2\mu}\Lambda|\xi|\right]\right\} \\ +e^{-|\xi|h}\left\{\lambda+3\mu+(\lambda+\mu)(\Lambda+2h)|\xi|-\frac{\tau^s}{2\mu}|\xi|\left[\lambda+2\mu+\frac{(\lambda+\mu)(\lambda+3\mu)}{\lambda+2\mu}\Lambda|\xi|+\frac{2(\lambda+\mu)^2}{\lambda+2\mu}\Lambda h\xi^2\right]\right\} \end{array}\right\} \tag{4.10f}$$

In the case of the internal horizontal loading, the arbitrary functions *A* to *F* take the form,

$$A=\frac{i\overline{q}(\xi)e^{-|\xi|h}}{2(\lambda+2\mu)\eta|\xi|\xi}\left\{[\mu-(\lambda+\mu)h|\xi|](1+\Lambda|\xi|)-\tau^s|\xi|\left[\frac{\lambda+2\mu}{2(\lambda+\mu)}-\frac{\lambda+2\mu}{2\mu}h|\xi|-\frac{\lambda+3\mu}{2(\lambda+2\mu)}\Lambda|\xi|-\frac{(\lambda+\mu)^2}{2\mu(\lambda+2\mu)}\Lambda h\xi^2\right]\right\} \tag{4.11a}$$

$$B=\frac{i\overline{q}(\xi)e^{-|\xi|h}}{2(\lambda+2\mu)\eta\xi}\left\{\lambda+3\mu-(\lambda+\mu)(\Lambda+2h)|\xi|+\frac{\tau^s}{2\mu}|\xi|\left[\lambda+2\mu-\frac{(\lambda+\mu)(\lambda+3\mu)}{\lambda+2\mu}\Lambda|\xi|+\frac{2(\lambda+\mu)^2}{\lambda+2\mu}\Lambda h\xi^2\right]\right\} \tag{4.11b}$$

$$C=-\frac{i\overline{q}(\xi)e^{-|\xi|h}[\mu-(\lambda+\mu)h|\xi|]}{2|\xi|\xi(\lambda+2\mu)} \tag{4.11c}$$

$$D=-\frac{i\overline{q}(\xi)e^{-|\xi|h}(\lambda+\mu)}{2\xi(\lambda+2\mu)} \tag{4.11d}$$

$$E=-\frac{i\overline{q}(\xi)}{2(\lambda+2\mu)\eta|\xi|\xi}\begin{Bmatrix}e^{|\xi|h}\left\{[\mu+(\lambda+\mu)h|\xi|](1+\Lambda|\xi|)+\tau^s|\xi|\left[\frac{\lambda+2\mu}{2(\lambda+\mu)}+\frac{\lambda+2\mu}{2\mu}h|\xi|+\frac{\lambda+3\mu}{2(\lambda+2\mu)}\Lambda|\xi|+\frac{(\lambda+\mu)(\lambda+3\mu)}{2\mu(\lambda+2\mu)}\Lambda h\xi^2\right]\right\}\\-e^{-|\xi|h}\left\{[\mu-(\lambda+\mu)h|\xi|](1+\Lambda|\xi|)-\tau^s|\xi|\left[\frac{\lambda+2\mu}{2(\lambda+\mu)}-\frac{\lambda+2\mu}{2\mu}h|\xi|-\frac{\lambda+3\mu}{2(\lambda+2\mu)}\Lambda|\xi|-\frac{(\lambda+\mu)^2}{2\mu(\lambda+2\mu)}\Lambda h\xi^2\right]\right\}\end{Bmatrix} \tag{4.11e}$$

$$F=\frac{i\overline{q}(\xi)}{2(\lambda+2\mu)\eta\xi}\begin{Bmatrix}e^{|\xi|h}\left\{(\lambda+\mu)(1+\Lambda|\xi|)+\frac{\tau^s}{2\mu}|\xi|\left[\lambda+2\mu+\frac{(\lambda+\mu)(\lambda+3\mu)}{\lambda+2\mu}\Lambda|\xi|\right]\right\}\\+e^{-|\xi|h}\left\{\lambda+3\mu-(\lambda+\mu)(\Lambda+2h)|\xi|+\frac{\tau^s}{2\mu}|\xi|\left[\lambda+2\mu-\frac{(\lambda+\mu)(\lambda+3\mu)}{\lambda+2\mu}\Lambda|\xi|+\frac{2(\lambda+\mu)^2}{\lambda+2\mu}\Lambda h\xi^2\right]\right\}\end{Bmatrix} \tag{4.11f}$$

4.2 Fundamental Solutions for Axisymmetric Problems

Consider a three-dimensional elastic layer of finite thickness t bonded to a rigid base, and subjected to axisymmetric vertical and tangential loading at a depth h below the free surface as shown in Figure 4.1(b). Similar to the case of plane problems, the corresponding solutions of elastic fields can be derived by dividing the elastic layer into two sub-domains. The sub-domain '1' corresponds to the region where $0 \le z \le h$ and the sub-domain '2' corresponds to the region where $h \le z \le t$. The general solutions of the sub-domain '1' are given by Eqs. (3.14a) to (3.14f) whereas the general solutions of the sub-domain '2' are also given by Eqs. (3.14a) to (3.14f) with the arbitrary functions A' to D' being replaced by E' to H' respectively. A superscript 'i' ($i = 1, 2$) is used hereafter to denote quantities associated with each sub-domain. The arbitrary functions A' to H' corresponding to each sub-domain can be obtained by solving the following boundary value problem.

$$\sigma_{zz}^{(1)}\Big|_{z=0}+\left[\frac{d\tau^{s}}{dr}\frac{du_{z}^{(1)}}{dr}+\tau^{s}\left(\frac{d^{2}u_{z}^{(1)}}{dr^{2}}+\frac{1}{r}\frac{du_{z}^{(1)}}{dr}\right)\right]_{z=0}=0 \tag{4.12a}$$

$$\sigma_{rz}^{(1)}\Big|_{z=0}+\left[\frac{d\tau^{s}}{dr}\left(1+\frac{u_{r}^{(1)}}{r}\right)+\kappa^{s}\left(\frac{d^{2}u_{r}^{(1)}}{dr^{2}}+\frac{1}{r}\frac{du_{r}^{(1)}}{dr}-\frac{u_{r}^{(1)}}{r^{2}}\right)\right]_{z=0}=0 \tag{4.12b}$$

$$\sigma_{zz}^{(1)}\Big|_{z=h^{-}}-\sigma_{zz}^{(2)}\Big|_{z=h^{+}}=p(r) \tag{4.12c}$$

$$\sigma_{rz}^{(1)}\Big|_{z=h^{-}}-\sigma_{rz}^{(2)}\Big|_{z=h^{+}}=q(r) \tag{4.12d}$$

$$u_{z}^{(1)}\Big|_{z=h^{-}}=u_{z}^{(2)}\Big|_{z=h^{+}} \tag{4.12e}$$

$$u_{r}^{(1)}\Big|_{z=h^{-}}=u_{r}^{(2)}\Big|_{z=h^{+}} \tag{4.12f}$$

$$u_{z}^{(2)}\Big|_{z=t}=0 \tag{4.12g}$$

$$u_{r}^{(2)}\Big|_{z=t}=0 \tag{4.12h}$$

where $p(r)$ and $q(r)$ denote the jump of the normal traction and shear traction across the plane $z=h$ due to the applied internal vertical and tangential loads respectively.

It should be noted that, similarly to the case of plane problems, the effect of surface stresses are only appeared in the equilibrium equations of the normal and shear stresses on the surface of an elastic layer (Eqs. (4.12a) and (4.12b)). The corresponding arbitrary functions A' to H' to determine the solutions of stresses and displacements can be obtained by solving a set of linear simultaneous equations constituted by applying Hankel integral transforms to Eqs. (4.12a) to (4.12h).

In this section, only the solutions for the case of surface vertical and tangential loading on an elastic layer of finite thickness are presented since it has many practical applications, such as indentation and other contact problems. Consider a three-dimensional elastic layer of finite thickness t bonded to a rigid base, and subjected to axisymmetric surface loads as shown in Figure 4.1(b) with h = 0. The corresponding solutions of stresses and displacements can be

determined from Eqs. (3.14a) to (3.14f) with the arbitrary functions A' to D' obtained by solving the following boundary value problem.

$$\sigma_{zz}\big|_{z=0}+\left[\frac{d\tau^s}{dr}\frac{du_z}{dr}+\tau^s\left(\frac{d^2u_z}{dr^2}+\frac{1}{r}\frac{du_z}{dr}\right)\right]_{z=0}=-p(r) \tag{4.13a}$$

$$\sigma_{rz}\big|_{z=0}+\left[\frac{d\tau^s}{dr}\left(1+\frac{u_r}{r}\right)+\kappa^s\left(\frac{d^2u_r}{dr^2}+\frac{1}{r}\frac{du_r}{dr}-\frac{u_r}{r^2}\right)\right]_{z=0}=-q(r) \tag{4.13b}$$

$$u_z\big|_{z=t}=0 \tag{4.13c}$$

$$u_r\big|_{z=t}=0 \tag{4.13d}$$

In view of Eqs. (3.14a) to (3.14f), the following set of linear simultaneous equations for determining the arbitrary functions can be constituted by applying Hankel integral transforms to Eqs. (4.13a) to (4.13d) together with the assumption that the residual surface stress is constant.

$$(\lambda+\mu)\left(1+\frac{\xi}{2\mu}\tau^s\right)\xi A'+\left(\mu+\xi\tau^s\right)B'-(\lambda+\mu)\left(1-\frac{\xi}{2\mu}\tau^s\right)\xi C'+\left(\mu-\xi\tau^s\right)D'=\frac{\overline{P}(\xi)}{2\xi^2} \tag{4.14a}$$

$$(\lambda+\mu)\left(1+\frac{\xi}{2\mu}\kappa^s\right)\xi A'-\left(\lambda+\frac{\lambda+\mu}{2\mu}\xi\kappa^s\right)B'+(\lambda+\mu)\left(1-\frac{\xi}{2\mu}\kappa^s\right)\xi C'+\left(\lambda-\frac{\lambda+\mu}{2\mu}\xi\kappa^s\right)D'=\frac{\overline{Q}(\xi)}{2\xi^2} \tag{4.14b}$$

$$\xi A'e^{-|\xi|t}-(1-\xi t)B'e^{-|\xi|t}-\xi C'e^{|\xi|t}-(1+\xi t)D'e^{|\xi|t}=0 \tag{4.14c}$$

$$\frac{\lambda+\mu}{\mu}\xi A'e^{-|\xi|t}+\left(2+\frac{\lambda+\mu}{\mu}\xi t\right)B'e^{-|\xi|t}+\frac{\lambda+\mu}{\mu}\xi C'e^{|\xi|t}-\left(2-\frac{\lambda+\mu}{\mu}\xi t\right)D'e^{|\xi|t}=0 \tag{4.14d}$$

where $p'(\xi)$ and $q'(\xi)$ are the Hankel transforms of $p(r)$ and $q(r)$ respectively and are given by

$$p'(\xi)=-\int_0^\infty rp(r)J_0(\xi r)dr \tag{4.15a}$$

$$q'(\xi)=-\int_0^\infty rq(r)J_1(\xi r)dr \tag{4.15b}$$

By solving the set of linear simultaneous equations displayed in Eqs. (4.12a) to (4.12d), the following solutions are obtained for the arbitrary functions A' to D'.

$$A' = \frac{1}{4}\frac{\left(A_{p0}+A_{p1}\right)}{I}\frac{p'(\xi)}{\xi^3} + \frac{1}{4}\frac{\left(A_{q0}+A_{q1}\right)}{I}\frac{q'(\xi)}{\xi^3}; \tag{4.16a}$$

$$B' = \frac{1}{4}\frac{\left(B_{p0}+B_{p1}\right)}{I}\frac{p'(\xi)}{\xi^3} + \frac{1}{4}\frac{\left(B_{q0}+B_{q1}\right)}{I}\frac{q'(\xi)}{\xi^3}; \tag{4.16b}$$

$$C' = \frac{1}{4}\frac{\left(C_{p0}+C_{p1}\right)}{I}\frac{p'(\xi)}{\xi^3} + \frac{1}{4}\frac{\left(C_{q0}+C_{q1}\right)}{I}\frac{q'(\xi)}{\xi^3}; \tag{4.16c}$$

$$D' = \frac{1}{4}\frac{\left(D_{p0}+D_{p1}\right)}{I}\frac{p'(\xi)}{\xi^3} + \frac{1}{4}\frac{\left(D_{q0}+D_{q1}\right)}{I}\frac{q'(\xi)}{\xi^3}; \tag{4.16d}$$

where

$$A_{p0} = \frac{\lambda\left(\lambda+3\mu\right)}{\left(\lambda+\mu\right)^2}e^{2\xi t} + 2t^2\xi^2 - \frac{2\lambda t\xi}{\lambda+\mu} + \frac{\lambda^2+3\lambda\mu+4\mu^2}{\left(\lambda+\mu\right)^2}; \tag{4.17a}$$

$$A_{p1} = \frac{\Lambda\xi}{\lambda+2\mu}\left[\left(\lambda+3\mu\right)\left(e^{2\xi t}-1\right) - 2t\xi\left(\lambda+\mu\right)\left(t\xi-1\right)\right]; \tag{4.17b}$$

$$A_{q0} = \frac{\mu\left(\lambda+3\mu\right)}{\left(\lambda+\mu\right)^2}e^{2\xi t} + 2t^2\xi^2 + \frac{2\mu t\xi}{\lambda+\mu} + \frac{\mu\left(3\lambda+5\mu\right)}{\left(\lambda+\mu\right)^2}; \tag{4.17c}$$

$$A_{q1} = \tau^s\left[\frac{\left(\lambda+3\mu\right)}{\left(\lambda+\mu\right)^2}\xi\left(e^{2\xi t}-1\right) - \frac{2t\xi^2}{\left(\lambda+\mu\right)} - \frac{t^2\xi^3}{\mu}\right]; \tag{4.17d}$$

$$B_{p0} = \frac{\lambda+3\mu}{\lambda+\mu}e^{2th} + \left(1-2t\xi\right); \tag{4.17e}$$

$$B_{p1} = \frac{\Lambda\xi}{\lambda+2\mu}\left[\left(\lambda+3\mu\right)\left(e^{2\xi t}-1\right) + 2t\xi\left(\lambda+\mu\right)\right]; \tag{4.17f}$$

$$B_{q0} = -\left[\frac{\lambda+3\mu}{\lambda+\mu}e^{2\xi t} + \left(1+2t\xi\right)\right]; \tag{4.17g}$$

$$B_{q1} = \tau^s\left[-\frac{\left(\lambda+3\mu\right)}{2\mu\left(\lambda+\mu\right)}\xi\left(e^{2\xi t}-1\right) + \frac{t\xi^2}{\mu}\right]; \tag{4.17h}$$

$$C_{p0} = -\left[\frac{\lambda\left(\lambda+3\mu\right)}{\left(\lambda+\mu\right)^2}e^{-2\xi t} + 2t^2\xi^2 + \frac{2\lambda t\xi}{\lambda+\mu} + \frac{\lambda^2+3\lambda\mu+4\mu^2}{\left(\lambda+\mu\right)^2}\right]; \tag{4.17i}$$

$$C_{p1} = -\frac{\Lambda\xi}{\lambda+2\mu}\left[\left(\lambda+3\mu\right)\left(1-e^{-2\xi t}\right) + 2t\xi\left(\lambda+\mu\right)\left(t\xi+1\right)\right]; \tag{4.17j}$$

$$C_{q0} = \frac{\mu\left(\lambda+3\mu\right)}{\left(\lambda+\mu\right)^2}e^{-2\xi t} + 2t^2\xi^2 - \frac{2\mu t\xi}{\lambda+\mu} + \frac{\mu\left(3\lambda+5\mu\right)}{\left(\lambda+\mu\right)^2}; \tag{4.17k}$$

$$C_{q1}=\tau^{s}\left[\frac{(\lambda+3\mu)}{(\lambda+\mu)^{2}}\xi\left(1-e^{-2\xi t}\right)-\frac{2t\xi^{2}}{(\lambda+\mu)}+\frac{t^{2}\xi^{3}}{\mu}\right]; \tag{4.17l}$$

$$D_{p0}=\frac{\lambda+3\mu}{\lambda+\mu}e^{-2\xi t}+(1+2t\xi); \tag{4.17m}$$

$$D_{p1}=\frac{\Lambda\xi}{\lambda+2\mu}\left[(\lambda+3\mu)\left(1-e^{-2\xi t}\right)+2t\xi(\lambda+\mu)\right]; \tag{4.17n}$$

$$D_{q0}=\frac{\lambda+3\mu}{\lambda+\mu}e^{-2t\xi}+(1-2t\xi); \tag{4.17o}$$

$$D_{q1}=\tau^{s}\left[\frac{(\lambda+3\mu)}{2\mu(\lambda+\mu)}\xi\left(1-e^{-2\xi t}\right)-\frac{t\xi^{2}}{\mu}\right]; \tag{4.17p}$$

The elastic field of a semi-infinite medium under surface loading can readily be obtained from the solutions in Eqs. (4.16a) and (4.16d), by taking the limit of $t\to\infty$. Note that the arbitrary functions C' and $D'\equiv 0$ to ensure the regularity of the solutions at infinity. In the case of the vertical load, the arbitrary functions A' and B' take the form,

$$A'=\frac{p'(\xi)}{2\eta'\xi^{3}}\frac{\lambda}{(\lambda+\mu)^{2}}\left[1+\frac{(\lambda+\mu)^{2}}{\lambda(\lambda+2\mu)}\Lambda\xi\right] \tag{4.18a}$$

$$B'=\frac{p'(\xi)}{2\eta'\xi^{2}(\lambda+\mu)}\left(1+\frac{\lambda+\mu}{\lambda+2\mu}\Lambda\xi\right) \tag{4.18b}$$

where

$$\eta'=(1+\Lambda\xi)+\frac{\tau^{s}}{2\mu}\xi\left[\frac{\lambda+2\mu}{\lambda+\mu}+\frac{\lambda+3\mu}{\lambda+2\mu}\Lambda\xi\right] \tag{4.19}$$

In the case of the horizontal loading,

$$A'=\frac{q'(\xi)}{2\eta'\xi^{3}}\frac{\mu}{(\lambda+\mu)^{2}}\left(1+\frac{\tau^{s}\xi}{\mu}\right) \tag{4.20a}$$

$$B'=-\frac{q'(\xi)}{2\eta'\xi^{2}(\lambda+\mu)}\left(1+\frac{\tau^{s}\xi}{2\mu}\right) \tag{4.20b}$$

4.3 Numerical Results

The complete fundamental solutions for displacements and stresses are given by Eqs. (3.10a) to (3.10e) with the solutions for arbitrary functions given by Eqs. (4.4a) to (4.4d) for the case of plane problems, whereas for the case of axisymmetric problems the solutions are given by Eqs. (3.14a) to (3.14f) with the solutions for arbitrary functions given by Eqs. (4.16a) to (4.16d). It is noted that the solutions for displacements and stresses for the case of plane problems given by Eqs. (3.10a) to (3.10e) can be reduced to semi-infinite integrals due to the even or odd behavior of the integrand with respect to ξ. A closed-form solution for both cases cannot be obtained due to the complexity of the integrands. Therefore, it is proposed to employ an accurate numerical scheme to evaluate these integrals. In this study, the integrals are evaluated by using globally adaptive numerical quadrature scheme based on 21-point Gauss-Kronrod rule (Piessens 1983). The surface elastic constants can be obtained by using atomistic simulations (Miller and Shenoy 2000, Shenoy 2005, Dingreville and Qu 2007). It is convenient to introduce the non-dimensional coordinates, $x_0 = x / \Lambda$ and $z_0 = z / \Lambda$ for the case of plane problems and $r_0 = r / \Lambda$ for the case of axisymmetric problems, in the numerical study. The numerical results in the present study correspond to the case of an elastic layer subjected to a distributed load applied over a strip $-a \le x \le a$. In addition, a hypothetical material with λ/μ = 2.226 and Λ = 1 nm are considered, and τ^s = 5 N/m is used to demonstrate the influence of residual surface stress.

4.3.1 Plane Problems

Figures 4.2 to 4.7 demonstrate the influence of surface elasticity and residual surface stress on the stress field of an elastic layer with very large value of t (a half-plane) under different loading cases. Figures 4.2 and 4.3 show the variation of non-dimensional stresses along the x-direction of a half-plane at various depths under a uniform vertical strip load of magnitude p_0 and a horizontal strip load of magnitude q_0 respectively applied at the surface. A non-

dimensional load width, $a_0 = a/\Lambda = 1$, is used in the numerical study. Only the solutions along the positive *x*-axis are presented due to the symmetry or anti-symmetry of the solutions about the z-axis.

The influence of surface elasticity on an identical problem was previously examined by Zhao and Rajapakse (2009) by ignoring the out-of-plane component of surface stresses. The dotted lines denote the classical elasticity solutions corresponding to zero surface stress (i.e. $\kappa^s = \tau^s = 0$) and the dash lines denote the solutions that neglect the out-of-plane component of surface stresses (Zhao and Rajapakse, 2009), which also disregard the influence of residual surface stress (τ^s) as previously discussed. It is evident from the figures that the influence of residual surface stress is more significant in the case of vertical strip load when compared to the horizontal strip load case. On the contrary, the influence of surface elasticity is more evident in the case of horizontal loading. It is also found that for the case of horizontal loading the influence of residual surface stress is negligible on horizontal normal and shear stresses but more evident on vertical normal stress, whereas in the case of vertical strip load all stress components depend significantly on the residual surface stress. This behavior can be described from the fact that the residual surface stress appears in the equilibrium equation of the vertical normal stress, Eq. (4.1a), but apparently vanishes in the shear stress equation, Eq. (4.1b), due to the assumption that the residual surface stress is constant. As expected, the influence of residual surface stress becomes significant only in a local region near the surface (i.e. $z_0 < 2.0$ for the vertical loading and $z_0 < 1.0$ for the horizontal loading) and would diminish with the distance from the free surface. In addition, the influence of the residual surface stress becomes negligible when $x_0/a_0 > 4$.

To investigate the influence of the surface material parameter Λ and the residual surface stress τ^s, the non-dimensional stress profiles along the x-direction of a half-plane due to a uniform vertical strip load p_0 are shown in

Figure 4.4 for different values of Λ and in Figure 4.5 for different values of τ^s respectively. Note that in Figures 4.4 and 4.5 stresses are calculated at z_0 = 0.1. In Figure 4.4, the non-dimensional stresses are presented for a hypothetical material with the surface material parameter Λ_1 being varied from 0 to 100Λ, whereas the residual surface stress parameter (τ^s) is unchanged. It can be seen from the figure that the free surface is stiffer with increasing values of Λ_1 resulting in the reduction of the stresses in the layer. The influence of the residual surface stress in Figure 4.5 shows a similar trend to Figure 4.4. It can be seen from Figure 4.5 that all bulk stress components decrease when residual surface stress (τ^s) increases from 0 to 100 N/m.

Figures 4.6 and 4.7 show the variation of non-dimensional stresses along the z-axis of an elastic half-plane subjected to an internal vertical strip load p_0 and an internal horizontal strip load q_0 over a region $2a$ (with a_0 = 1) at various depths. A non-dimensional quantity, $h_0 = h/\Lambda$, is used in the numerical analysis. Numerical results shown in Figures 4.6 and 4.7 indicate that the stresses increase when approaching the plane of applied loading. A discontinuity in both vertical and horizontal stresses is observed at the level where the vertical strip load is applied, whereas for the case of a horizontal strip load the shear stress is discontinuous at the loading plane. It is found that the residual surface stress shows more significant influence on the stress field in the case of a vertical strip loading, especially at points closer to the free surface (z_0 < 2) when compared to the case of a horizontal strip loading. It should be noted that the vertical stress in Figure 4.6 is no longer zero at the surface due to the presence of the residual surface stress.

To investigate the influence of layer thickness, the profiles of non-dimensional stresses in elastic layers of different thicknesses bonded to a rigid base and subjected to uniformly distributed vertical strip load p_0 and horizontal strip load q_0 over a region $2a$ (with a_0 = 1) at the free surface are presented in Figures 4.8 and 4.9 respectively. In this case, it is convenient to define the non-

dimensional layer thickness, $t_0 = t/\Lambda$. Once again, the residual surface stress shows more significant influence in the case of a vertical strip load when compared to a horizontal strip load. It is clear from these figures that the thickness of a layer has a significant influence on the stress field for both classical and non-classical cases. The stresses in both cases are mainly compressive and decrease with increasing layer thickness, except for the horizontal stresses under vertical strip load in Figure 4.8(b), in which tensile stresses are also noted for layers with finite thickness.

4.3.2 Axisymmetric Problems

Figures 4.10 to 4.13 demonstrate the influence of surface elasticity and residual surface stress on the displacement fields of an elastic layer with finite thickness under surface axisymmetric vertical and tangential loading. Since an arbitrary axisymmetric load can be approximated by the summation of axisymmetric polynomial functions, $p(r) = \sum_{m=1}^{\infty} \alpha_m r^{m-1}$, elastic fields of an elastic layer under arbitrary axisymmetric load can be obtained by superposition techniques. Figures 4.10 to 4.12 show the variation of normalized displacements along the z-direction of an elastic layer with finite thickness t_0/a_0 = 5 at r_0/a_0 = 0.5 under a parabolic vertical load $p(r) = p_0 r^2 / a^2$ and tangential load $q(r) = q_0 r^2 / a^2$, and a uniformly distributed vertical load of magnitude p_0 in a circular region of radius a respectively. The normalized displacements are presented for different values of a .i.e. $a_0 = a/\Lambda$ = 0.5, 1 and 1.5. Numerical results shown in Figures 4.10 and 4.11 indicate that, similar to the case of plane problems, the residual surface stress shows more significant influence for the case of vertically applied load whereas the surface elasticity shows more significant influence for the case of tangential load. It is also found that for the case of tangential loading the influence of residual surface stress is negligible on radial displacement but more evident on vertical displacement, whereas in the case of vertical loading both vertical and radial displacements depend

significantly on the residual surface stress. The normalized displacements under a uniformly distributed vertical load presented in Figure 4.12 show similar trends when compared to the displacements under a parabolic vertical load presented in Figure 4.10 except that the maximum negative value of radial displacement under uniform loading is located at the surface. It can be seen from the figures that an elastic layer becomes stiffer with the presence of surface stress. In addition, all displacements reduce to zero when approach the bottom of the layer. It is obvious from the figures that, with the consideration of surface stresses, normalized displacements show the size-dependent behavior and the influence of surface stresses becomes more significant when the radius of applied load decreases.

In Figure 4.13, normalized vertical displacements of an elastic layer with finite thickness t_0/a_0 = 5 subjected to a parabolic vertical load $p(r) = p_0 r^2 / a^2$ are presented at various depths with r_0 = 0 for different values of a .It is observed from the figure that the influence of surface stress decreases when a_0 increases and the solution will converge to the classical solution. Figure 4.14 demonstrate the influence of surface elasticity and residual surface stress on the stress field of an elastic layer with finite thickness t_0/a_0 = 5 under surface axisymmetric vertical loading. Figures 4.14 show the variation of non-dimensional stresses along the r-direction of a layer at various depths under a parabolic distributed vertical load $p(r) = p_0 r^2 / a^2$ in a circular region of radius a for $a_0 = a/\Lambda$ = 1. Similar to the case of plane problems, all stress components depend significantly on the surface stresses especially in the plane near the surface, i.e. z_0 < 2, In addition, the influence of the residual surface stress becomes negligible when r_0/a_0 > 4. Numerical results shown in Figures 4.2 to 4.14 confirm the fact that the influence of the surface stresses is significant in the analysis of the problems involving nanoscale layers or soft elastic materials and cannot be ignored.

4.4 Conclusion

A theoretical formulation based on the Gurtin-Murdoch continuum theory of elastic material surfaces is presented to study the elastic response of a nanoscale layer under two-dimensional and three-dimensional axisymmetric loading. An important aspect of the present study is the consideration of the out-of-plane term of the surface displacement gradient in the formulation. It is shown that the elastic field can be solved explicitly for the case of plane problems and axisymmetric problems by using Fourier and Hankel integral transform techniques respectively. The final solution is expressed in terms of semi-infinite integrals that can be accurately computed by employing a numerical quadrature scheme. It is found from the analytical solution and numerical results that the effects of the surface energy on the elastic field are characterized by both the characteristic length parameter Λ that is related to the surface and bulk elastic moduli and the residual surface stress (τ^s). As expected, the influence of the surface elasticity and the residual surface stress becomes more significant in the vicinity of the layer surface. Numerical results also indicate that increasing Λ and τ^s result in a decrease in bulk stresses and displacements. In addition, unlike in the classical elasticity approach, the behavior of the material becomes size-dependent when the surface stress is considered. The fundamental solutions presented in this study can be used to examine a variety of practical problems involving nanoscale/soft material systems and to develop boundary integral equations methods for such systems.

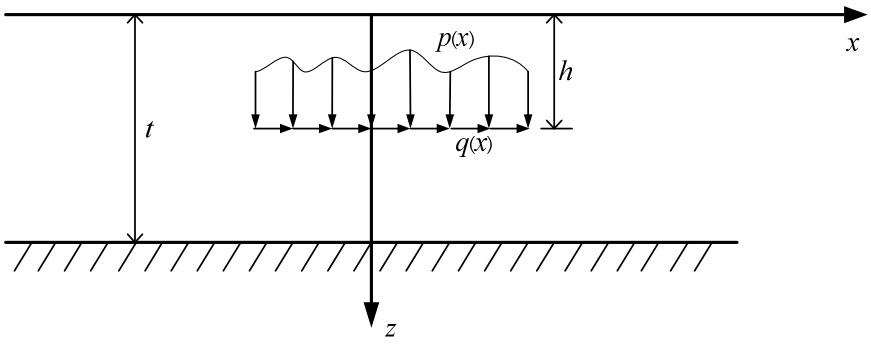

(a)

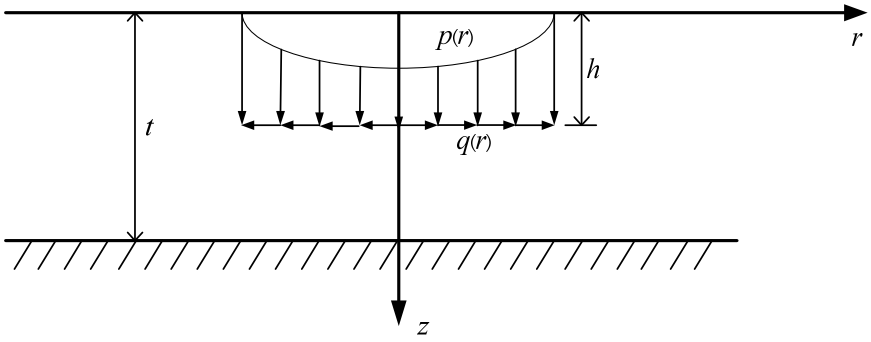

(b)

Figure 4.1 An isotropic elastic layer subjected to internal vertical and tangential loading: (a) plane strain case (b) axisymmetric case.

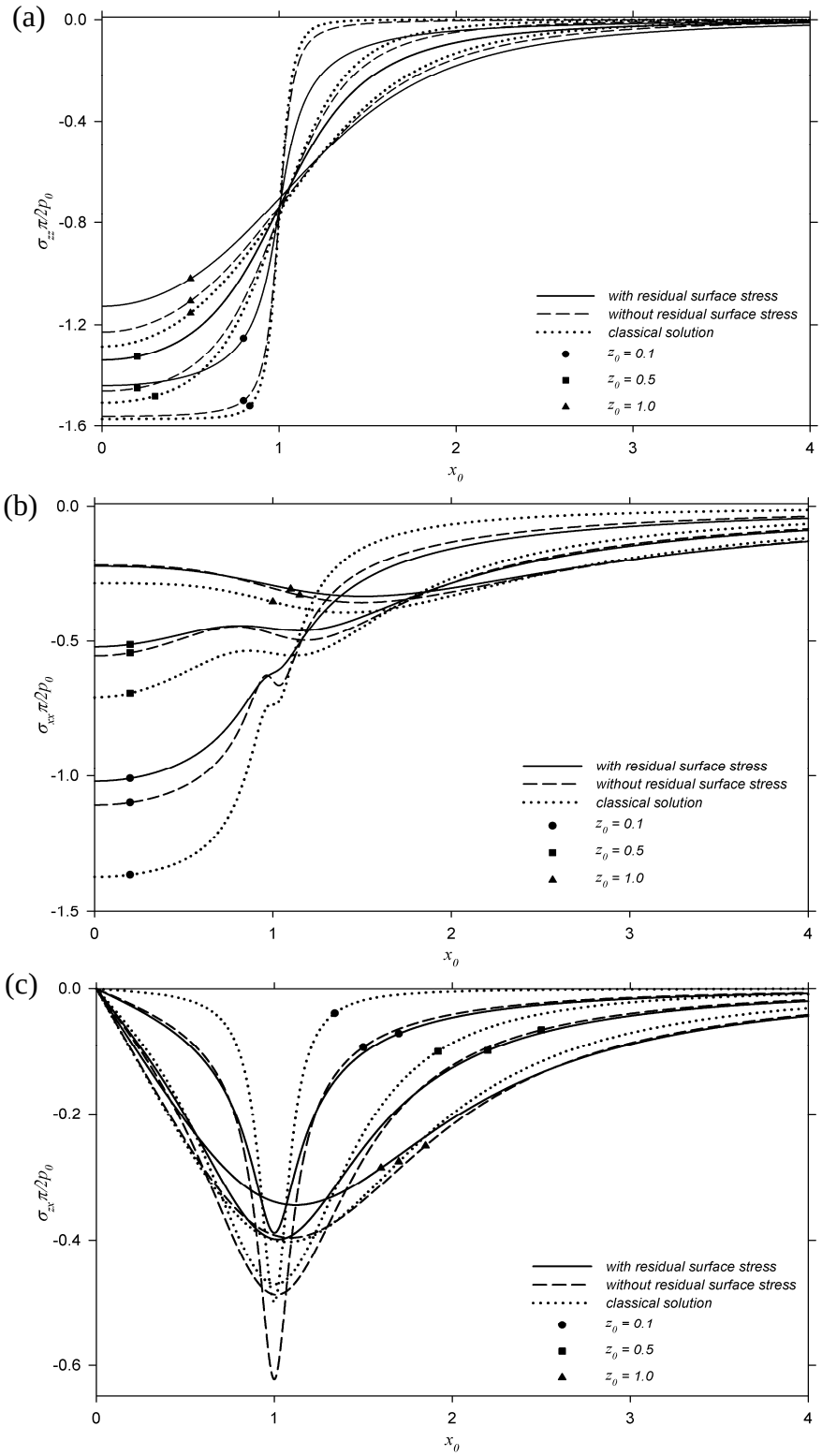

Figure 4.2 Non-dimensional stress profiles of a half-plane under vertical surface load: (a) Vertical stress (b) Horizontal stress (c) Shear stress.

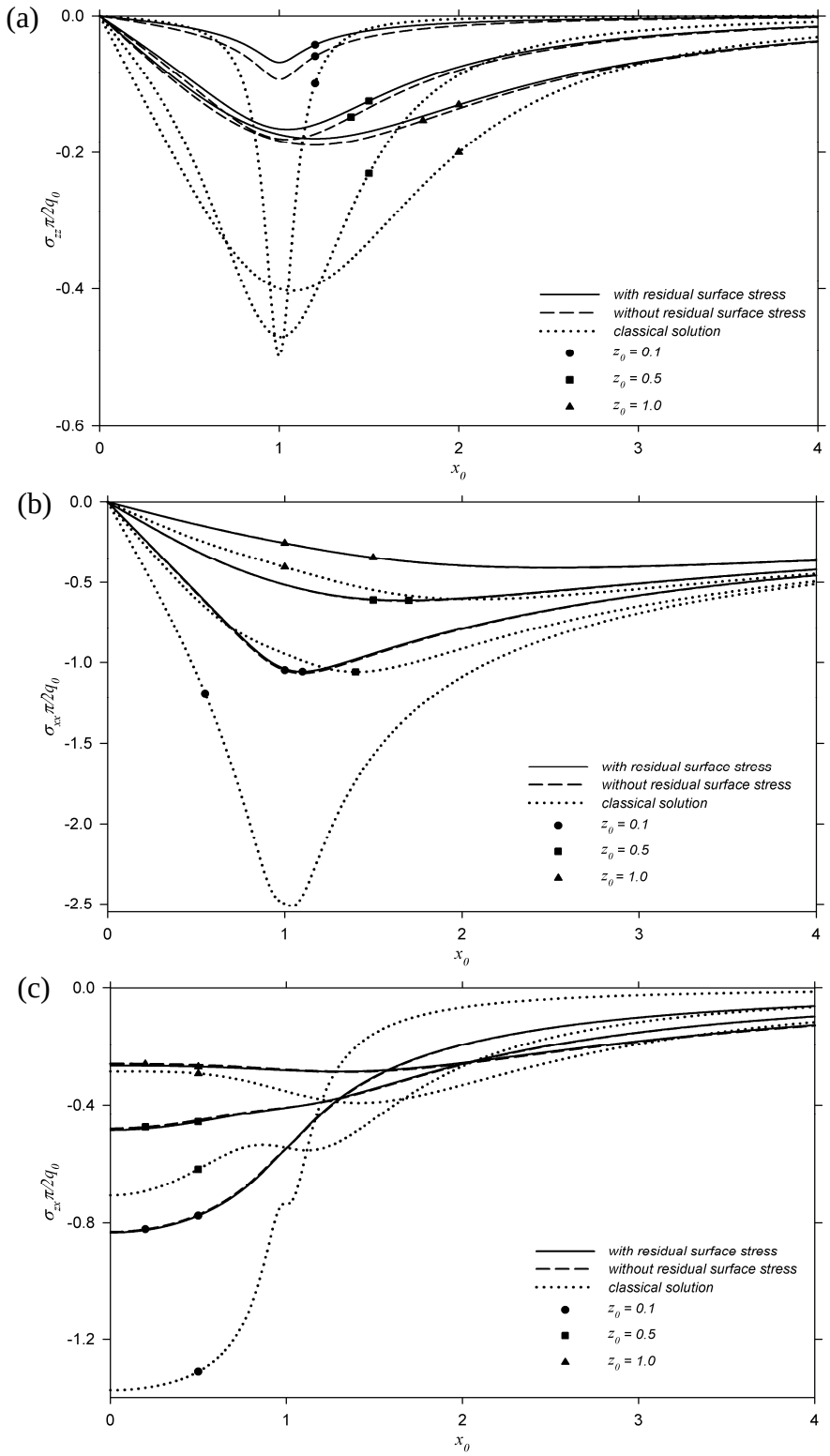

Figure 4.3 Non-dimensional stress profiles of a half-plane under horizontal surface load: (a) Vertical stress (b) Horizontal stress (c) Shear stress.

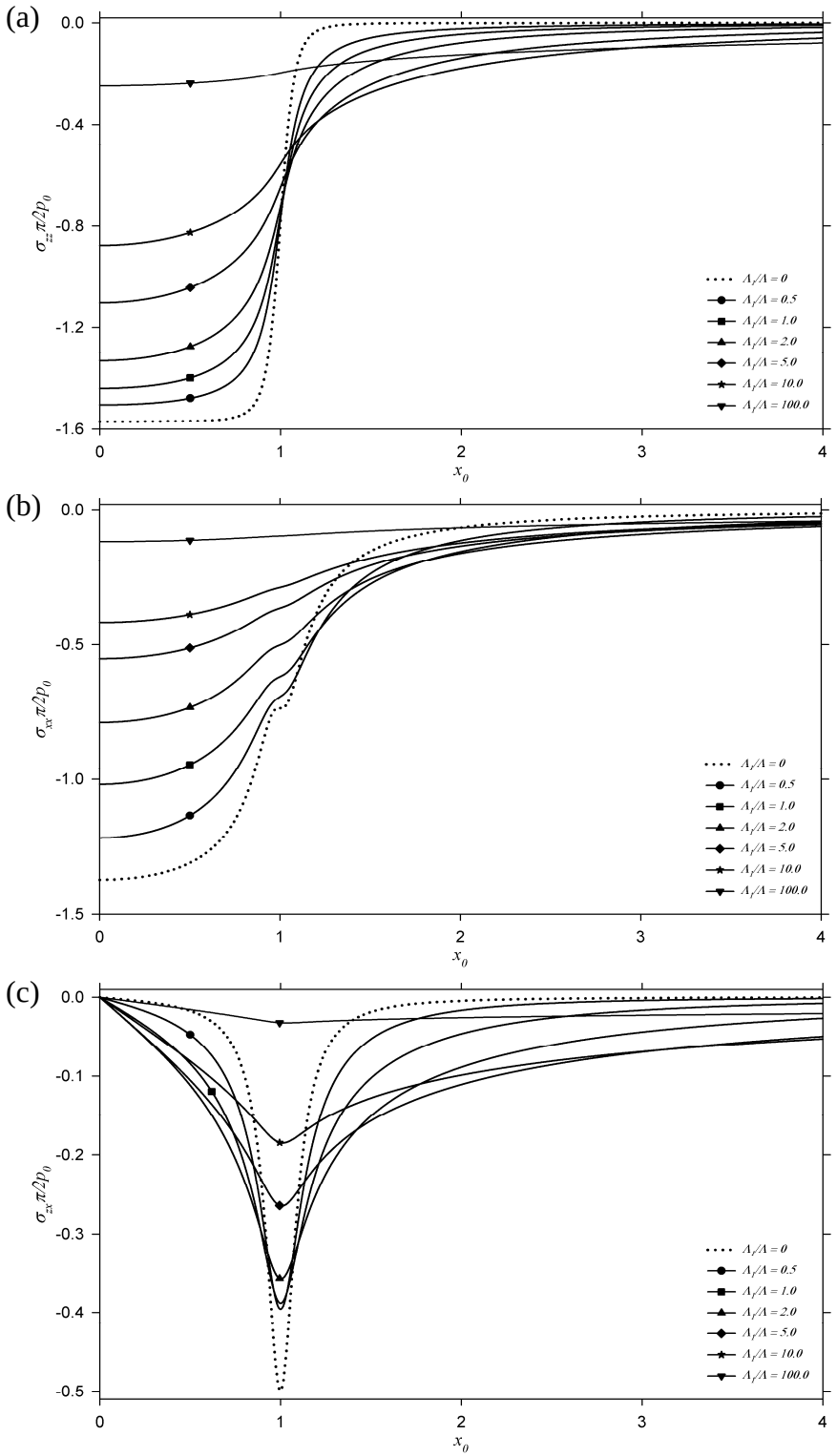

Figure 4.4 Non-dimensional stress profiles of a half-plane at z_0 = 0.1 under vertical surface load for different surface material constants (Λ): (a) Vertical stress (b) Horizontal stress (c) Shear stress.

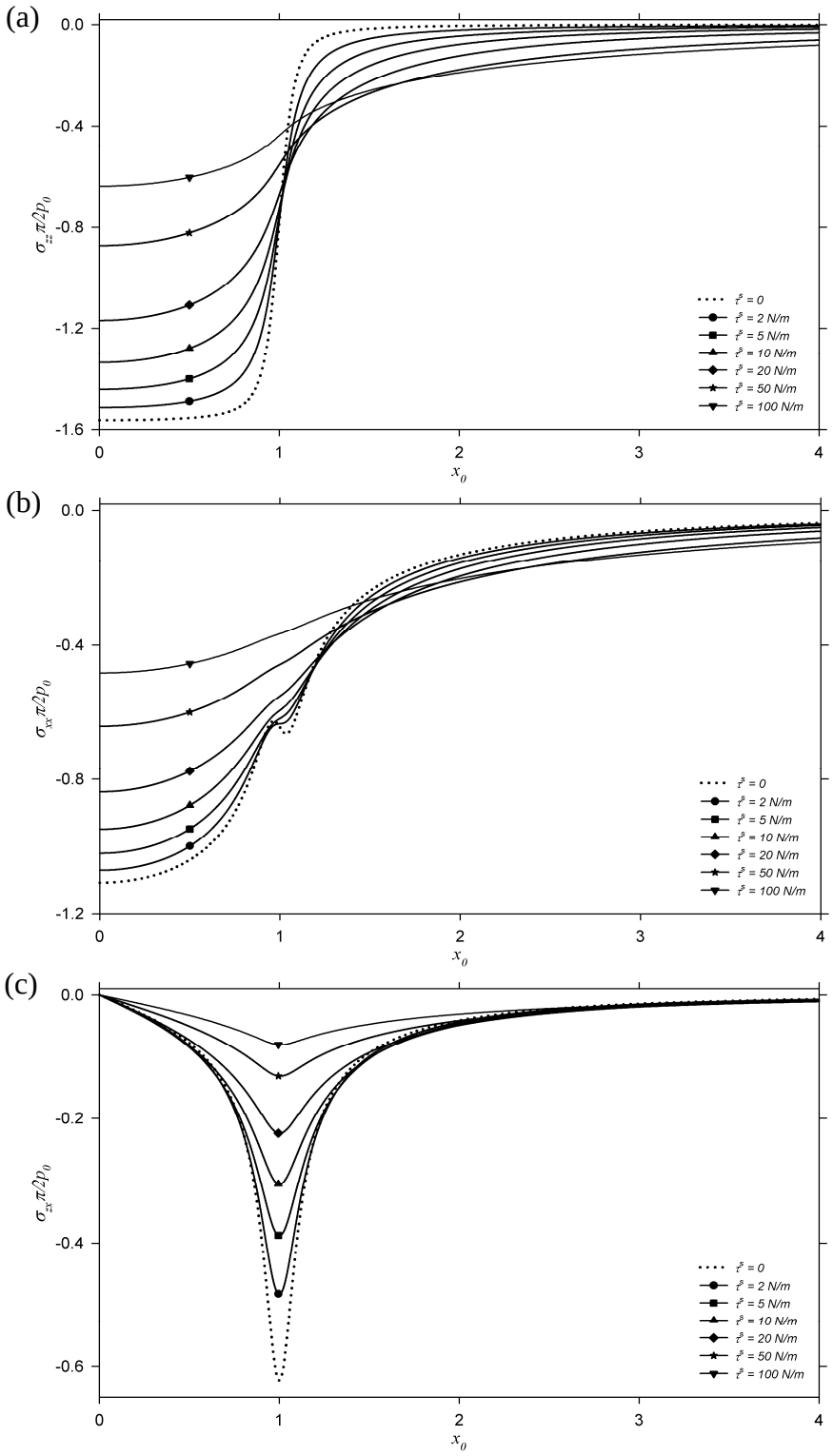

Figure 4.5 Non-dimensional stress profiles of a half-plane at z_0 = 0.1 under vertical surface load for different residual surface stresses (τ^s): (a) Vertical stress (b) Horizontal stress (c) Shear stress.

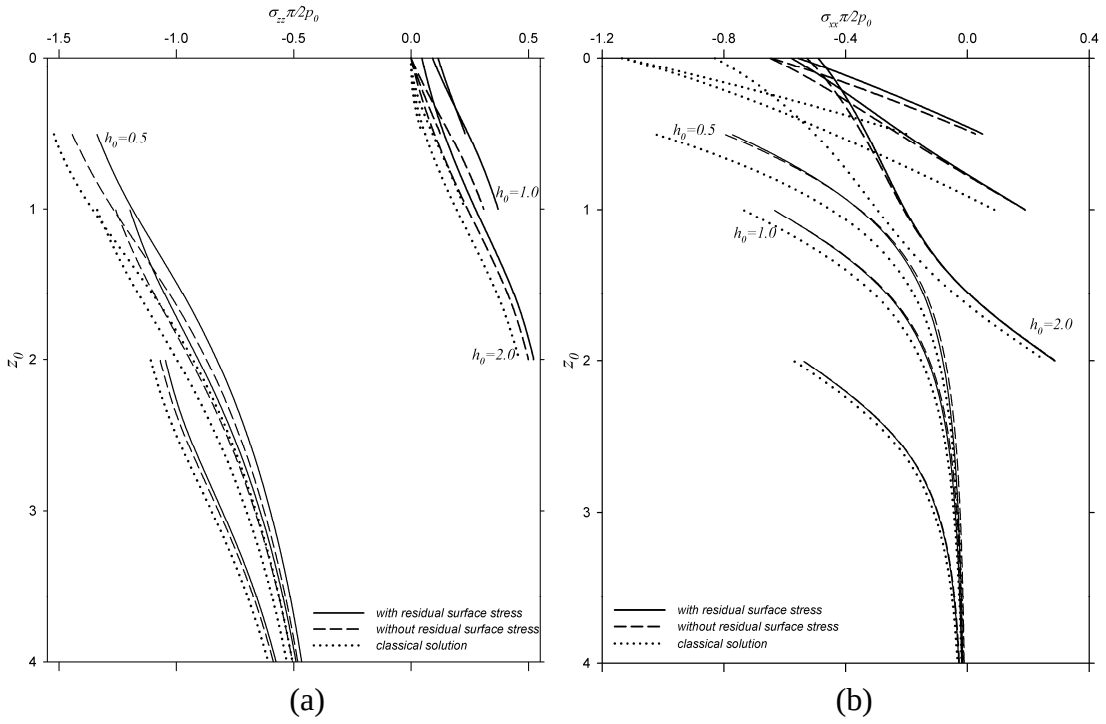

Figure 4.6 Non-dimensional stress profiles along the z-axis of a half-plane under internal vertical load: (a) Vertical stress (b) Horizontal stress.

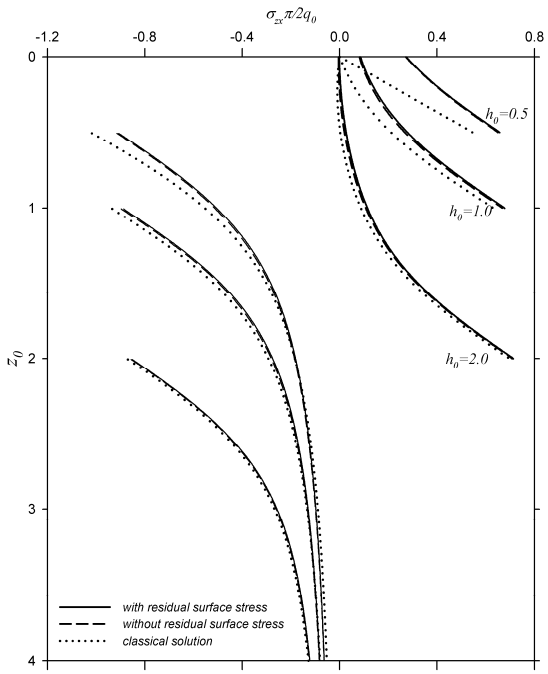

Figure 4.7 Non-dimensional shear stress profiles along the z-axis of a half-plane under internal horizontal load.

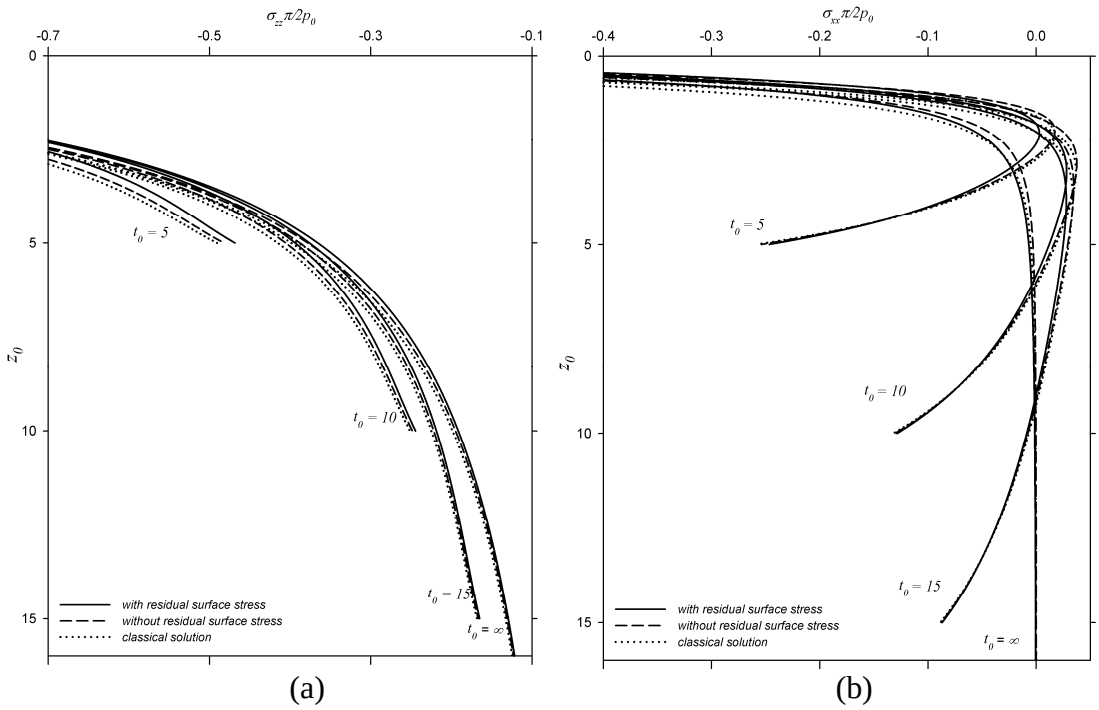

Figure 4.8 Non-dimensional stress profiles along the z-axis of a finite thickness layer under vertical surface load: (a) Vertical stress (b) Horizontal stress.

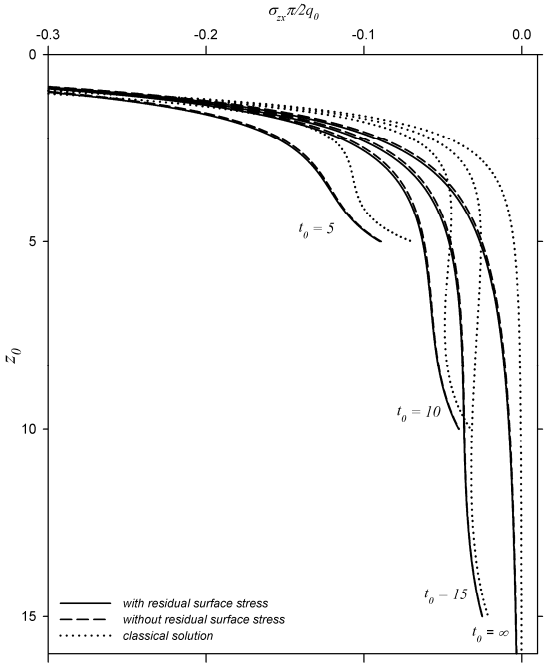

Figure 4.9 Non-dimensional shear stress along the z-axis of a finite thickness layer under horizontal surface load.

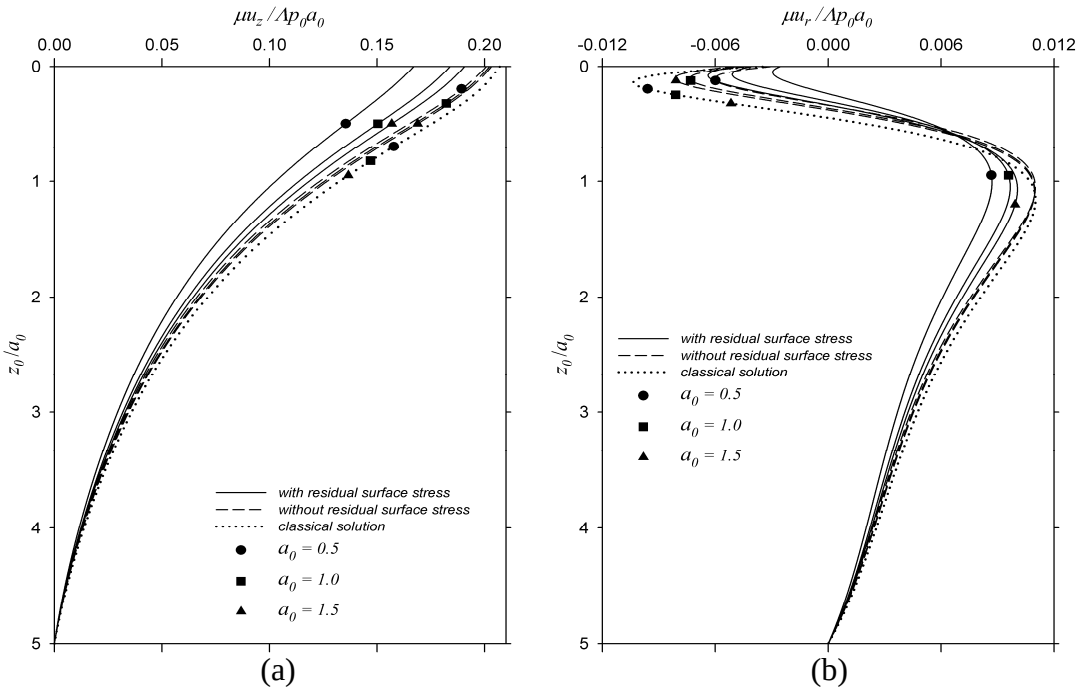

Figure 4.10 Normalized displacement profiles at r_0/a_0 = 0.5 of a layer with finite thickness t_0/a_0 = 5 under parabolic vertical load at the surface: (a) Vertical displacement (b) Radial displacement.

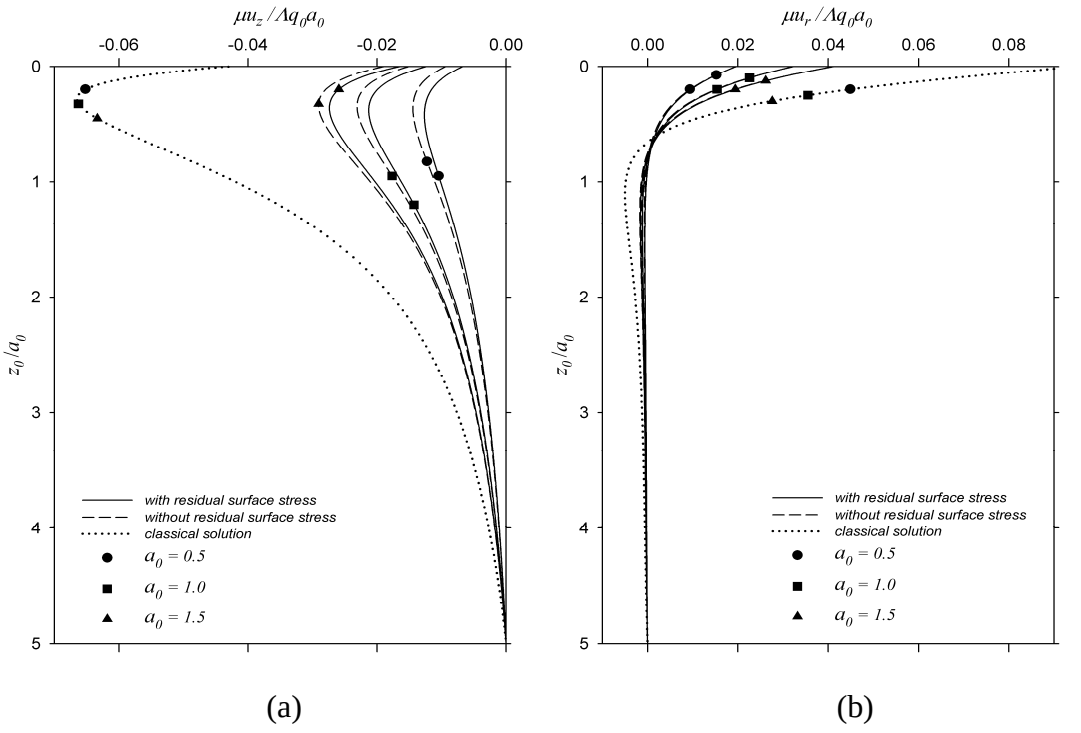

Figure 4.11 Normalized displacement profiles at r_0/a_0 = 0.5 of a layer with finite thickness t_0/a_0 = 5 under parabolic tangential load at the surface: (a) Vertical displacement (b) Radial displacement.

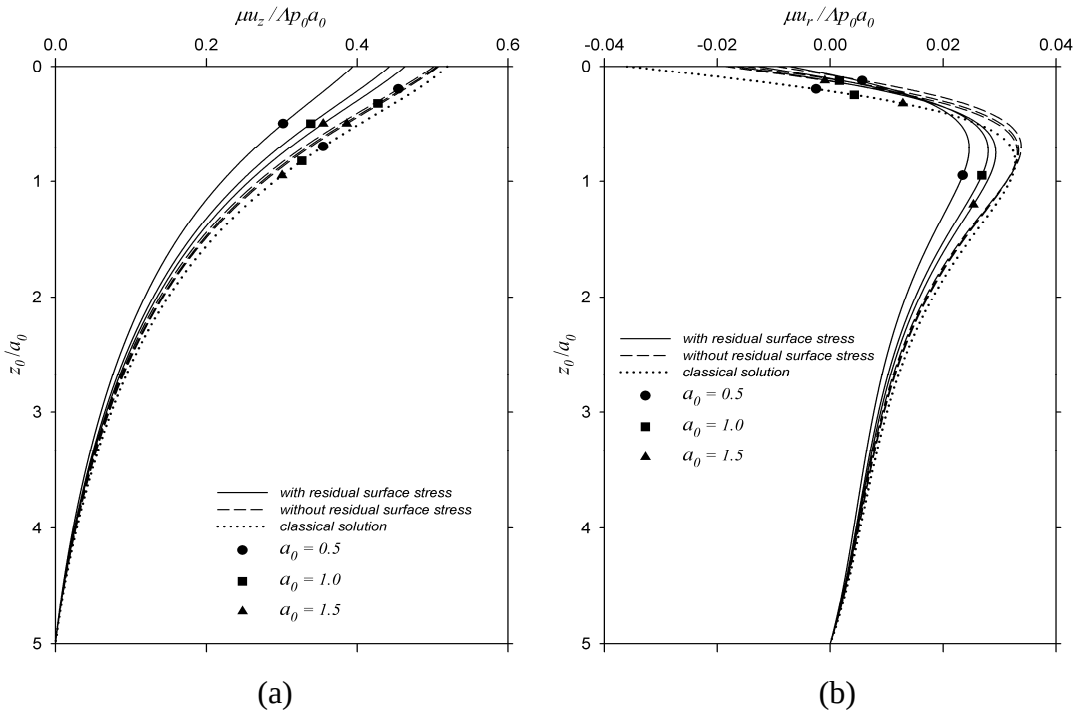

Figure 4.12 Normalized displacement profiles at r_0/a_0 = 0.5 of a layer with finite thickness t_0/a_0 = 5 under uniformly distributed vertical load at the surface: (a) Vertical displacement (b) Radial displacement.

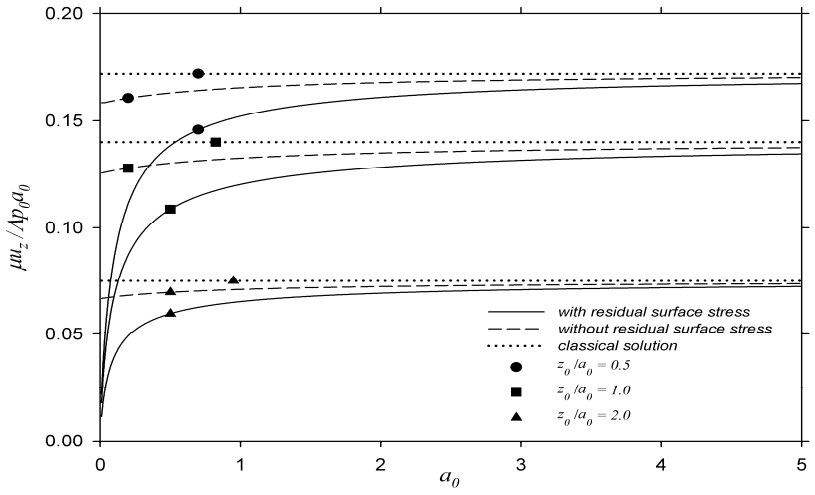

Figure 4.13 Normalized vertical displacement at r_0 = 0 of a layer with finite thickness t_0/a_0 = 5 under parabolic vertical load at the surface.

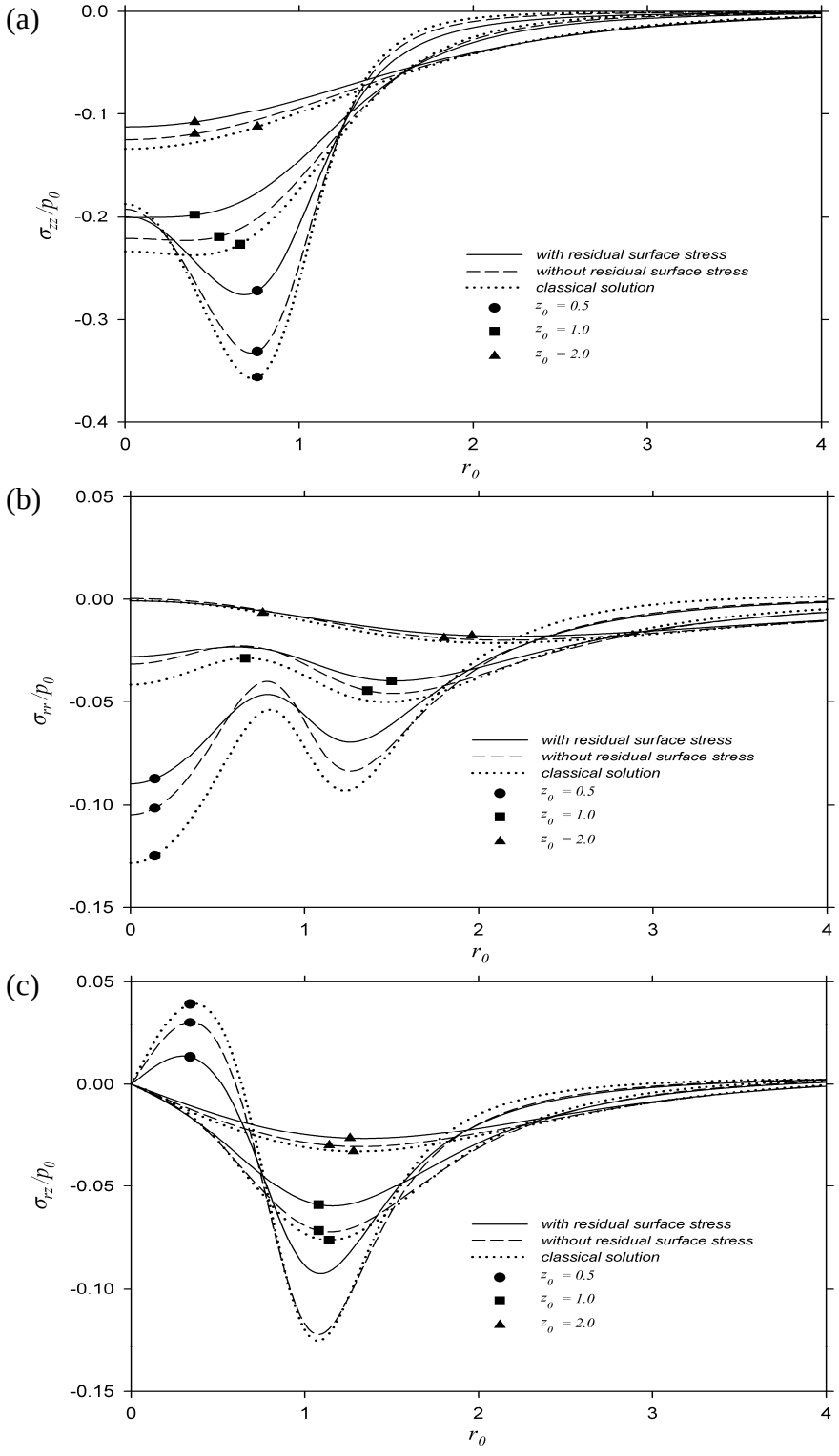

Figure 4.14 Non-dimensional stress profiles of a layer with finite thickness t_0/a_0 = 5 under parabolic vertical load at the surface: (a) Vertical stress (b) Radial stress (c) Shear stress.

CHAPTER V

DISLOCATIONS AND CRACK IN ELASTIC MEDIUM

In this chapter, the fundamental solutions of an isotropic elastic medium involving defects, i.e. dislocations and crack, are derived with the consideration of the influence of surface stresses by employing Gurtin-Murdoch continuum theory of elastic material surfaces. The boundary value problems corresponding to shear (gliding edge) and opening (climbing edge) dislocations in an elastic half-plane are solved by using Fourier integral transform technique. In addition, a penny-shaped crack in an infinite elastic medium is investigated for mode-I crack by the application of Hankel integral transform technique. Selected numerical results are presented to portray the influence of surface stresses on these problems.

5.1 Dislocations in Semi-Infinite Elastic Medium

Consider an elastic half-plane with shear (gliding edge) and opening (climbing edge) dislocations located at a depth h below the free surface as shown in Figure 5.1. The solution to this problem can be derived by considering the half-plane as a two sub-domain. The sub-domain '1' corresponds to the region where $0 \le z \le h$ and the sub-domain '2' corresponds to the region where $h \le z < \infty$. The general solutions of sub-domain '1' are given by Eqs. (3.10a) to (3.10e) whereas the general solution of sub-domain '2' are also given by Eqs. (3.10a) to (3.10e) with C and $D \equiv 0$ to satisfy the regularity conditions at infinity, and the constants A and B being replaced by E and F respectively. A superscript 'i' ($i = 1, 2$) is used hereafter to denote the quantities associated with each sub-domain. The arbitrary functions A to F corresponding to each sub-domain can be obtained by solving the following boundary value problem.

$$\sigma_{zz}^{(1)}\Big|_{z=0}+\left(\frac{d\tau^s}{dx}\frac{du_z^{(1)}}{dx}+\tau^s\frac{d^2u_z^{(1)}}{dx^2}\right)_{z=0}=0 \tag{5.1a}$$

$$\sigma_{zx}^{(1)}\Big|_{z=0}+\left(\frac{d\tau^s}{dx}+\kappa^s\frac{d^2u_x^{(1)}}{dx^2}\right)_{z=0}=0 \tag{5.1b}$$

$$\sigma_{zz}^{(1)}\Big|_{z=h^-}=\sigma_{zz}^{(2)}\Big|_{z=h^+} \tag{5.1c}$$

$$\sigma_{zx}^{(1)}\Big|_{z=h^-}=\sigma_{zx}^{(2)}\Big|_{z=h^+} \tag{5.1d}$$

$$u_z^{(2)}\Big|_{z=h^+}-u_z^{(1)}\Big|_{z=h^-}=b_zH(-x) \tag{5.1e}$$

$$u_x^{(2)}\Big|_{z=h^+}-u_x^{(1)}\Big|_{z=h^-}=b_xH(-x) \tag{5.1f}$$

where $b_\alpha(\alpha=x,z)$ denotes the magnitude of the dislocations, which are the components of the Burger's vector; and $H(x)$ denotes the unit step function.

It should be noted that both Eqs. (5.1a) and (5.1b) are non-classical boundary conditions obtained from Eqs. (3.4a) and (3.4b). Application of Fourier integral transforms to Eqs. (5.1a) to (5.1f) together with the assumption that residual surface stress is constant and the substitution of Eqs. (3.10a) to (3.10e) yield,

$$\left(1+\frac{|\xi|}{2\mu}\tau^s\right)A+\frac{\tau^s}{2(\lambda+\mu)}(B+D)+\left(1-\frac{|\xi|}{2\mu}\tau^s\right)C=0 \tag{5.2a}$$

$$\left(1+\frac{|\xi|}{2\mu}\kappa^s\right)|\xi|A-\left(1+\frac{(\lambda+2\mu)}{2\mu(\lambda+\mu)}|\xi|\kappa^s\right)B-\left(1-\frac{|\xi|}{2\mu}\kappa^s\right)|\xi|C-\left(1-\frac{(\lambda+2\mu)}{2\mu(\lambda+\mu)}|\xi|\kappa^s\right)D=0 \tag{5.2b}$$

$$(A-E)e^{-|\xi|h}+(B-F)he^{-|\xi|h}+Ce^{|\xi|h}+Dhe^{|\xi|h}=0 \tag{5.2c}$$

$$|\xi|(A-E)e^{-|\xi|h}-(1-|\xi|h)(B-F)e^{-|\xi|h}-|\xi|Ce^{|\xi|h}-(1+|\xi|h)De^{|\xi|h}=0 \tag{5.2d}$$

$$|\xi|(A-E)e^{-|\xi|h}+\left(|\xi|h+\frac{\mu}{\lambda+\mu}\right)(B-F)e^{-|\xi|h}-|\xi|Ce^{|\xi|h}-\left(|\xi|h-\frac{\mu}{\lambda+\mu}\right)De^{|\xi|h}=\frac{2\mu b_z i}{\xi} \tag{5.2e}$$

$$|\xi|(A-E)e^{-|\xi|h}+\left(|\xi|h-\frac{\lambda+2\mu}{\lambda+\mu}\right)(B-F)e^{-|\xi|h}+|\xi|Ce^{|\xi|h}+\left(|\xi|h+\frac{\lambda+2\mu}{\lambda+\mu}\right)De^{|\xi|h}=\frac{2\mu b_x}{|\xi|} \tag{5.2f}$$

The following solutions are obtained for the arbitrary functions A, B, C, D, E and F by solving a set of linear simultaneous equations presented above.

5.1.1 Shear Dislocation

The arbitrary functions corresponding to the shear dislocation of intensity b_x are

$$A=\frac{b_x\mu(\lambda+\mu)e^{-|\xi|h}}{|\xi|\eta(\lambda+2\mu)}\left[(1+|\xi|\Lambda)h-\frac{\tau^s}{2\mu}|\xi|\left(\frac{\lambda+2\mu}{\lambda+\mu}h+\frac{2\mu}{\lambda+\mu}\Lambda+\frac{\lambda+\mu}{\lambda+2\mu}|\xi|h\Lambda\right)\right] \tag{5.3a}$$

$$B=\frac{b_x\mu(\lambda+\mu)e^{-|\xi|h}}{|\xi|\eta(\lambda+2\mu)}\left[-1+2|\xi|h+|\xi|\Lambda-\frac{\tau^s}{2\mu}|\xi|\left(\frac{\lambda+2\mu}{\lambda+\mu}-\frac{\lambda+\mu}{\lambda+2\mu}|\xi|\Lambda(1-2|\xi|h)\right)\right] \tag{5.3b}$$

$$C=-\frac{hb_x\mu(\lambda+\mu)e^{-|\xi|h}}{|\xi|(\lambda+2\mu)} \tag{5.3c}$$

$$D=\frac{b_x\mu(\lambda+\mu)e^{-|\xi|h}}{|\xi|(\lambda+2\mu)} \tag{5.3d}$$

$$E=-\frac{b_x\mu(\lambda+\mu)}{|\xi|\eta(\lambda+2\mu)}\left\{\begin{array}{l}e^{|\xi|h}\left[(1+|\xi|\Lambda)h+\frac{\tau^s}{2\mu}|\xi|\left(\frac{\lambda+2\mu}{\lambda+\mu}h+\frac{\lambda+3\mu}{\lambda+2\mu}|\xi|h\Lambda\right)\right]\\-e^{-|\xi|h}\left[(1+|\xi|\Lambda)h-\frac{\tau^s}{2\mu}|\xi|\left(\frac{\lambda+2\mu}{\lambda+\mu}h+\frac{2\mu}{\lambda+\mu}\Lambda+\frac{\lambda+\mu}{\lambda+2\mu}|\xi|h\Lambda\right)\right]\end{array}\right\} \tag{5.3e}$$

$$F=\frac{b_x\mu(\lambda+\mu)}{|\xi|\eta(\lambda+2\mu)}\left\{\begin{array}{l}e^{|\xi|h}\left[1+|\xi|\Lambda+\frac{\tau^s}{2\mu}|\xi|\left(\frac{\lambda+2\mu}{\lambda+\mu}+\frac{\lambda+3\mu}{\lambda+2\mu}|\xi|\Lambda\right)\right]\\+e^{-|\xi|h}\left[-1+2|\xi|h+|\xi|\Lambda-\frac{\tau^s}{2\mu}|\xi|\left(\frac{\lambda+2\mu}{\lambda+\mu}-\frac{\lambda+\mu}{\lambda+2\mu}|\xi|\Lambda(1-2|\xi|h)\right)\right]\end{array}\right\} \tag{5.3f}$$

where η is given by Eq.(4.8)

5.1.2 Opening Dislocation

The arbitrary functions corresponding to the opening dislocation of intensity b_z are

$$A=\frac{ib_z\mu(\lambda+\mu)e^{-|\xi|h}}{\xi|\xi|\eta(\lambda+2\mu)}\left[(1+|\xi|\Lambda)(1+|\xi|h)-\frac{\tau^s}{2\mu}|\xi|\left(\frac{\lambda+2\mu}{\lambda+\mu}(1+|\xi|h)+\frac{\lambda^2+4\lambda\mu+5\mu^2}{(\lambda+\mu)(\lambda+2\mu)}|\xi|\Lambda+\frac{\lambda+\mu}{\lambda+2\mu}\xi^2h\Lambda\right)\right] \tag{5.4a}$$

$$B=\frac{ib_z\mu(\lambda+\mu)e^{-|\xi|h}}{\xi\eta(\lambda+2\mu)}\left[1+2|\xi|h+|\xi|\Lambda-\frac{\tau^s}{2\mu}|\xi|\left(\frac{\lambda+2\mu}{\lambda+\mu}+\frac{\lambda+\mu}{\lambda+2\mu}|\xi|\Lambda(1+2|\xi|h)\right)\right] \tag{5.4b}$$

$$C=-\frac{i(1+|\xi|h)b_z\mu(\lambda+\mu)e^{-|\xi|h}}{\xi|\xi|(\lambda+2\mu)} \tag{5.4c}$$

$$D=\frac{ib_z\mu(\lambda+\mu)e^{-|\xi|h}}{\xi(\lambda+2\mu)} \tag{5.4d}$$

$$E=\frac{ib_z\mu(\lambda+\mu)}{\xi|\xi|\eta(\lambda+2\mu)}\left\{\begin{array}{l}(-1+|\xi|h)e^{|\xi|h}\left[1+|\xi|\Lambda+\frac{\tau^s}{2\mu}|\xi|\left(\frac{\lambda+2\mu}{\lambda+\mu}+\frac{\lambda+3\mu}{\lambda+2\mu}|\xi|\Lambda\right)\right]+\\ e^{-|\xi|h}\left[(1+|\xi|\Lambda)(1+|\xi|h)-\frac{\tau^s}{2\mu}|\xi|\left(\frac{\lambda+2\mu}{\lambda+\mu}(1+|\xi|h)+\frac{\lambda^2+4\lambda\mu+5\mu^2}{(\lambda+\mu)(\lambda+2\mu)}|\xi|\Lambda+\frac{\lambda+\mu}{\lambda+2\mu}\xi^2h\Lambda\right)\right]\end{array}\right\} \tag{5.4e}$$

$$F=-\frac{ib_z\mu(\lambda+\mu)}{\xi\eta(\lambda+2\mu)}\left\{\begin{array}{l}e^{|\xi|h}\left[1+|\xi|\Lambda+\frac{\tau^s}{2\mu}|\xi|\left(\frac{\lambda+2\mu}{\lambda+\mu}+\frac{\lambda+3\mu}{\lambda+2\mu}|\xi|\Lambda\right)\right]\\ -e^{-|\xi|h}\left[1+2|\xi|h+|\xi|\Lambda-\frac{\tau^s}{2\mu}|\xi|\left(\frac{\lambda+2\mu}{\lambda+\mu}+\frac{\lambda+\mu}{\lambda+2\mu}|\xi|\Lambda(1+2|\xi|h)\right)\right]\end{array}\right\} \tag{5.4f}$$

From the above solutions, it is evident that the elastic field of the half-plane is influenced by both surface material constant κ^s (or Λ) and residual surface stress τ^s. Note that Λ and τ^s vanish in the absence of surface stresses and the above solutions reduce to the classical elasticity solutions.

5.1.3 Numerical Results

The complete fundamental solutions for displacements and stresses corresponding to shear and opening dislocations are given by Eqs. (3.10a) to (3.10e) with the solutions for arbitrary functions, *A* to *F*, given by Eqs. (5.3a) to (5.3f) and (5.4a) to (5.4f). The solutions for displacements and stresses given by Eqs. (3.10a) to (3.10e) can be reduced to semi-infinite integrals due to the even or odd behavior of the integrand with respect to ξ. Since, closed-form solutions cannot be obtained similar to the case of internally loaded elastic layer in Chapter 4, the numerical quadrature scheme based on 21-point Gauss-Kronrod rule (Piessens 1983) is then employed. It is convenient to introduce the following non-dimensional quantities in the numerical study: $x_0 = x/\Lambda$; $z_0 = z/\Lambda$; $h_0 = h/\Lambda$. In addition, the material properties of λ/μ = 2.226 (e.g. Aluminum (Dingreville and Qu 2007)), and Λ = 0.15288 nm for Al [1 1 1] surface (Miller and Shenoy 2000) are used in the present study, and τ^s = 5 N/m is used to demonstrate the influence of residual surface stress.

Figures 5.2 and 5.3 show the non-dimensional stresses along the x-direction of a half-plane at various depths due to a shear dislocation of magnitude b_x and an opening dislocation of magnitude b_z ,respectively, at the plane h_0 = 1.0 . Only the solutions along the positive x-axis are plotted due to the symmetry or anti-symmetry of the solutions about the z-axis. For the shear dislocation, vertical and horizontal normal stresses are symmetric whereas shear stress is anti-symmetric about the z-axis. For the case of opening dislocation, vertical and horizontal stresses are anti-symmetric, while shear stress is symmetric, about the z-axis. Note that the dotted lines in Figures 5.2 and 5.3 denote the classical elasticity solutions corresponding to zero surface stress (i.e. $\kappa^s = \tau^s = 0$) and the dash lines denote the solutions that neglect the out-of-plane component of surface stresses. It is evident from both figures that some components of the bulk stress field are significantly influenced by the presence of surface stresses. Horizontal normal stresses of the bulk material show more influence of surface elasticity Λ when compared to vertical and shear stresses. In addition, vertical normal stresses of the bulk material show more influence of residual surface stress τ^s when compared to horizontal and shear stresses. This observation is true for both types of dislocations. It should be noted that at z_0 = 1.0 horizontal normal stress and shear stress are infinite at the dislocation core under a shear dislocation, whereas for an opening dislocation, horizontal and vertical normal stresses are infinite at the dislocation core. For both types of dislocations, the influence of surface elasticity on bulk shear stress is negligible especially at points closer to the dislocation core whereas the residual surface stress show more significant influence on bulk shear stress in the vicinity of dislocation core (e.g. when $x_0 < 3$). On the other hand, the influence of residual surface stress on bulk horizontal normal stress is negligible especially at points closer to the dislocation core whereas the horizontal normal stress for both types of dislocation shows more significant influence of surface elasticity in the vicinity of the dislocation core (e.g. when $x_0 < 3$) especially in the domain above the slip

plane. In addition, the influence of surface elasticity and residual surface stress on the vertical normal stress show more significant at points closer to the dislocation core (e.g. when x_0 < 3) except in the case of shear dislocation, the influence of surface elasticity is negligible. It is obvious that the region above the slip plane has the most influence of surface stress due to its proximity to the free surface. In all cases, the stresses become quite negligible for x_0 > 5.

To investigate the influence of the depth of dislocation plane; surface material parameter Λ and residual surface stress τ^s, the non-dimensional stress field along the x-direction due to an opening dislocation of magnitude b_z are presented in Figure 5.4 for different depths of dislocation plane, in Figure 5.5 for different values of Λ and in Figure 5.6 for different values of τ^s respectively. Note that in Figure 5.4 stresses are calculated at z_0 = 1.0. From Figure 5.4, it is clear that the depth of dislocation has a significant influence on the stress field and the stresses increase as the dislocation plane approaches z_0 = 1.0. Furthermore, the influence of surface elasticity and residual surface stress are more significant when the slip plane is near the free surface. As in Figures 5.2 and 5.3, horizontal normal stress shows the highest influence of surface elasticity whereas vertical normal stress shows the highest influence of residual surface stress. In Figure 5.5 the non-dimensional stresses are presented for a hypothetical material with the surface material parameter Λ_1 being varied from 0 to 1000 Λ (where Λ = 0.15288 nm for aluminum), whereas the residual surface stress parameter (τ^s) is unchanged. On the other hand, the non-dimensional stresses displayed in Figure 5.6 are presented for a hypothetical material with the residual surface stress parameter τ^s being varied from 0 to 1000 N/m, whereas the surface material parameter is unchanged. Note that in Figures 5.5 and 5.6 stresses are calculated at z_0 = 0.1 to maximize the influence of surface stress. As expected, the influence of surface stresses on the bulk stress components becomes more significant with increasing Λ_1 and τ^s (i.e. when the surface becomes more rigid). In addition, the stress field shows an asymptotic solution

with respect to Λ_1 and τ^s, which is reached when $\Lambda_1 > 100\,\Lambda$ and $\tau^s > 500$ N/m, respectively. Another important observation is that horizontal normal stress near the free surface shown in Figures 5.5 and 5.6 experience a change in sign as the surface material parameter or residual surface stress parameter increases. Numerical results shown in Figures 5.2 to 5.6 confirm the fact that the influence of surface stresses cannot be ignored in modeling of near-surface cracks and other defects in materials where the surface energy effects are not negligible.

5.2 Penny-Shaped Crack in Infinite Elastic Medium

5.2.1 Formulation of Dual Integral Equations

Consider a penny-shaped crack with a radius a subjected to axisymmetric applied internal pressure $p(r)$ in an infinite elastic medium as shown in Figure 5.7. The corresponding solutions for bulk stresses and displacements are given by Eqs. (3.14a) to (3.14f) with C' and $D' \equiv 0$ to satisfy the regularity conditions at infinity and the arbitrary functions A' and B' can be obtained by solving the boundary value problem on the crack surface (z = 0).

$$\sigma_{zz} + \left[\frac{d\tau^s}{dr}\frac{du_z}{dr} + \tau^s\left(\frac{d^2u_z}{dr^2} + \frac{1}{r}\frac{du_z}{dr} \right) \right] = -p(r), \qquad 0 \le r < a \quad (5.5a)$$

$$u_z = 0, \qquad a < r < \infty \quad (5.5b)$$

$$\sigma_{rz} + \left[\frac{d\tau^s}{dr}\left(1 + \frac{u_r}{r} \right) + \kappa^s\left(\frac{d^2u_r}{dr^2} + \frac{1}{r}\frac{du_r}{dr} - \frac{u_r}{r^2} \right) \right] = 0, \qquad 0 \le r < a \quad (5.5c)$$

$$\sigma_{rz} = 0, \qquad a < r < \infty \quad (5.5d)$$

It is noted that the residual surface stress of the crack surface is assumed to be constant and the analysis is only concerned with the elastic field induced by the external loading, i.e. the influence of point loads at crack-tip induced by residual surface stress (Wu,1999) is not considered. By substituting the solutions of stresses and displacements from Eqs. (3.14a) to (3.14f) into Eqs. (5.5a) to (5.5d), we then obtain

$$\int_0^\infty \left\{ \left[2(\lambda+\mu)\xi^4 + \frac{\lambda+\mu}{\mu}\tau^s\xi^5 \right] A + \left(2\mu\xi^3 + 2\tau^s\xi^4 \right) B \right\} J_0(\xi r) d\xi = -p(r), \quad 0 \le r < a \qquad (5.6a)$$

$$\int_0^\infty \left(\frac{\lambda+\mu}{\mu}\xi^3 A + 2\xi^2 B \right) J_0(\xi r) d\xi = 0, \qquad a < r < \infty \qquad (5.6b)$$

$$\int_0^\infty \left\{ \left[2(\lambda+\mu)\xi^4 + \frac{\lambda+\mu}{\mu}\kappa^s\xi^5 \right] A - \left(2\lambda\xi^3 + \frac{\lambda+\mu}{\mu}\kappa^s\xi^4 \right) B \right\} J_1(\xi r) d\xi = 0, \quad 0 \le r < a \qquad (5.6c)$$

$$\int_0^\infty \left[2(\lambda+\mu)\xi^4 A - 2\lambda\xi^3 B \right] J_1(\xi r) d\xi = 0, \qquad a < r < \infty \qquad (5.6d)$$

By introducing the non-dimensional parameters; $\bar{r} = r/a$ and $\bar{\xi} = \xi a$, Eqs. (5.6a) to (5.6d) can be expressed to a set of simultaneous dual integral equations as

$$\int_0^\infty \sum_{j=1}^{2} c_{ij}\left(\bar{\xi}\right) f_j\left(\bar{\xi}\right) J_{\nu_i}\left(\bar{\xi}\bar{r}\right) d\bar{\xi} = h_i\left(\bar{r}\right), \qquad 0 \le \bar{r} < 1 \qquad (5.7a)$$

$$\int_0^\infty \sum_{j=1}^{2} d_{ij}\left(\bar{\xi}\right) f_j\left(\bar{\xi}\right) J_{\nu_i}\left(\bar{\xi}\bar{r}\right) d\bar{\xi} = g_i\left(\bar{r}\right), \qquad 1 < \bar{r} < \infty \qquad (5.7b)$$

where i = 1, 2;

$$c = \begin{bmatrix} 2(\lambda+\mu)\dfrac{\bar{\xi}^4}{a^4} + \dfrac{\lambda+\mu}{\mu}\tau^s\dfrac{\bar{\xi}^5}{a^5} & 2\mu\dfrac{\bar{\xi}^3}{a^3} + 2\tau^s\dfrac{\bar{\xi}^4}{a^4} \\ 2(\lambda+\mu)\dfrac{\bar{\xi}^4}{a^4} + \dfrac{\lambda+\mu}{\mu}\dfrac{\bar{\xi}^5}{a^5}\kappa^s & -2\lambda\dfrac{\bar{\xi}^3}{a^3} + \dfrac{\lambda+\mu}{\mu}\kappa^s\dfrac{\bar{\xi}^4}{a^4} \end{bmatrix};$$

$$d = \begin{bmatrix} \dfrac{\lambda+\mu}{\mu}\dfrac{\bar{\xi}^3}{a^3} & 2\dfrac{\bar{\xi}^2}{a^2} \\ 2(\lambda+\mu)\dfrac{\bar{\xi}^4}{a^4} & -2\lambda\dfrac{\bar{\xi}^3}{a^3} \end{bmatrix}; \quad f = \begin{bmatrix} A'\left(\bar{\xi}\right) \\ B'\left(\bar{\xi}\right) \end{bmatrix}; \quad v = \begin{bmatrix} 0 \\ 1 \end{bmatrix}; \quad h = \begin{bmatrix} -\bar{p}\left(\bar{r}\right) \\ 0 \end{bmatrix}; \quad g = \begin{bmatrix} 0 \\ 0 \end{bmatrix}$$

and $\bar{p}\left(\bar{r}\right) = ap\left(a\bar{r}\right)$

The above equation can be easily reduced to

$$\int_0^\infty \sum_{j=1}^{2} e_{ij}\left(\bar{\xi}\right) \psi_j\left(\bar{\xi}\right) J_{\nu_i}\left(\bar{\xi}\bar{r}\right) d\bar{\xi} = h_i\left(\bar{r}\right), \qquad 0 \le \bar{r} < 1 \qquad (5.8a)$$

$$\int_0^\infty \psi_i\left(\bar{\xi}\right) J_{\nu_i}\left(\bar{\xi}\bar{r}\right) d\bar{\xi} = 0, \qquad 1 < \bar{r} < \infty \qquad (5.8b)$$

where $\psi_i\left(\overline{\xi}\right)=\sum_{j=1}^{2} d_{ij}\left(\overline{\xi}\right) f_j\left(\overline{\xi}\right)$ and

$$e=cd^{-1}=\begin{bmatrix} \dfrac{2\mu\left(\lambda+\mu\right)}{\lambda+2\mu}\dfrac{\overline{\xi}}{a}+\tau^s\dfrac{\overline{\xi}^2}{a^2} & \dfrac{\mu}{\lambda+2\mu} \\ -\dfrac{\mu}{\lambda+2\mu}\kappa^s\dfrac{\overline{\xi}^2}{a^2} & 1+\dfrac{\lambda+3\mu}{2\mu\left(\lambda+2\mu\right)}\kappa^s\dfrac{\overline{\xi}}{a} \end{bmatrix}$$

To solve Eqs. (5.8a) and (5.8b), ψ is defined as (Erdogan and Bahar, 1964);

$$\psi_j\left(\overline{\xi}\right)=\overline{\xi}^{1-\beta_j}\sum_{m=0}^{\infty}\varphi_{jm}J_{\nu_j+2m+\beta_j}\left(\overline{\xi}\right) \tag{5.9}$$

Hence, Eq.(5.8b) will be automatically satisfied due to the following properties of Sonine-Schafheitlin integrals (Magnus and Oberhettinger, 1954).

$$\int_0^{\infty}\overline{\xi}^{1-\beta_j}J_{\nu_j}\left(\overline{\xi}\overline{r}\right)J_{\nu_j+2m+\beta_j}\left(\overline{\xi}\right)d\overline{\xi}=0, \qquad \overline{r}>1;\ 2\left(\nu_j+m+1\right)>0 \text{ and } \beta_j>0 \tag{5.10}$$

and Eq.(5.8a) may then be written as

$$\sum_{m=0}^{\infty}\sum_{j=1}^{2}\varphi_{jm}\int_0^{\infty}\overline{\xi}^{1-\beta_j}e_{ij}\left(\overline{\xi}\right)J_{\nu_i}\left(\overline{\xi}\overline{r}\right)J_{\nu_j+2m+\beta_j}\left(\overline{\xi}\right)d\overline{\xi}=h_i\left(\overline{r}\right), \qquad 0\le\overline{r}<1 \tag{5.11}$$

where φ_{jm} are the unknown coefficients to be determined. Multiplying both sides of Eq. (5.11) by

$$\overline{r}^{1+\nu_i}\left(1-\overline{r}^2\right)^{\beta_i-1}\Im_k\left(\nu_i+\beta_i,1+\nu_i,\overline{r}^2\right);\ k\ =0,1,2,\ldots,\ m;$$

and then integrating with respect to $\overline{r}$ from 0 to 1, yield (Tranter, 1956)

$$\sum_{m=0}^{\infty}\sum_{j=1}^{2}\varphi_{jm}\int_0^{\infty}\overline{\xi}^{1-\beta_j-\beta_i}e_{ij}\left(\overline{\xi}\right)J_{\nu_i+2k+\beta_i}\left(\overline{\xi}\right)J_{\nu_j+2m+\beta_j}\left(\overline{\xi}\right)d\overline{\xi}=Q_i\left(\nu_i,\beta_i,k\right) \tag{5.12}$$

where

$$Q_i\left(\nu_i,\beta_i,k\right)=\frac{\Gamma(\nu_i+k+1)}{2^{\beta_i-1}\Gamma(\nu_i+1)\Gamma(k+\beta_i)}\int_0^1 h_i\left(\overline{r}\right)\overline{r}^{1+\nu_i}\left(1-\overline{r}^2\right)^{\beta_i-1}\Im_k\left(\nu_i+\beta_i,1+\nu_i,\overline{r}^2\right)d\overline{r}$$

and $\Im_n$ is the Jacobi polynomial, which is defined in terms of hypergeometric series by (Magnus and Oberhettinger, 1954) as

$$\Im_n(\alpha,\gamma,x) = {}_2F_1(-n,\alpha+n;\gamma;x)$$

The coefficients φ_{jm} can be obtained by solving Eq. (5.12). Note that the unspecified constant, β_j, in Eq. (5.12) must be positive and makes the integral appearing in Eq. (5.12) converged. The arbitrary functions A' and B' for calculate stresses and displacements can be expressed in term of ψ_i (i = 1,2) as

$$A'(\bar{\xi}) = \frac{\lambda\mu}{(\lambda+\mu)(\lambda+2\mu)}\frac{a^3}{\bar{\xi}^3}\left[\psi_1(\bar{\xi}) + \frac{a}{\lambda\bar{\xi}}\psi_2(\bar{\xi})\right] \tag{5.13a}$$

$$B'(\bar{\xi}) = \frac{\mu}{(\lambda+2\mu)}\frac{a^2}{\bar{\xi}^2}\left[\psi_1(\bar{\xi}) - \frac{a}{2\mu\bar{\xi}}\psi_2(\bar{\xi})\right] \tag{5.13b}$$

5.2.2 Numerical Results

In this section, selected numerical results are presented to portray the influence of surface stresses on the elastic field of the medium. It is noted that the solutions for stresses and displacements can be calculated by Eqs.(3.14a) to (3.14f) with the arbitrary functions, A' and B', given by Eqs.(5.13a) and (5.13b). In this study, the semi-infinite integrals in Eqs.(3.14a) to (3.14f) are evaluated by using globally adaptive numerical quadrature scheme based on 21-point Gauss-Kronrod rule (Piessens 1983). In the numerical study, it is convenient to introduce the following non-dimensional quantities, $r_0 = r/\bar{\Lambda}$; $z_0 = z/\bar{\Lambda}$ and $a_0 = a/\bar{\Lambda}$, where $\bar{\Lambda} = \left|\kappa^s/\mu\right|$ and it has the dimension of length. The numerical results in the present study corresponding to the case of a penny-shaped crack in an infinite elastic medium subjected to a uniformly distributed applied internal pressure, p_0. In addition, the material properties of λ/μ = 1.94, $\bar{\Lambda}$ = .24983 nm and τ^s = 0.6056 N/m for Si [100] (Miller and Shenoy, 2000) are used in the present study.

Since the arbitrary function, A' and B', given by Eqs.(5.13a) and (5.13b) are evaluated by the combination of ψ_1 and ψ_2, which are defined by infinite

series in Eq.(5.9), the convergence of the solution is plotted to verify the validity and accuracy of the solution technique and to determine the appropriate number of terms, m, in the series that can be used to predict the behavior of the problem accurately. Figure 5.8 shows the convergence of non-dimensional vertical stress in the vicinity of crack tip for the classical case where the surface stress is excluded (i.e. $\kappa^s = \tau^s = 0$). It can be seen from the figure that the present solution shows very good agreement with classical elasticity solution proposed by Fabricant (1989) especially when m is larger than 60. In Figure 5.9, the numerical solutions for the classical vertical stress and classical crack opening displacement from the present study, using 65 terms in the approximation (m = 65), are compared with the benchmark solutions. It is evident from Figure 5.9 that numerical results obtained from the present study are almost indistinguishable from the exact solutions proposed by Fabricant (1989). In this study, the elastic field of the medium are therefore calculated by using m = 65.

Figures 5.10 and 5.11 demonstrate the influence of surface stresses on the elastic field of an elastic medium near the crack region. A non-dimensional crack radius, a_0 = 1.0 is considered in the numerical study. In Figure 5.10, the variation along the r-axis of non-dimensional vertical stresses in the region near the crack tip is presented, whereas Figure 5.11 displays the non-dimensional crack opening displacements. The non-dimensional stresses and displacements shown in Figures 5.10 and 5.11 are presented for Si [100] and hypothetical material (λ / μ = 1.94, $\bar{\Lambda}$ = .24983 nm) with different values of residual surface stress (i.e. τ^s = 0.1 and 1.0 N/m). Note that the broken lines in Figures 5.10 and 5.11 denote the classical elasticity solution (Fabricant, 1989), which can also be obtained from the present solution with the absence of surface stress (i.e. $\kappa^s = \tau^s = 0$).

The variation of non-dimensional vertical stress on the crack plane in the region near the crack tip shown in Figure 5.10 reveals that the surface stresses have a significant influence on the vertical stress, especially in the vicinity of the

crack tip where the vertical stress approaches infinity for both classical and present solutions. It is observed from the figure that the presence of surface stress effects results in the reduction of vertical stress. Similar aspect is also found in the case of plane strain cracks (Kim et al., 2011). Note that their paper assumes that the stress at the crack tip is finite. In Figure 5.11 the influence of the surface stresses on the crack opening displacement is presented. As in classical elasticity, the maximum displacement is located at the center of the crack before gradually reduces to zero at the crack tip. In addition, it can be seen from the figure that the presence of surface stresses causes the reduction of the crack opening displacement.

Figure 5.12 demonstrate the size-dependent behavior of the elastic medium with the presence of surface stresses. In Figure 5.12, the variation along the r-axis of non-dimensional vertical stress profile in the region near the crack tip is presented for Si [100] with different values of crack radius (i.e. a_0 = 0.5, 1.0 and 1.5). It is obvious from the figure that with the consideration of surface stresses, the non-dimensional vertical stress depends significantly on crack size in contrast with the classical solutions, where the non-dimensional vertical stresses are independent of crack size. In addition, it is observed from Figure 5.12 that the influence of surface stresses decreases when crack size increases and the solution will converge to the classical solution. Numerical results shown in Figures 5.10 to 5.12 confirm the fact that the influence of surface stresses is significant in the analysis of the problems involving nanoscale cracks and other defects in materials where the surface energy effects are not negligible.

5.3 Conclusion

The fundamental solutions of an elastic medium with dislocations and crack are derived with the consideration of surface stress influence by adopting the Gurtin-Murdoch continuum theory of surface elasticity. The elastic fields corresponding to plane strain and axisymmetric problems are obtained by using

Fourier and Hankel integral transforms, respectively. It is found that analytical solutions can be expressed in terms of semi-infinite integrals that cannot be evaluated in closed-form but can be computed accurately by employing a numerical quadrature scheme. For crack problems, a set of simultaneous dual integral equations is solved by employing appropriate solution scheme. It is found from the numerical results that the surface stresses have a significant influence on the elastic field especially in the region near the surface. In addition, numerical results in this study show similar trends with their classical solutions. However, unlike in the classical elasticity approach, the behavior of the material becomes size-dependent when the surface stresses are accounted for. The fundamental solutions for gliding and climbing edge dislocations presented in this study are essential to the extension of the displacement discontinuity method (DDM) to analyze fracture problems involving nanoscale systems and soft elastic solids.

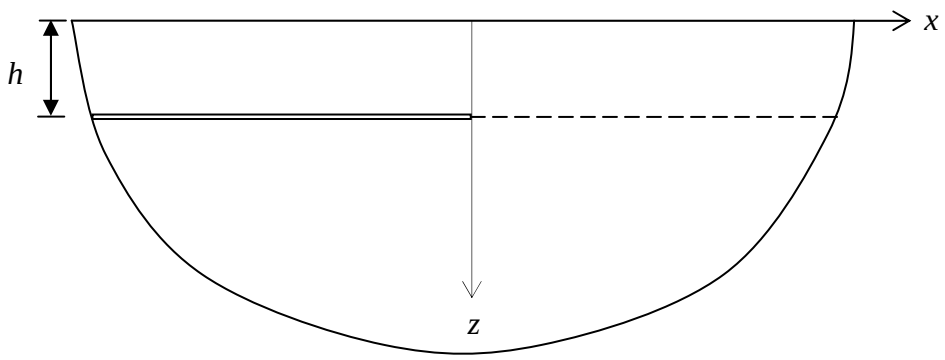

Figure 5.1 Dislocations in a semi-infinite elastic medium at a depth h below the surface.

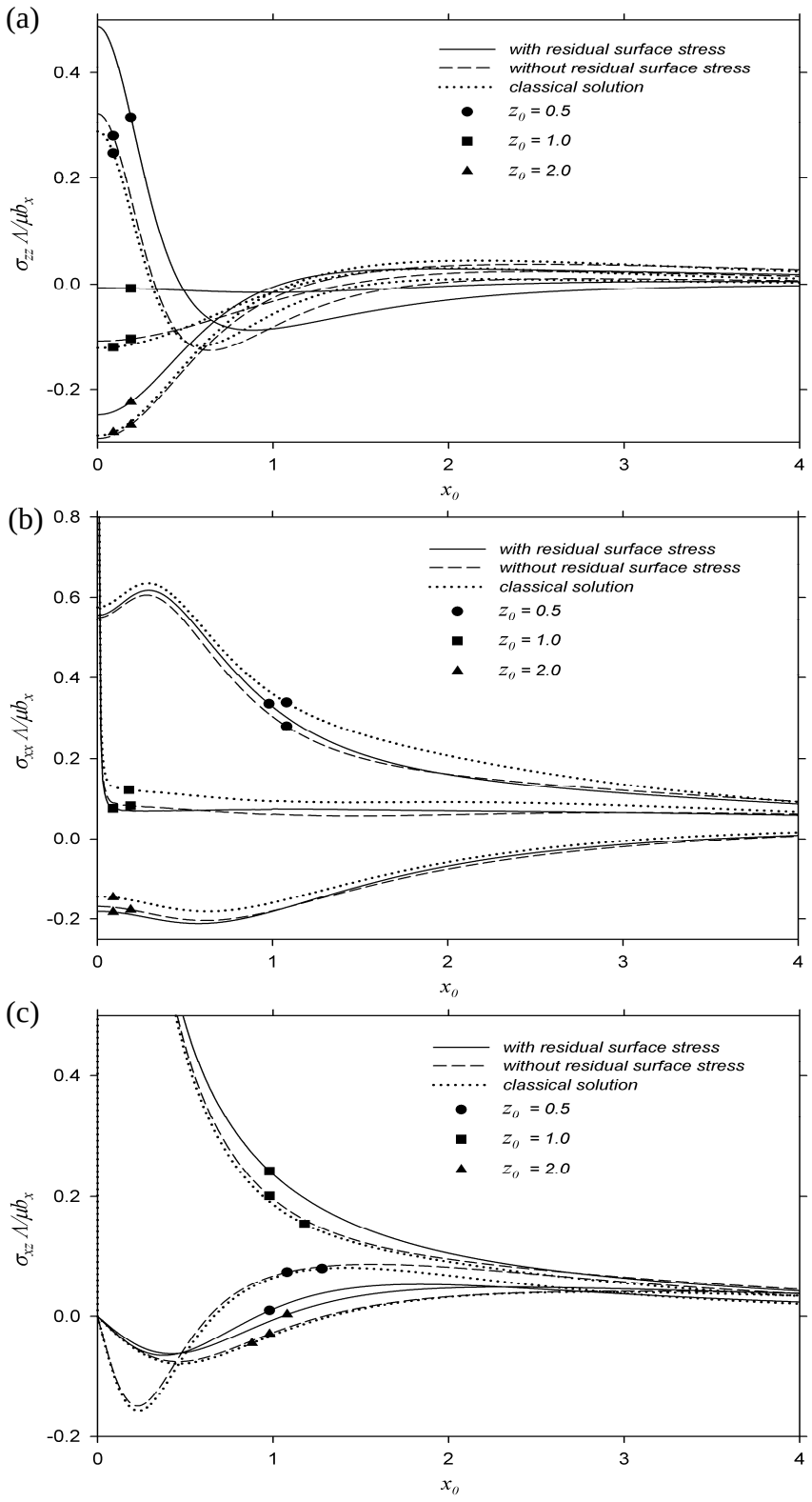

Figure 5.2 Non-dimensional stress profiles under shear dislocation at h_0 = 1.0: (a) Vertical stress (b) Horizontal stress (c) Shear stress.

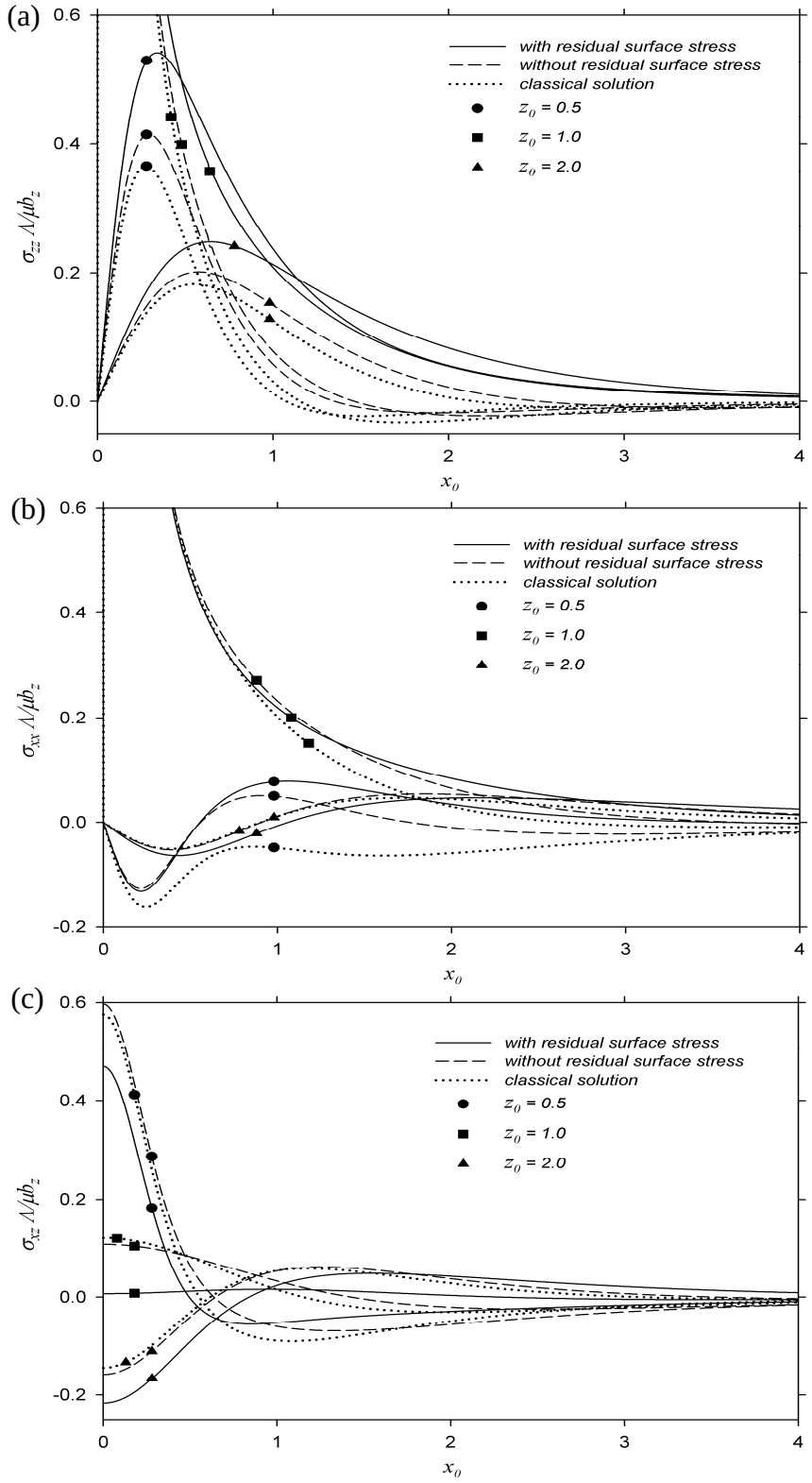

Figure 5.3 Non-dimensional stress profiles under opening dislocation at h_0 = 1.0: (a) Vertical stress (b) Horizontal stress (c) Shear stress.

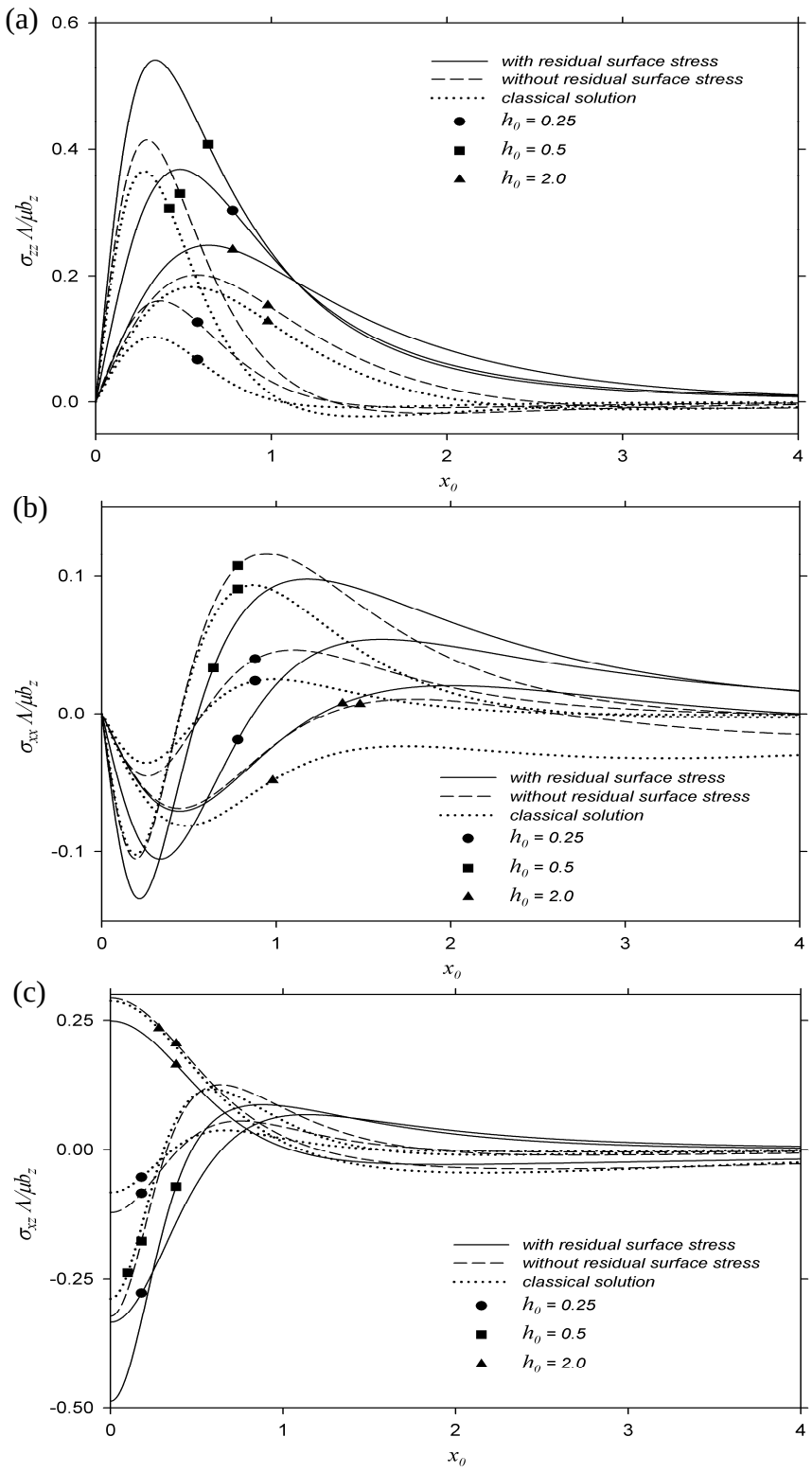

Figure 5.4 Non-dimensional stress profiles under opening dislocation for different depths of dislocation plane (z_0 = 1.0): (a) Vertical stress (b) Horizontal stress (c) Shear stress.

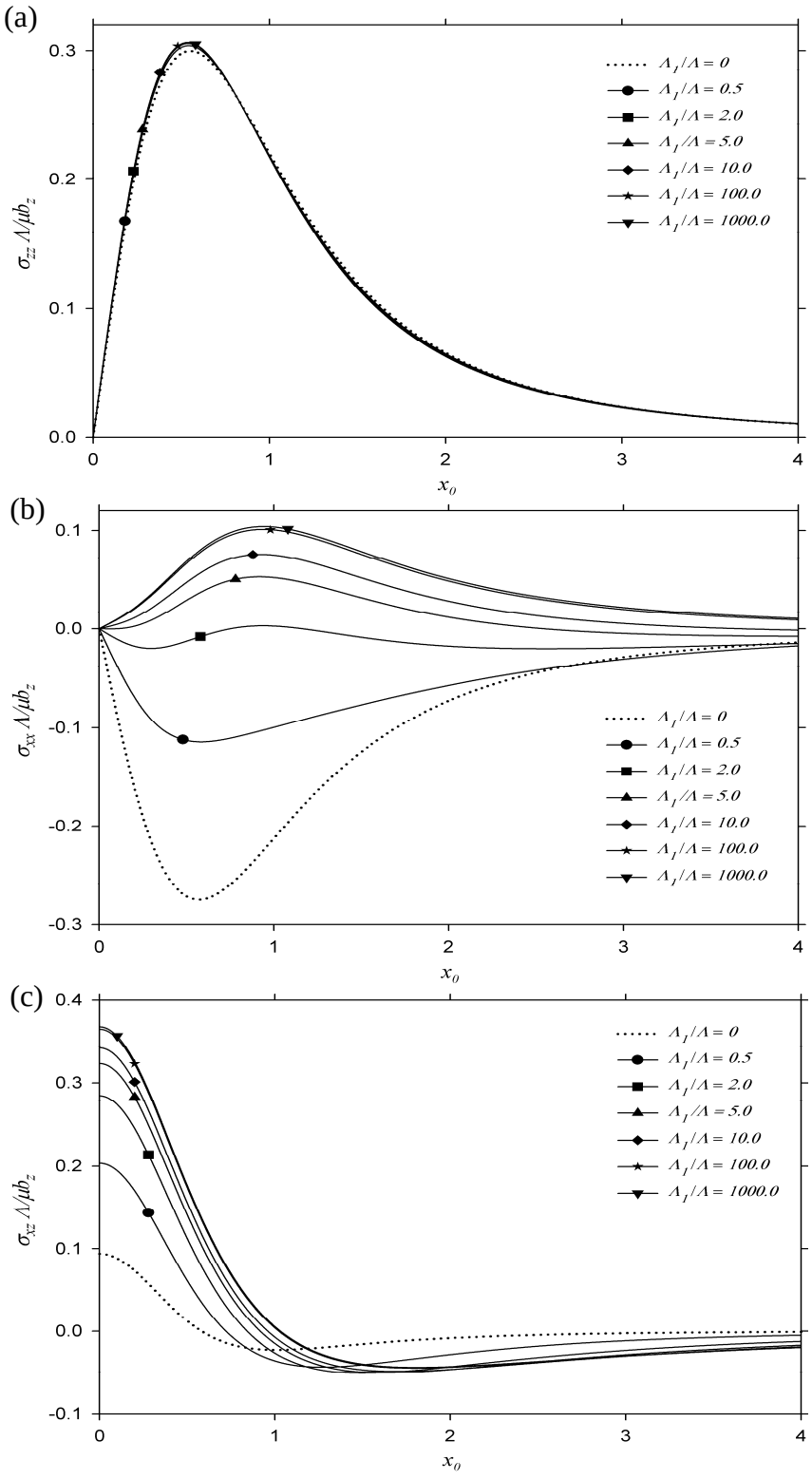

Figure 5.5 Non-dimensional stress profiles under opening dislocation for different material constants (h_0 = 1.0 and z_0 = 0.1): (a) Vertical stress (b) Horizontal stress (c) Shear stress.

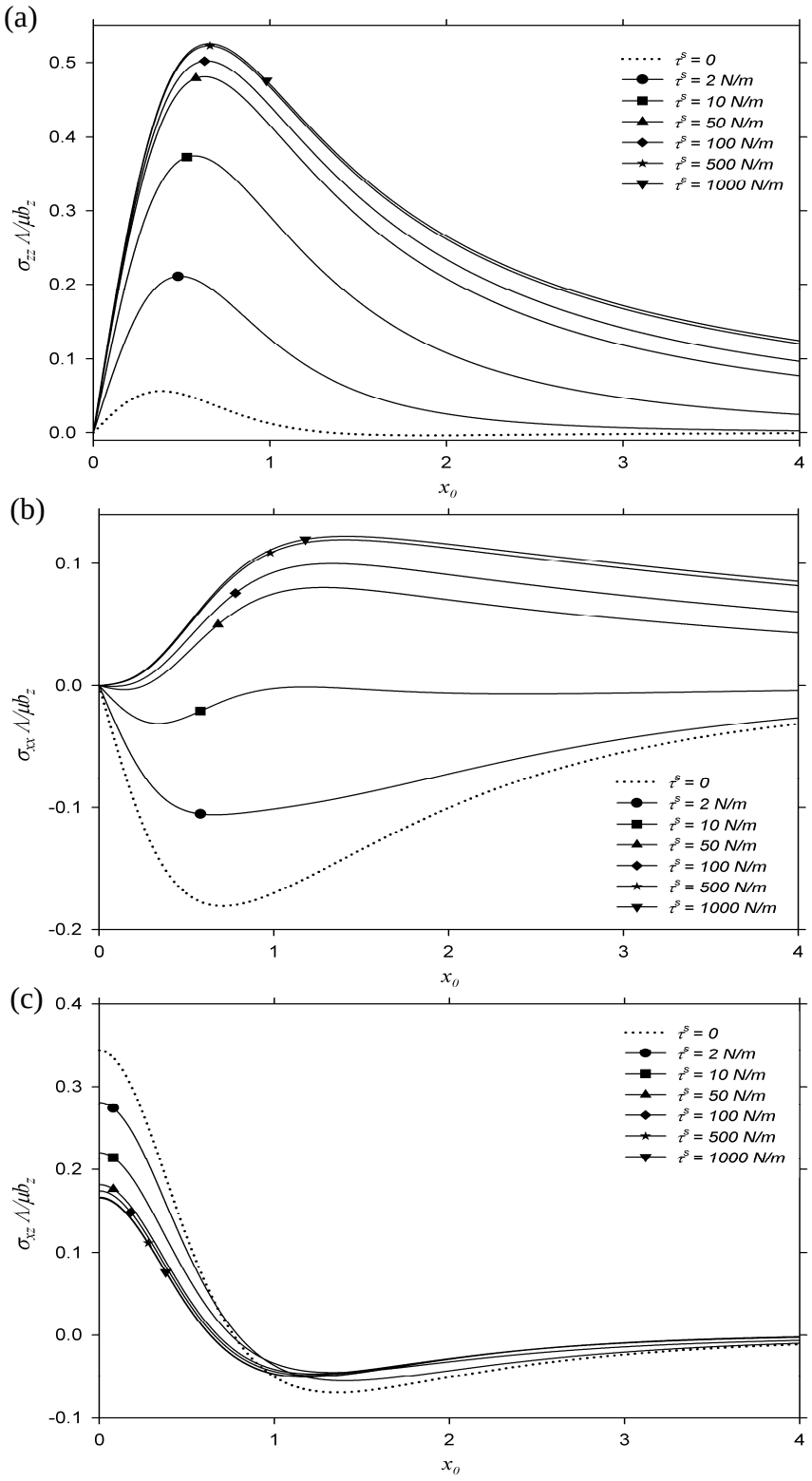

Figure 5.6 Non-dimensional stress profiles under opening dislocation for different residual surface stresses (h_0 = 1.0 and z_0 = 0.1): (a) Vertical stress (b) Horizontal stress (c) Shear stress.

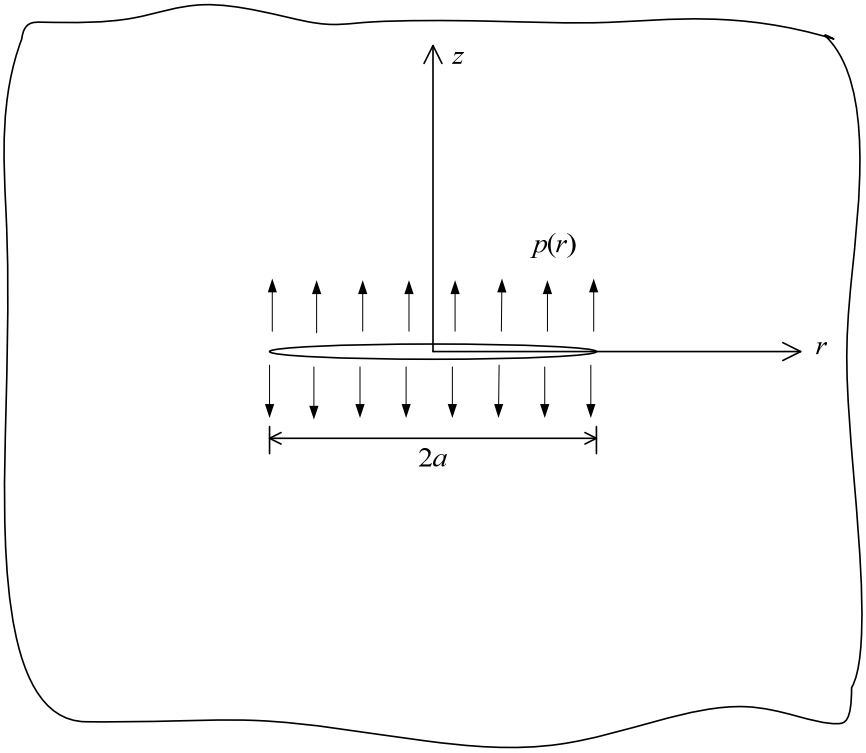

Figure 5.7 A penny-shaped crack in an infinite elastic medium subjected to applied internal pressure.

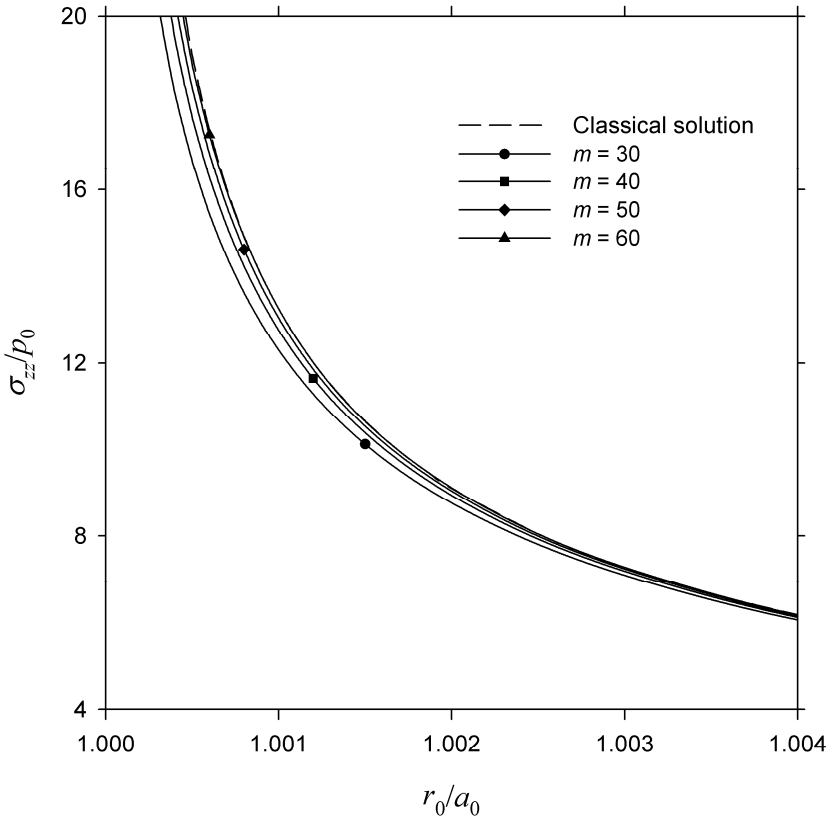

Figure 5.8 Convergence of non-dimensional vertical stress profile in the vicinity of crack tip.

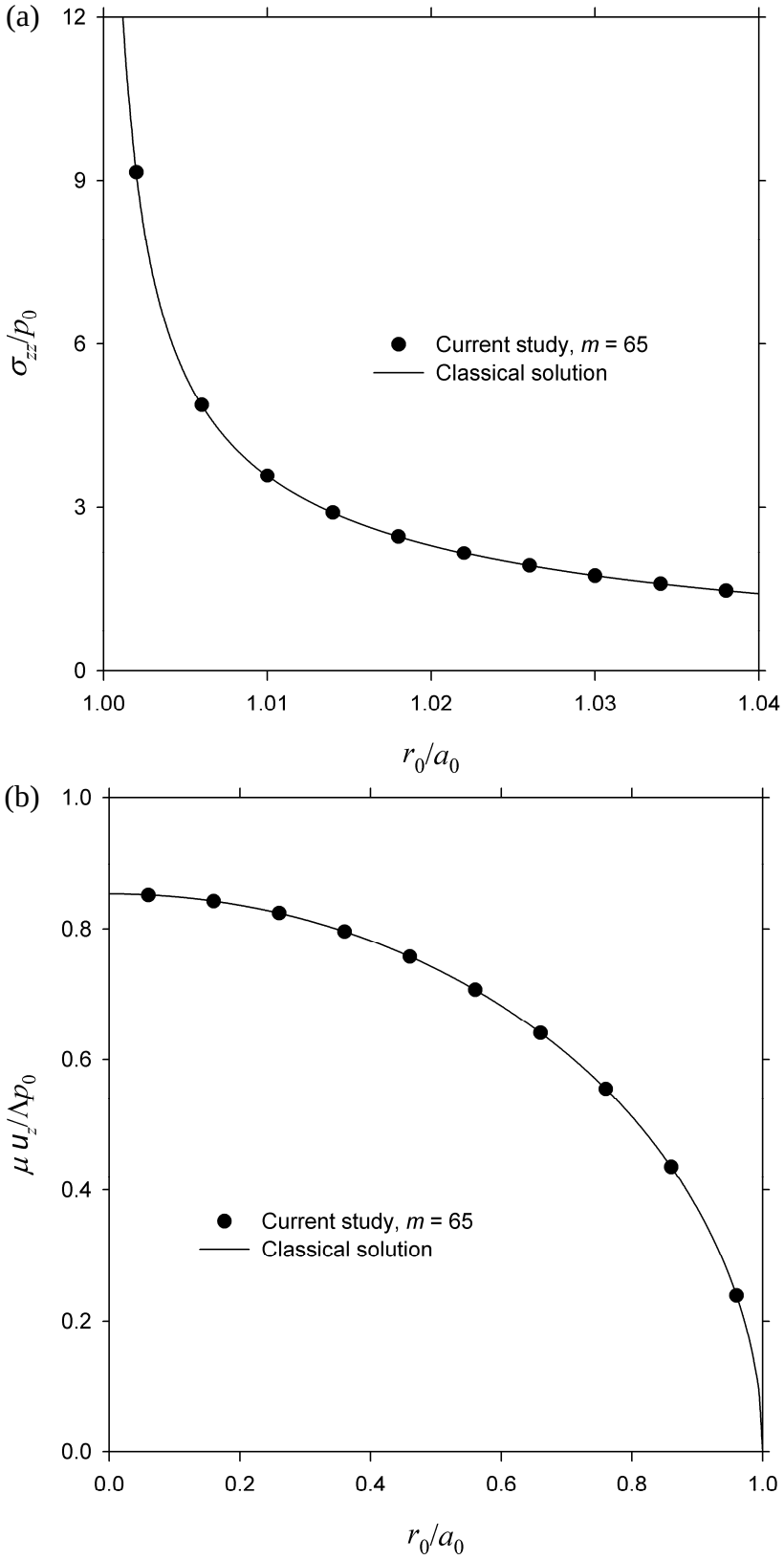

Figure 5.9 Comparison of classical numerical solution with exact solution: (a) Vertical stress (b) Crack opening displacement.

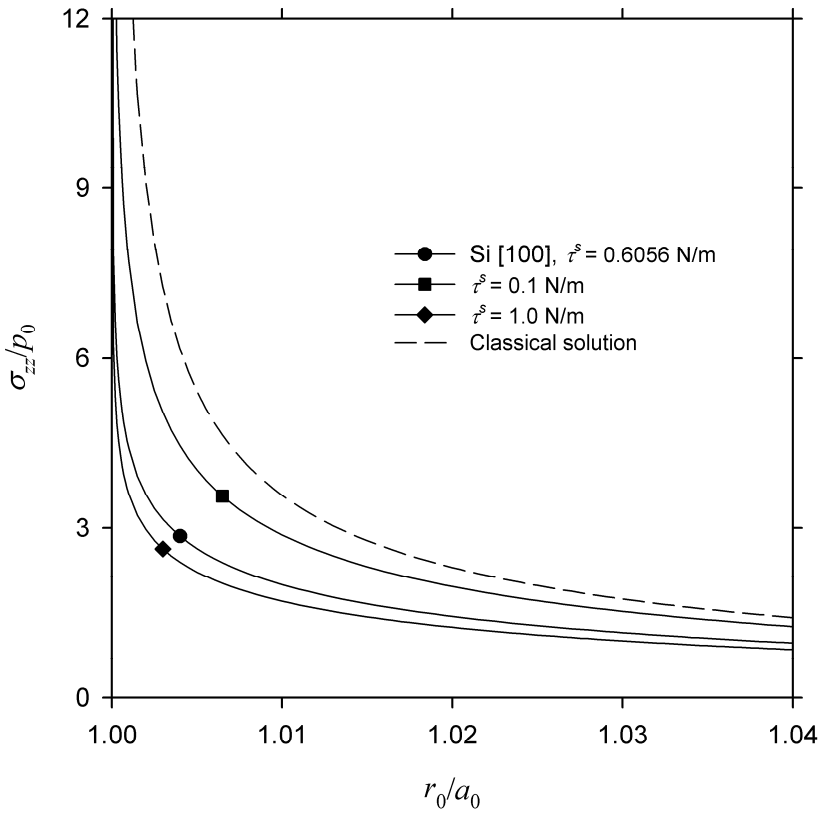

Figure 5.10 Non-dimensional vertical stress profile in the vicinity of crack tip for different residual surface stresses (τ^s).

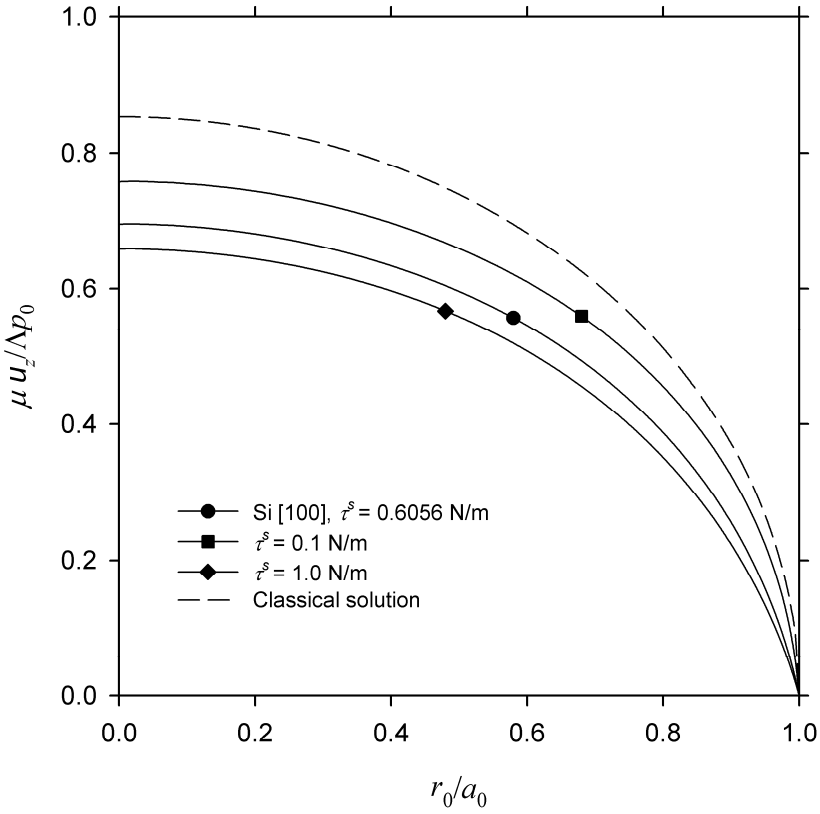

Figure 5.11 Non-dimensional crack opening displacement for different residual surface stresses (τ^s).

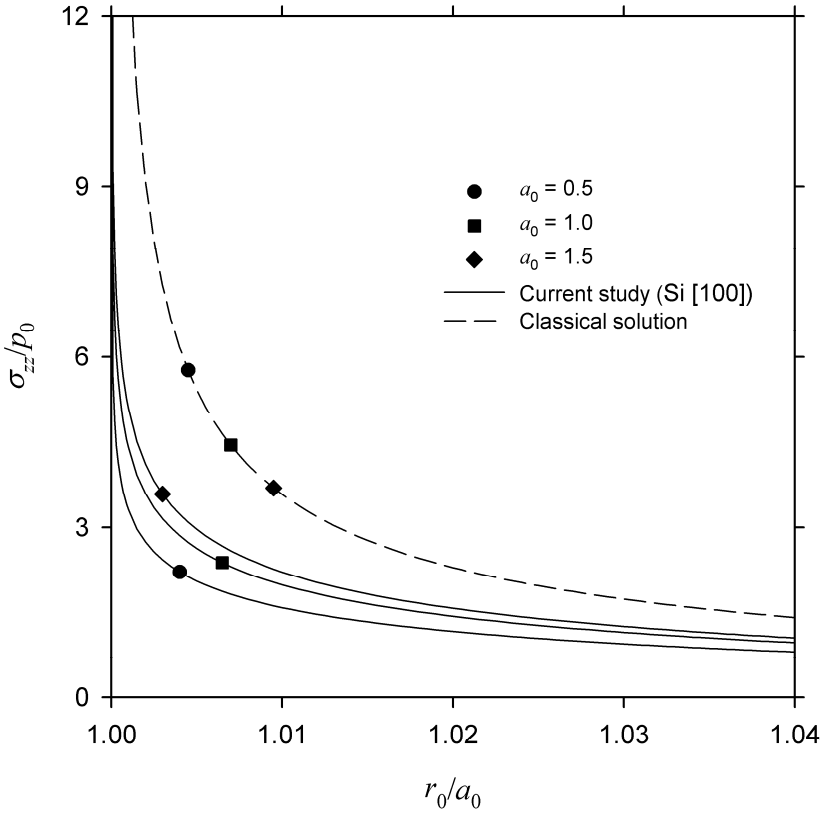

Figure 5.12 Non-dimensional vertical stress profile in the vicinity of crack tip for different sizes of crack (a_0).

CHAPTER VI

RIGID-INDENTATION ON ELASTIC LAYER

In this chapter, the fundamental solutions derived in Chapter 4 are employed in the formulation of axisymmetric indentation problems. Green functions of surface displacements of an isotropic elastic layer with the consideration of surface stresses are first constructed from the fundamental solutions presented in Section 4.2. The integral equations for solving nano-indentation problems of a finite thickness elastic layer under axisymmetric punch profile are then formulated for several indentation models. Selected numerical results are presented to portray the influence of surface stresses for a special case of rigid, flat-ended cylindrical punch with frictionless model.

6.1 Axisymmetric Green Functions for Elastic Layer

Consider a three-dimensional finite thickness elastic layer bonded to a rigid base, and subjected to axisymmetric normal and tangential traction on the surface. The required fundamental solutions for the problems are presented in Section 4.2 for arbitrary axisymmetric load cases. Green functions, which are defined by the solutions of surface displacements of an elastic layer under unit normal ring load, p, and unit tangential ring loads, q, can be respectively constructed by Eqs. (3.14e) and (3.14f) with the arbitrary functions given by Eqs. (4.16a) to (4.16d). Note that the Hankel transforms of unit normal ring load and unit tangential ring load applied at the radius r^* are given by

$$p'(\xi) = -\int_0^\infty rp\delta(r - r^*)J_0(\xi r)dr = -pr^*J_0(\xi r^*) \tag{6.1a}$$

$$q'(\xi) = -\int_0^\infty rq\delta(r - r^*)J_1(\xi r)dr = -qr^*J_1(\xi r^*) \tag{6.1b}$$

By using a method of superposition, the vertical and radial displacements at any distance r on the surface due to arbitrary axisymmetric normal traction $p\left(r^*\right)$ and tangential traction $q\left(r^*\right)$ can be expressed in the integral equation as

$$u_r(r)=\int_0^\infty U_r^N\left(r,r^*\right)p\left(r^*\right)dr^*+\int_0^\infty U_r^T\left(r,r^*\right)q\left(r^*\right)dr^* \tag{6.2}$$

$$u_z(r)=\int_0^\infty U_z^N\left(r,r^*\right)p\left(r^*\right)dr^*+\int_0^\infty U_z^T\left(r,r^*\right)q\left(r^*\right)dr^* \tag{6.3}$$

where $U_r^N\left(r,r^*\right)$ and $U_z^N\left(r,r^*\right)$ denote radial and vertical displacements respectively at any distance r on the surface due to a unit normal ring load applied on the layer at the radius r^*, whereas $U_r^T\left(r,r^*\right)$ and $U_z^T\left(r,r^*\right)$ denote radial and vertical displacements at any distance r on the surface due to a unit tangential ring load applied on the layer at the radius r^* respectively . Similarly, all other elastic fields at any point (r,z) within the bulk material, denoted generically by $R(r,z)$, due to arbitrary axisymmetric normal and tangential traction can also be expressed in the integral equation as

$$R(r,z)=\int_0^\infty R^N\left(r,z,r^*\right)p\left(r^*\right)dr^*+\int_0^\infty R^T\left(r,z,r^*\right)q\left(r^*\right)dr^* \tag{6.4}$$

where $R^N\left(r,z,r^*\right)$ and $R^T\left(r,z,r^*\right)$ denote the responses at any point (r,z) due to a unit normal ring load and unit tangential ring load applied on the layer at the radius r^* respectively. It is clear that for a problem where the surface traction $p\left(r^*\right)$ and $q\left(r^*\right)$ are fully prescribed, all field quantities can be directly computed by Eq. (6.4). The derived Green functions have important applications in contact problems such as indentation problems, where the surface traction is unknown, as demonstrated in the subsequent sections.

6.2 Axisymmetric Rigid Punch Problems

For indentation problems, normal traction and tangential traction in the contact region are unknown a priori and have to be determined with the appropriate assumption of the contact condition in the contact region between the punch and the layer. Consider an isotropic elastic layer under an

axisymmetric rigid punch with a profile $v^p(r)$ as shown in Figure 6.1. It is noted that the profile of the punch is conveniently defined by choosing v^p = 0 at r = 0. The radius of a contact region and the indentation depth induced by a resultant force P at the center of the punch are denoted by a and d respectively. The integral equation for solving the unknown traction can be summarized for the cases of frictionless and frictional indentation models as follows:

6.2.1 Rigid Frictionless Punch Problems

In the study of indentation problems, the model of a frictionless punch is the most common model, and has been widely employed in classical mechanics. For a special case of axisymmetric frictionless nano-indentation problems, the tangential traction in the contact region identically vanishes whereas the vertical displacement is prescribed via the punch profile, v^p, and the prescribed indentation depth, d. The integral equation for determining the normal traction in the contact region can then be deduced from Eq. (6.3) as

$$u_z(r) = \int_0^a U_z^N(r,r^*)\, p(r^*)\, dr^* = d - v^p(r), \qquad 0 \le r \le a \qquad (6.5)$$

where a denotes the contact radius.

6.2.2 Rigid Fully Bonded Punch Problems

For the case of rigid fully bonded nano-indentation problems, the tangential displacement in the contact region identically vanishes whereas the vertical displacement is prescribed via the punch profile, v^p, and the prescribed indentation depth, d. The integral equations for determining normal and tangential traction in the contact region can then be deduced from Eqs. (6.2) and (6.3) as

$$u_r(r) = \int_0^a U_r^N(r,r^*)\, p(r^*)\, dr^* + \int_0^a U_r^T(r,r^*)\, q(r^*)\, dr^* = 0, \qquad 0 \le r \le a \qquad (6.6)$$

$$u_z(r) = \int_0^a U_z^N(r,r^*)\, p(r^*)\, dr^* + \int_0^a U_z^T(r,r^*)\, q(r^*)\, dr^* = d - v^p(r), \qquad 0 \le r \le a \qquad (6.7)$$

6.2.3 Rigid Rough Punch Problems

For the case of rigid rough nano-indentation problems, the tangential traction in the contact region can be related to the normal traction via an appropriate friction model whereas the vertical displacement is prescribed via the arbitrary punch profile, v^p, and the prescribed indentation depth, d. The integral equation for determining normal traction in the contact region can be deduced from Eq. (6.3) as

$$u_z(r)=\int_0^a U_z^N\left(r,r^*\right)p\left(r^*\right)dr^*+\int_0^a U_z^T\left(r,r^*\right)f\left(p\left(r^*\right)\right)dr^*=d-v^p(r),\ 0\le r\le a \qquad (6.8)$$

where a function f denotes the relation between normal traction and tangential traction. Once the normal traction $p\left(r^*\right)$ is determined, the tangential traction $q\left(r^*\right)$ can readily be obtained.

It is noted that by solving the integral equations (6.5) to (6.8), the unknown surface traction are obtained for each case. The elastic field of an elastic layer can readily be determined from the integral relation (6.4)

6.3 Rigid Frictionless Flat-Ended Cylindrical Punch

Consider a three-dimensional elastic layer of a finite thickness t bonded to a rigid material base under a rigid flat-ended cylindrical punch of a radius a as shown in Figure 6.2. The punch is subjected to a resultant force P at the center of the punch, and results in the indentation depth d as shown in the figure. In this study, it is assumed that there is no friction between the punch and the layer. For the special case of rigid flat-ended punch, the punch profile is set to be zero, i.e. $v^p(r)$ = 0, the integral equation for solving the pressure distribution in the contact region can be expressed as

$$\int_0^a U_z^N\left(r,r^*\right)p\left(r^*\right)dr^*=d, \qquad 0\le r\le a \qquad (6.9)$$

In order to solve the above equation, the pressure distribution in the contact region is assumed in the following form.

$$p\left(r^*\right)=\sum_{j=1}^{m}\alpha_j f_j\left(r^*\right), \tag{6.10}$$

By substitution pressure distribution in Eq. (6.10) into Eq. (6.9), we then obtain

$$\sum_{j=1}^{m}\alpha_j\int_0^a U_z^N\left(r,r^*\right)f_j\left(r^*\right)dr^*=d\,, \qquad 0\le r\le a \tag{6.11}$$

By adopting collocation technique, the above integral equation can be discretized into the following form

$$\sum_{j=1}^{m}\alpha_j\int_0^a U_z^N\left(r_i,r^*\right)f_j\left(r^*\right)dr^*=d_i\,, \qquad \text{for all } r_i,\ i = 1, 2, 3, \ldots, n \tag{6.12}$$

where d_i denotes the indentation depth at r_i.

The coefficient α_j can be obtained by solving Eq. (6.12). In this study the pressure distribution is approximated by the summation of axisymmetric polynomial functions as follow:

$$p\left(r^*\right)=\sum_{j=1}^{m}\alpha_j(r^*)^{j-1}, \tag{6.13}$$

More importantly, unlike classical solution, it is noted that for this particular case the resultant force P is not only transferred to the pressure distribution in the contact region but it also produced a normal ring load at the edge of the punch due to the influence of surface tension when the out-of-plane surface stresses is considered. Once the normal traction is obtained, all other field quantities can be computed from the integral relation in Eq. (6.4).

6.4 Numerical Results

In this section, selected numerical results are presented to portray the influence of surface stresses on the elastic field of the layer. It is noted that the relevant Green functions constructed by Eqs. (3.14e) and (3.14f) with the arbitrary functions given by Eqs. (4.16a) to (4.16d) are expressed as semi-infinite

integrals where closed form solutions cannot be obtained as previously discussed in Chapter 4. The numerical quadrature scheme based on 21-point Gauss-Kronrod rule (Piessens 1983) is then employed to evaluate these integrals. In the numerical study, it is convenient to introduce the following non-dimensional quantities, $r_0 = r/\Lambda$; $z_0 = z/\Lambda$; $t_0 = t/\Lambda$; $a_0 = a/\Lambda$ and $d_0 = d/\Lambda$, where $\Lambda = \kappa^s\left(\lambda+2\mu\right)/2\mu\left(\lambda+\mu\right)$, and it has the dimension of length. The numerical results in the present study correspond to the case of an elastic layer with finite thickness t_0/a_0 = 5 under rigid frictionless flat-ended cylindrical punch with the contact radius a_0 = 0.5 and the indentation depth d_0. In addition, the material properties used in Chapter 4 are considered in the numerical study, i.e. λ/μ = 2.226; Λ = 1 nm and τ^s = 5 N/m.

Since the pressure distribution is approximated by the summation of axisymmetric polynomial functions, the convergence of the solution is plotted to verify the accuracy of the solution technique and to determine the appropriate number of terms, m, in the series that can be used to predict the behavior of the problem accurately. Figure 6.3 shows the convergence of normallized contact pressure with the consideration of complete surface stresses. It can be seen from the figure that the present solution shows good agreement with benchmark solution proposed by Pinyochotiwong (2010) especially when m is larger than 12. In Figure 6.4, the numerical solutions for the normalized vertical displacement from the present study, using 15 terms in the approximation (m = 15), are compared with the benchmark solutions. It is evident from Figure 6.4 that numerical results obtained from the present study show excellent agreement with the solutions proposed by Pinyochotiwong (2010). In this study, all solutions are therefore calculated by using m = 15.

Figures 6.5 and 6.6 demonstrate the influence of surface stresses on the pressure distribution in the contact region and vertical displacement respectively, for difference values of contact radius (i.e. a_0 = 0.5, 1.0 and 1.5). It can be seen from Figure 6.5 that the contact pressure significantly decreases when the

influence of surface stresses is considered. On the contrary, the vertical displacement outside of the contact region obtained from current study is comparative higher than that in classical elasticity due to the fact that surface stresses make elastic layer stiffer and hence larger indentation force is needed in order to produce the same indentation depth. It is obvious from the figure that with the consideration of surface stress influence, normalized contact pressure and vertical displacement depend significantly on crack radius (or size of the punch for this particular case). In addition, the influence of surface stresses decreases when the radius on contact region increases, and the solution will converge to the classical solution.

In Figures 6.7 and 6.8, the variation of normalized displacement profiles and stress profiles along r-direction of an elastic layer with finite thickness t_0/a_0 = 5 under flat-ended cylindrical punch with contact radius a_0 = 0.5 are presented at various depths. It can be seen from Figure 6.7 that both vertical and radial displacements show significant influence on surface stresses especially at the plane near surface. In addition, both vertical and radial displacements from the present study are comparative higher than classical solutions as previously discussed except that radial displacement at the region close to the surface where the negative values occur. From Figure 6.8, it is obvious that all components of stress show significant influence of surface stress especially at the plane near surface, i.e. z_0 < 2. In addition, the influence of the residual surface stress becomes negligible when r_0/a_0 > 3. It should be noted that stresses and displacements presented in this study show similar trend with classical solutions.

6.5 Conclusion

The indentation problem of an isotropic elastic layer under an axisymmetric punch is examined with the consideration of surface stresses by adopting Gurtin-Murdoch continuum theory of surface elasticity. The interaction problem is formulated by employing the Green functions constructed from the

derived fundamental solutions in Section 4.2. It is noted that Green functions can be expressed in terms of semi-infinite integrals that cannot be evaluated in closed-form but can be computed accurately by employing a numerical quadrature scheme. It is found from the numerical results that the surface stresses have a significant influence on the elastic field especially in the region near the surface. In addition, numerical results in this study show similar trends with their classical solutions. However, unlike classical elasticity, the behavior of the material becomes size-dependent when the surface stresses are accounted for. More importantly, for this particular case of flat-ended cylindrical punch, the presence of surface tension induces a normal ring load at the edge of the punch.

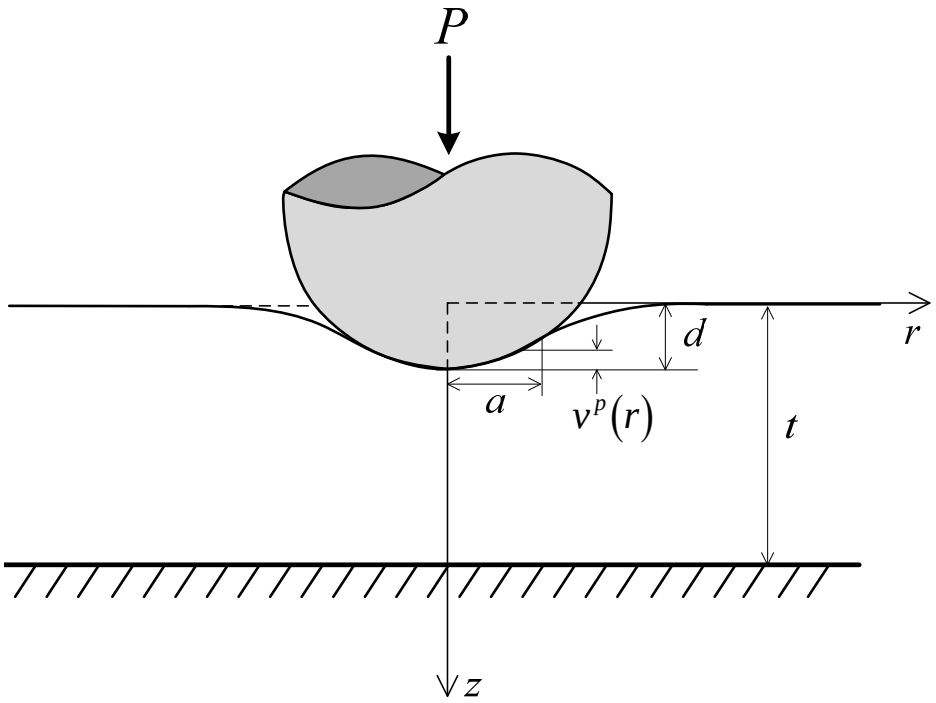

Figure 6.1 An isotropic elastic layer under axisymmetric rigid punch.

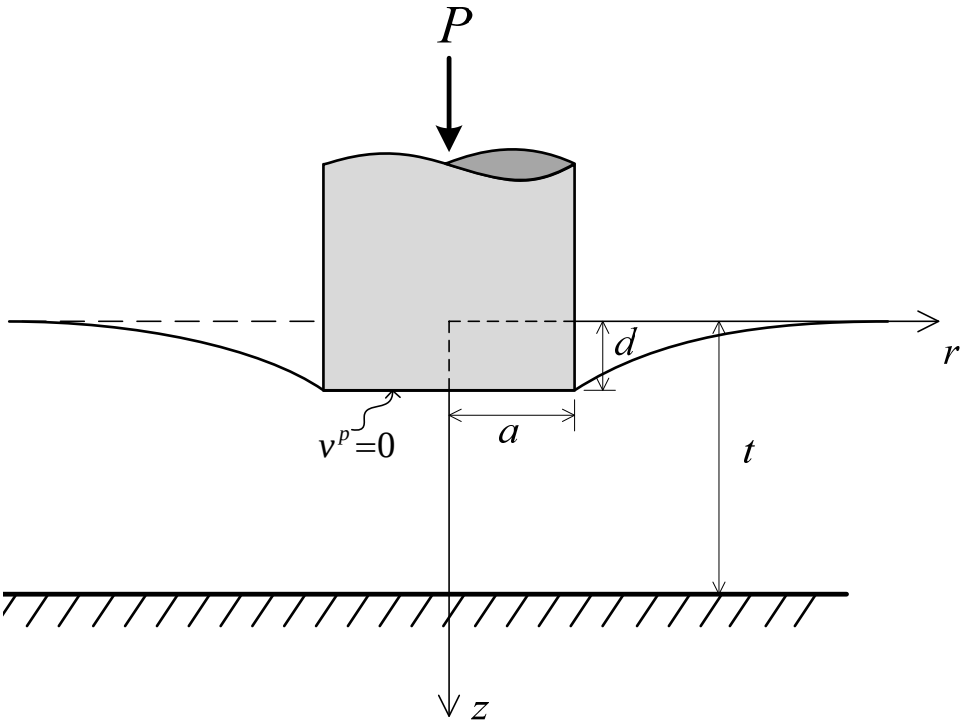

Figure 6.2 An isotropic elastic layer under rigid frictionless flat-ended cylindrical punch of a radius a.

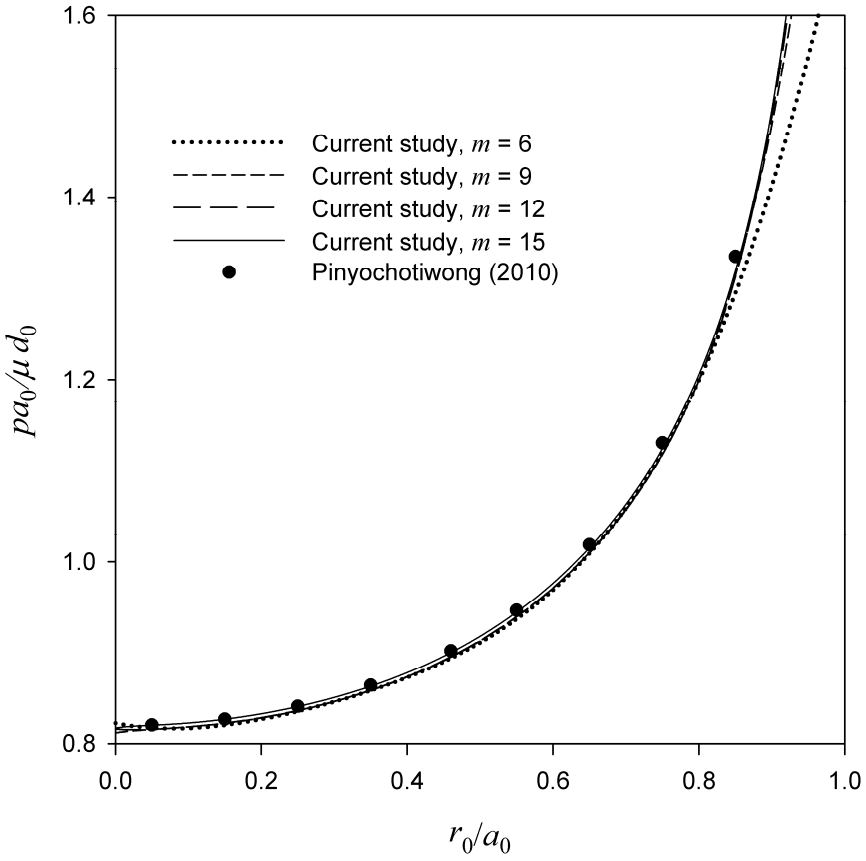

Figure 6.3 Convergence of normalized contact pressure of a half space ($t_0 \to \infty$) under flat-ended cylindrical punch with contact radius a_0 = 0.5.

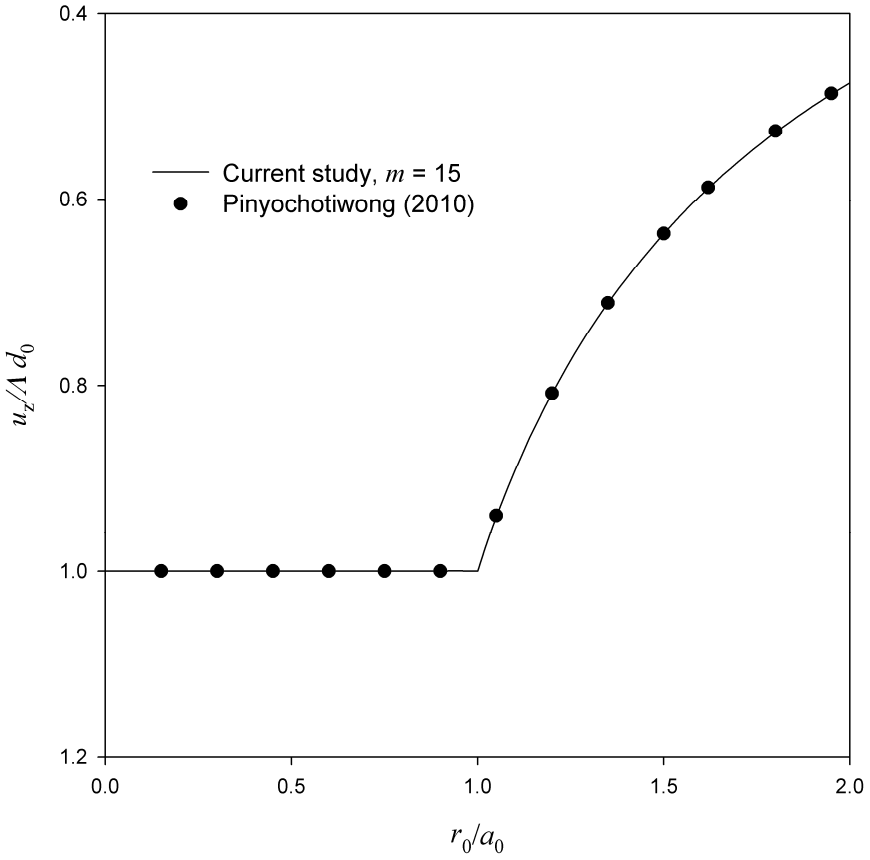

Figure 6.4 Comparison of numerical vertical displacement with benchmark solutions.

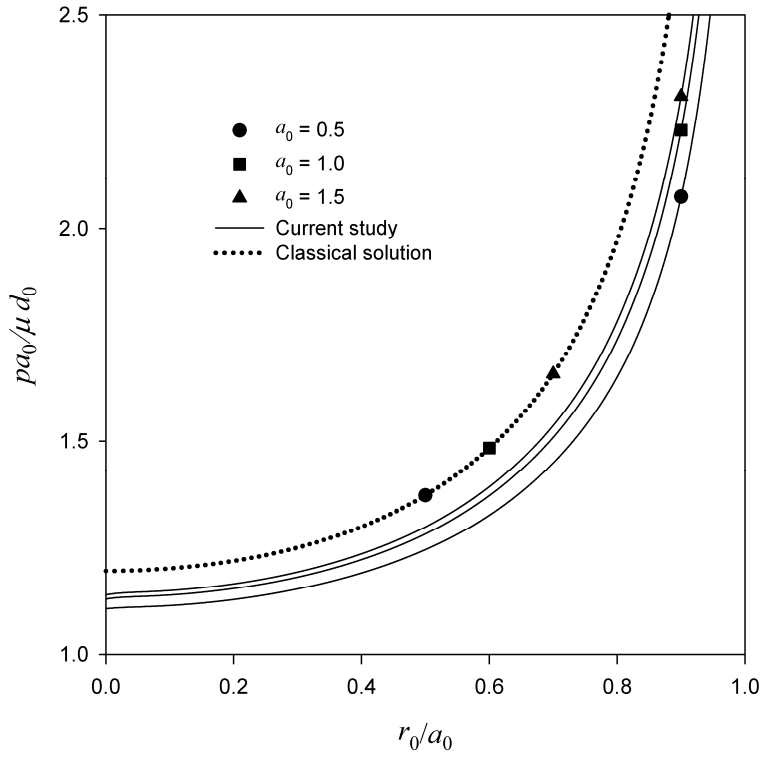

Figure 6.5 Distribution of normalized contact pressure under flat-ended cylindrical punch with various contact radii.

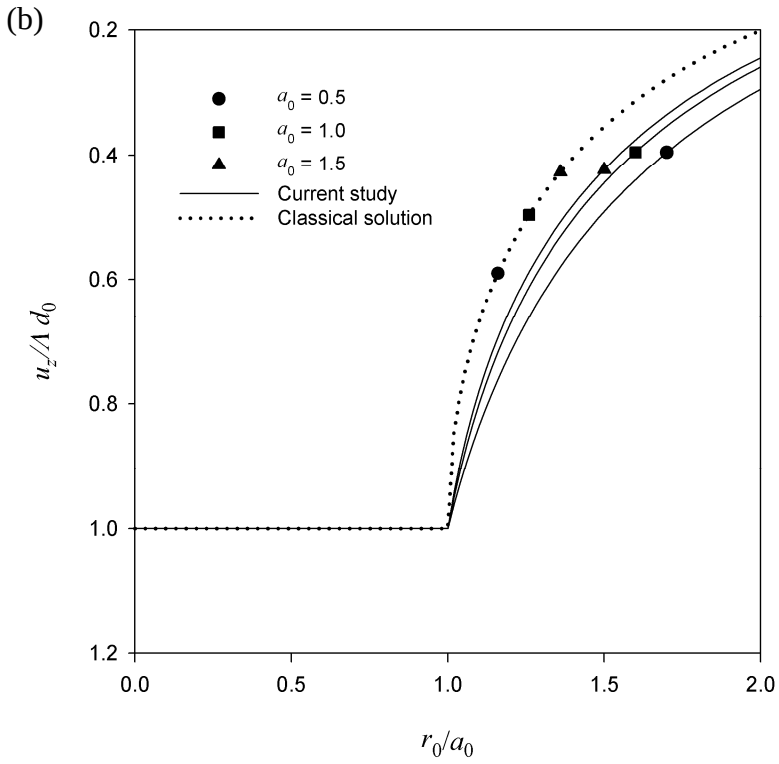

Figure 6.6 Normalized vertical displacement of the surface layer under flat-ended cylindrical punch with various contact radii.

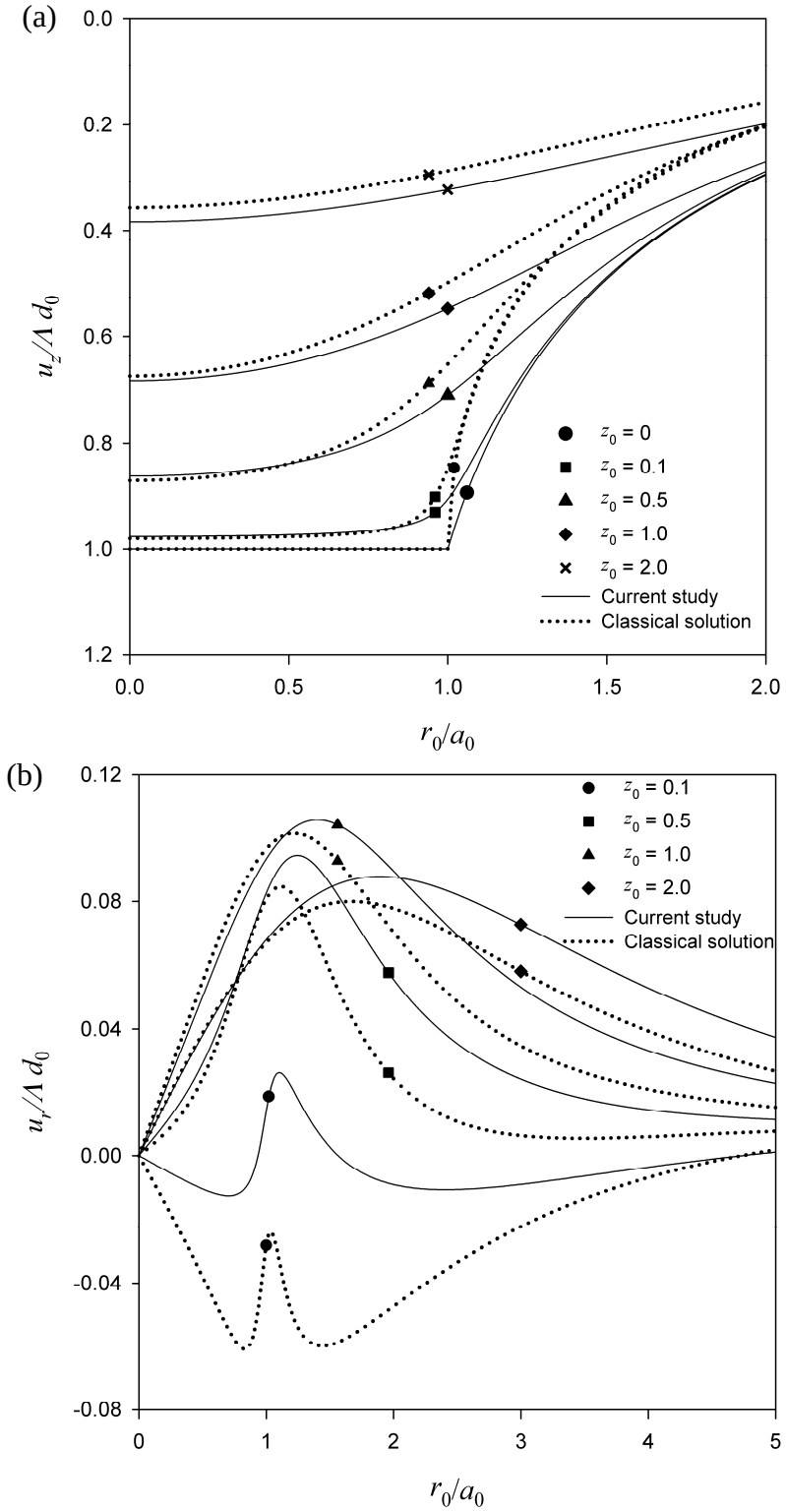

Figure 6.7 Normalized displacement profiles of a layer with finite thickness t_0/a_0 = 5 under flat-ended cylindrical punch with contact radius a_0 = 0.5: (a) Vertical displacement (b) Radial displacement.

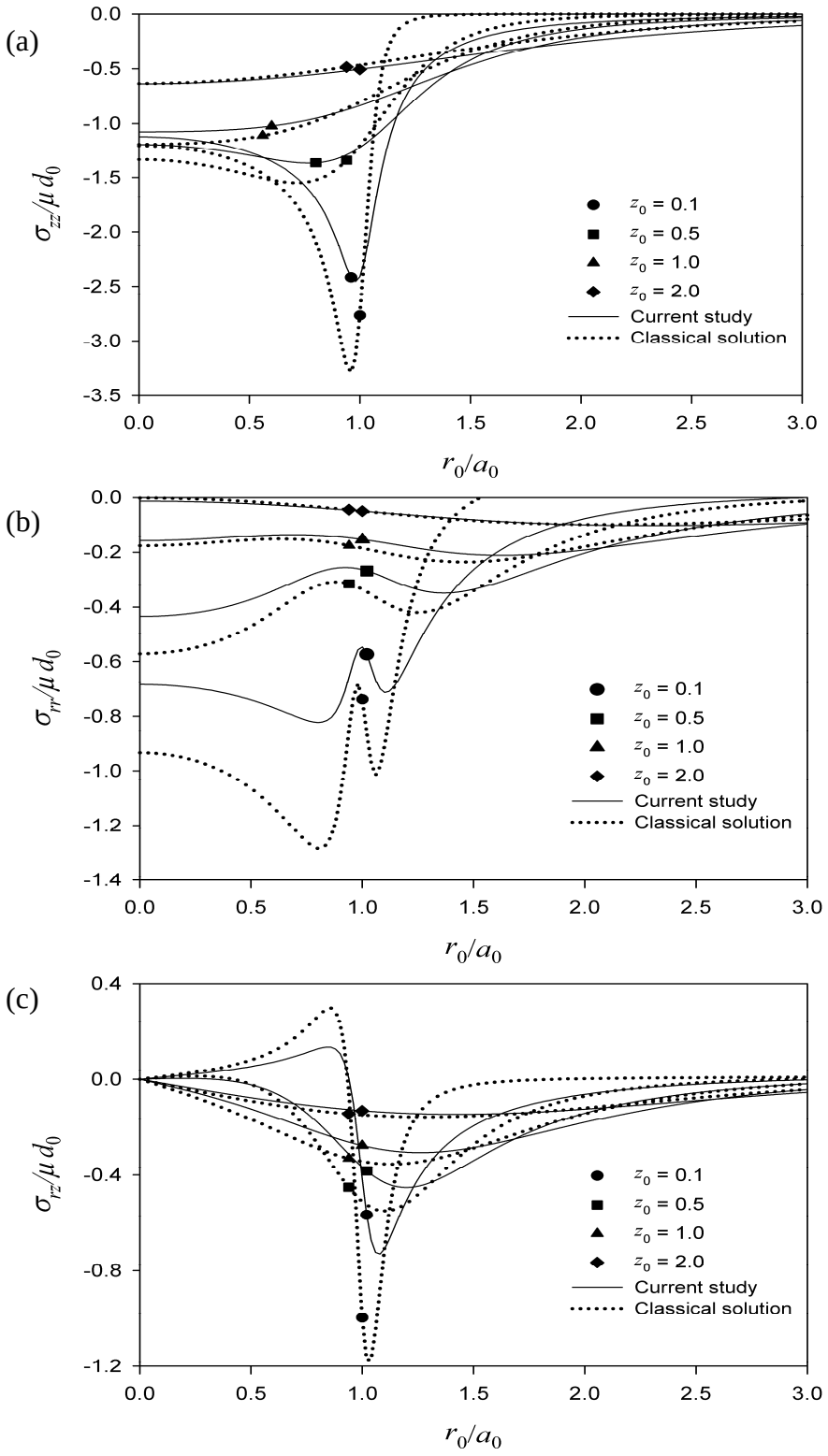

Figure 6.8 Normalized stress profiles of a layer with finite thickness t_0/a_0 = 5 under flat-ended cylindrical punch with contact radius a_0 = 0.5: (a) Vertical stress (b) Radial stress (c) Shear stress.

CHAPTER VII

CONCLUSIONS

7.1 Summary

This research presents a theoretical study of an isotropic elastic material with the consideration of surface energy effects by employing Gurtin-Murdoch continuum theory of elastic material surfaces. The fundamental solutions of an isotropic elastic layer under different loading cases, and an elastic medium with dislocations and cracks are presented. A set of general solutions corresponding to each problem is obtained from the governing equations of the bulk material by applying appropriate integral transform techniques. In addition, solution procedures for indentation problems are also presented to demonstrate the application of the derived fundamental solutions corresponding to an isotropic elastic layer under vertical and radial loads. Selected numerical results together with discussion and conclusion are given separately for each problem in the corresponding chapters. The major findings and conclusions of this research can be summarized as follows:

1. The analytical solutions are expressed in terms of semi-infinite integrals for problems involving different loading cases, dislocations and cracks with the presence of surface stresses, in which, closed-form solutions cannot be obtained due to the complexity of the integrands. The solutions can be accurately computed by employing a numerical quadrature scheme. In this research, a globally adaptive numerical quadrature scheme based on 21-point Gauss-Kronrod rule is employed in the evaluation of the integrals. The validity and accuracy of the present solution schemes are confirmed by comparing with available benchmark solutions.

2. As shown in the numerical results for each problem, surface stresses show a significant influence on the elastic fields of an isotropic elastic material especially in the vicinity of the surface. In addition, the bulk material becomes stiffer with the presence of surface energy effects for the fundamental problems presented in this research. An extensive parametric study observed in numerical results indicates that, unlike classical elasticity, the elastic fields of the bulk material become size-dependent with the consideration of surface stresses. Numerical results presented in this study indicate that the influence of surface stresses is significant in the analysis of the problem involving nanoscale structures and soft elastic materials where the surface energy effects are not negligible.

7.2 Suggestions for Further Work

The fundamental solutions presented in this thesis provide an insight into fundamental understanding on the mechanical behavior of nanoscale structures and soft elastic solids, and can be used as benchmark solutions for verification purpose. The analytical solutions presented in this study can also be employed to construct Green functions which are useful for various boundary value problems in practical situations. The suggestions for further study on mechanics of nanoscale material are

1. In most practical situations, the substrate material is generally not rigid. The fundamental solutions for multilayer problems with the surface stresses are therefore very useful. In such problems, the surface energy effects on the interface between layers could become significant. The current methodology based on Fourier and Hankel transforms can be readily extended to solve the case of a flexible substrate.

2. The consideration of more complex problems, e.g., indentation problems with non-axisymmetric geometry and indenter shape, the elastic medium with arbitrary crack shape or multiple cracks, etc.

REFERENCES

Bilby, B. and Eshelby, J.D. 1968. Dislocations and the theory of fracture. In: Liebowitz, editors. Fracture. New York : Academic Press.

Cammarata, R.C. 1994. Surface and interface stress effects in thin films. Progress in Surface Science 46: 1-38.

Crouch, S.L. and Starfield, A.M. 1983. Boundary Element Methods in Solid Mechanics. London : George Allen and Unwin.

Dingreville, R., Qu, J. and Cherkaoui, M. 2005. Surface free energy and its effect on the elastic behavior of nano-sized particles, wires and films. Journal of the Mechanics and Physics of Solids 53: 1827-1854.

Duan, H.L., Wang, J., Huang, Z.P. and Karihaloo, B.L. 2005. Eshelby formalism for nano-inhomogeneities. Proceedings of the Royal Society A 461: 3335-3353.

Erdogan, F. and Bahar, L.Y. 1964. On the solution of simultaneous dual integral equations. Journal of the Society for Industrial and Applied Mathematics 12: 666-675.

Fabrikant, V.I. 1989. Applications of potential theory in mechanics: a selections of new results. The Netherlands : Kluwer Academic.

Fu, X.L., Wang, G.F. and Feng, X.Q. 2008. Surface effects on the near-tip stress fields of a mode-II crack. International Journal of Fracture 151: 95–106.

Gibbs, J. W. 1906. The scientific papers of J. Willard Gibbs. Vol. 1. London : Longmans Green.

Gross, D. 1982. Stress intensity factor of systems of cracks. Ingenieur-Archiv 51: 301-310.

Gurtin, M.E. and Murdoch, A.I. 1975. A continuum theory of elastic material surfaces. Archive for Rational Mechanics and Analysis 57: 291-323.

Gurtin, M.E. and Murdoch, A.I. 1978. Surface stress in solids. International Journal of Solids and Structures 14: 431-440.

Gurtin, M.E., Weissmüller, J., and Larché, F. 1998. A general theory of curved deformable interfaces in solids at equilibrium. Philosophical Magazine A 78: 1093-1109.

He, L.H., Lim, C.W. and Wu, B.S. 2004. A continuum model for size-dependent deformation of elastic films of nano-scale thickness. International Journal of Solids and Structures 41: 847–857.

He, L.H., and Lim, C.W. 2006. Surface green function for a soft elastic half-space: Influence of surface stress. International Journal of Solids and Structures 43: 132–143.

Hoagland, R.G., Daw, M.S. and Hirth, J.P. 1991. Some aspects of forces and fields in atomic models of crack tips. Journal of Materials Research 6: 2565–2571.

Huang, D.W. 2008. Size-dependent response of ultra-thin films with surface effects. International Journal of Solids and Structures 45: 568-579.

Iijima, S. 1991. Helical microtubules of graphitic carbon. Nature 354: 56-58.

Ji, B. and Gao, H. 2004. A study of fracture mechanisms in biological nano-composites via the virtual internal bond model. Materials Science and Engineering: A 366: 96-103.

Kim, C.I., Schiavone, P. and Ru, C.Q. 2010. The effects of surface elasticity on an elastic solid with mode-III crack: complete solution. Journal of Applied Mechanics - ASME 77, 021011: 1-7.

Kim, C.I., Schiavone, P. and Ru, C.Q. 2011. Analysis of plane-strain crack problems (Mode-I & Mode-II) in the presence of surface elasticity. Journal of Elasticity 104: 397-420.

Kim, C.I., Ru, C. Q. and Schiavone, P. 2012. A clarification of the role of crack-tip conditions in linear elasticity with surface effects. Mathematics and Mechanics of Solids 18(1): 59-66.

Liang, H., Upmanyu, M. and Huang, H. 2005. Size-dependent elasticity of nanowires: nonlinear effects. Physical Review B 71.241403: 1-4.

Lu, P., He, L.H., Lee, H.P. and Lu, C. 2006. Thin plate theory including surface effects. International Journal of Solids and Structures 43: 4631-4647.

Magnus, W. and Oberhettinger, F. 1954. Formulas and theorems for the functions of mathematical physics New York : Chelsea.

Mao, S.X., Zhao, M. and Wang, Z.L. 2003. Nanoscale mechanical behavior of individual semiconducting nanobelts. Applied Physics Letters 83: 993-995.

Melan, E. 1932. The stress state of a single force in the interior of the claimed half disc. ZAMM - Journal of Applied Mathematics and Mechanics 12: 343-346.

Miller, R.E., and Shenoy, V.B. 2000. Size-dependent elastic properties of nanosized structural elements. Nanotechnology 11: 139-147.

Mogilevskaya, S.G., Crouch, S.L. and Stolarski H.K. 2008. Multiple interacting circular nano-inhomogeneities with surface/interface effects. Journal of the Mechanics and Physics of Solids 56: 2298–327.

Oh, E., Walton, J.R. and Slattery, J.C. 2006. A theory of fracture based upon an extension of continuum mechanics to the nanoscale. Journal of Applied Mechanics - ASME 73: 792-798.

Park, H.S., Klein, P.A. and Wagner, G.J. 2006. A surface Cauchy-Born model for nanoscale materials. International Journal for Numerical Methods in Engineering 68: 1072-1095.

Perez, N. 2004. Fracture Mechanics. Boston : Kluwer Academic Publishers.

Pickett G. 1938. Stress distribution in a loaded soil with some rigid boundaries. In: Proceedings, Highway Research Board 18: 35-47.

Piessens, R., Doncker-Kapenga, E., Uberhuber, C.W. and Kahaner, D.K. 1983. QUADPACK: A subroutine package for automatic integration. Berlin : Springer.

Pinyochotiwong, Y. 2010. Rigid frictionless indentation on half-space with surface stresses. Master's thesis, Faculty of engineering (Civil engineering). Chulalongkorn University.

Povstenko, Y.Z. 1993. Theoretical investigation of phenomena caused by heterogeneous surface tension in solids. Journal of the Mechanics and Physics of Solids 41: 1499-1514.

Selvadurai, A.P.S. 2000. Partial differential equations in mechanics 2. Germany : Springer.

Sendova, T. and Walton, J.R. 2010. A new approach to the modeling and analysis of fracture through extension of continuum mechanics to the nanoscale. Mathematics and Mechanics of Solids 15: 368-413.

Sharma, P., Ganti, S. and Bhate, N. 2003. Effect of surfaces on the size-dependent elastic state of nano-inhomogeneities. Applied Physics Letters 82: 535-537.

Shodja, H.M., Gutkin, M.Y. and Moeini-Ardakani, S.S. 2011. Effect of surface stresses on elastic behavior of a screw dislocation inside the wall of nanotube. Physica Status Solidi (b) 248(6): 1437-1441.

Shenoy, V.B. 2005. Atomistic calculations of elastic properties of metallic fcc crystal surfaces. Physical Review B 71: 094104.

Shuttleworth, R. 1950. The surface tension of solids. Proceedings of the Physical Society Section A 63: 444-457.

Slattery, J.C., Oh, E. and Fu, K. 2004. Extension of continuum mechanics to the nanoscale. Chemical Engineering Science 59: 4621-4635.

Sneddon, I.N. 1951. Fourier Transform. New York : McGraw-Hill

Sun, C.T. and Zhang, H. 2002. Size-dependent elastic moduli of platelike nanomaterials. Journal of Applied Physics 93(2): 1212-1218.

Tian, L. and Rajapakse, R.K.N.D. 2007. Analytical solution for size-dependent elastic field of a nanoscale circular inhomogeneity. Journal of Applied Mechanics - ASME 74: 568-574.

Tranter, C.J. 1956. Integral transforms in mathematical physics New York : John Wiley.

Wang, G.F. and Feng, X.Q. 2007. Effects of surface stresses on contact problems at nanoscale. Journal of Applied Physics 101: 013510.

Wang, G.F., Feng, X.Q., Wang, T.J. and Gao, W. 2008 Surface effects on the near-tip stresses for Mode-I and Mode-III cracks. Journal of Applied Mechanics - ASME 75 . 011001: 1-5.

Wang, Z.Q., Zhao, Y.P. and Huang, Z.P. 2010. The effects of surface tension on the elastic properties of nano structures. International Journal of Engineering Science 48: 140-150.

Weissmuller, J. and Cahn, J.W., 1997. Mean stresses in microstructures due to interface stresses: A generalization of a capillary equation for solids. Acta Materialia 45(5): 1899-1906.

Wong, E.W., Sheehan, P.E., and Lieber, C.M. 1997. Nanobeam mechanics: Elasticity, strength, and toughness of nanorods and nanotubes. Science 277: 1971-1975.

Woodward, C. and Rao, S.I. 2001. Ab initio simulation of isolated screw dislocations in bcc Mo and Ta. Philosophical Magazine A 81: 1305-1316.

Wu, C.H. 1999. The effect of surface stress on the configurational equilibrium of voids and cracks. Journal of the Mechanics and Physics of Solids 47: 2469-2402.

Wu, C.H. and Wang, M.L. 2000. The effect of crack-tip point loads on fracture. Journal of the Mechanics and Physics of Solids 48: 2283-2296.

Wu, C.H. and Wang, M.L. 2001. Configurational equilibrium of circular-arc cracks with surface stress. International Journal of Solids and Structures 38: 4279-4292.

Yakobson, B.I. 2003. Nanomechanics. In W. A. Goddard; D. W. Brenner; S. E. Lyshevski; and G. J. Iafrate (eds.). Handbook of nanoscience, engineering, and technology, chapter 17. Florida: CRC Press.

Zhao, X.J. 2009. Surface loading and rigid indentation of an elastic layer with surface energy effects. Master's thesis, Faculty of graduate studies (mechanical engineering). The university of British Columbia (Vancouver).

Zhao, X.J., and Rajapakse, R.K.N.D. 2009. Analytical solutions for a surface-loaded isotropic elastic layer with surface energy effects. International Journal of Engineering Science 47: 1433-1444.

APPENDIX

APPENDIX A

The expressions of A_i to H_i ($i = p, q$) and I appearing in Eqs. (4.4a) to (4.4d) are given as follows:

$$A_p=\left\{\begin{array}{l}
(\lambda+3\mu)\left[\left(\frac{\lambda+\mu}{\lambda+2\mu}h+\Lambda\right)|\xi|\cosh\left(\xi(2t-h)\right)+\left(1+\frac{\lambda+\mu}{\lambda+2\mu}\Lambda h\xi^2\right)\sinh\left(|\xi|(2t-h)\right)\right] \\
-(\lambda+\mu)\left[\left(2t+\frac{\lambda+3\mu}{\lambda+\mu}\Lambda-\frac{\lambda+\mu}{\lambda+2\mu}\left(2t(t-h)\Lambda\xi^2+h\right)\right)|\xi|\cosh(\xi h)+\left(\frac{\lambda+3\mu}{\lambda+\mu}+\frac{\lambda+\mu}{\lambda+2\mu}\left(2t(t-h)-\Lambda h\right)\xi^2+2\Lambda t\xi^2\right)\sinh\left(|\xi|h\right)\right] \\
-\frac{\tau^s}{2\mu}|\xi|\left\{(\lambda+3\mu)\left[\left(\frac{\lambda+3\mu}{\lambda+2\mu}\Lambda+h\right)|\xi|\cosh\left(\xi(2t-h)\right)+\frac{\lambda+2\mu}{\lambda+\mu}\sinh\left(|\xi|(2t-h)\right)+\frac{(\lambda+\mu)^2}{2(\lambda+2\mu)^2}\left(e^{|\xi|(2t-h)}-\frac{\lambda+3\mu}{\lambda+\mu}e^{-|\xi|(2t-h)}\right)\Lambda h\xi^2\right]\right. \\
+(\lambda+\mu)\left[\left(h-\frac{2(\lambda+2\mu)}{\lambda+\mu}t-\frac{\lambda+3\mu}{\lambda+2\mu}\left(\frac{\lambda+3\mu}{\lambda+\mu}+2t|\xi|\right)\Lambda\right)|\xi|\cosh(\xi h)-\left(\frac{(\lambda+2\mu)(\lambda+3\mu)}{(\lambda+\mu)^2}+2t(t-h)\xi^2\right)\sin(|\xi|h)\right] \\
\left.+\frac{(\lambda+\mu)^3}{(\lambda+2\mu)^2}\Lambda\xi^2\left[\frac{(\lambda+3\mu)^2}{2(\lambda+\mu)^2}h-\left(t(t-h)|\xi|\right)e^{|\xi|h}-\frac{\lambda+3\mu}{2(\lambda+\mu)}\left(2t(t-h)|\xi|+h\right)e^{-|\xi|h}\right]\right\}
\end{array}\right\}\frac{\overline{p}(\xi)}{2\xi^2} \tag{A.1}$$

$$B_p=\left\{\begin{array}{l}
(\lambda+\mu)(\lambda+3\mu)\left[2\Lambda|\xi|\left(\cosh\left(\xi(2t-h)\right)-\cosh(\xi h)\right)+\left(2h|\xi|+\frac{\lambda+3\mu}{\lambda+\mu}\right)e^{|\xi|(2t-h)}-e^{-|\xi|(2t-h)}-\left(\frac{\lambda+3\mu}{\lambda+\mu}+2t|\xi|\right)e^{|\xi|h}\right] \\
+(\lambda+\mu)^2\left[4(t-h)\left(\Lambda\sinh\left(|\xi|h\right)-te^{|\xi|h}\right)\xi^2+\left(\frac{\lambda+3\mu}{\lambda+\mu}-2(t-h)|\xi|\right)e^{-|\xi|h}\right] \\
-\frac{\tau^s}{2\mu}|\xi|\left\{(\lambda+3\mu)\left[\frac{2(\lambda+\mu)(\lambda+3\mu)}{(\lambda+2\mu)}\Lambda|\xi|\cosh\left(\xi(2t-h)\right)+2(\lambda+2\mu)\left(\sinh\left(|\xi|(2t-h)\right)+\sinh\left(|\xi|h\right)\right)\right]\right. \\
-2(\lambda+\mu)\left[2(\lambda+2\mu)(t-h)+\frac{(\lambda+3\mu)^2}{\lambda+2\mu}\Lambda\right]|\xi|\cosh(\xi h)+\frac{2(\lambda+\mu)^2(\lambda+3\mu)}{\lambda+2\mu}\Lambda h\xi^2e^{|\xi|(2t-h)} \\
\left.-\frac{2(\lambda+\mu)^2}{\lambda+2\mu}\Lambda\xi^2\left[\left((\lambda+3\mu)t+2(\lambda+\mu)t(t-h)|\xi|\right)e^{|\xi|h}-(\lambda+3\mu)(t-h)e^{-|\xi|h}\right]\right\}
\end{array}\right\}\frac{\overline{p}(\xi)}{4(\lambda+2\mu)|\xi|} \tag{A.2}$$

$$C_p=\left\{\begin{array}{l}
(\lambda+3\mu)\left[\left(\frac{\lambda+\mu}{\lambda+2\mu}h+\Lambda\right)|\xi|\cosh\left(\xi(2t-h)\right)+\left(1+\frac{\lambda+\mu}{\lambda+2\mu}\Lambda h\xi^2\right)\sinh\left(|\xi|(2t-h)\right)\right] \\
-(\lambda+\mu)\left[\left(2t+\frac{\lambda+3\mu}{\lambda+\mu}\Lambda+\frac{\lambda+\mu}{\lambda+2\mu}\left(2t(t-h)\Lambda\xi^2-h\right)\right)|\xi|\cosh(\xi h)+\left(\frac{\lambda+3\mu}{\lambda+\mu}+\frac{\lambda+\mu}{\lambda+2\mu}\left(2t(t-h)-\Lambda h\right)\xi^2+2\Lambda t\xi^2\right)\sinh\left(|\xi|h\right)\right] \\
+\frac{\tau^s}{2\mu}|\xi|\left\{(\lambda+3\mu)\left[\left(\frac{\lambda+3\mu}{\lambda+2\mu}\Lambda+h\right)|\xi|\cosh\left(\xi(2t-h)\right)+\frac{\lambda+2\mu}{\lambda+\mu}\sinh\left(|\xi|(2t-h)\right)+\frac{(\lambda+\mu)^2}{2(\lambda+2\mu)^2}\left(\frac{\lambda+3\mu}{\lambda+\mu}e^{|\xi|(2t-h)}-e^{|\xi|(2t-h)}\right)\Lambda h\xi^2\right]\right. \\
+(\lambda+\mu)\left[\left(h|\xi|-\frac{2(\lambda+2\mu)}{(\lambda+\mu)}t|\xi|-\frac{\lambda+3\mu}{\lambda+\mu}\left(\frac{\lambda+3\mu}{\lambda+2\mu}\Lambda|\xi|-\frac{\lambda+2\mu}{\lambda+\mu}\right)\right)\cosh(\xi h)-\left(2(t-h)+\frac{2(\lambda+3\mu)}{\lambda+2\mu}\Lambda\right)t\xi^2\sin(|\xi|h)\right] \\
\left.-\frac{(\lambda+\mu)^3}{(\lambda+2\mu)^2}\Lambda\xi^2\left[\frac{\lambda+3\mu}{\lambda+\mu}\left(t(t-h)|\xi|-\frac{\lambda+3\mu}{2(\lambda+\mu)}h\right)e^{|\xi|h}+\left(\frac{(\lambda+3\mu)^2}{2(\lambda+\mu)^2}h-t(t-h)|\xi|\right)e^{-|\xi|h}\right]\right\}
\end{array}\right\}\frac{-\overline{p}(\xi)}{2\xi^2} \tag{A.3}$$

$$D_p=\left\{\begin{array}{l}(\lambda+\mu)(\lambda+3\mu)\left[2\Lambda|\xi|\left(\cosh\left(\xi(2t-h)\right)-\cosh\left(\xi h\right)\right)+e^{|\xi|(2t-h)}+\left(2h|\xi|-\dfrac{\lambda+3\mu}{\lambda+\mu}\right)e^{-|\xi|(2t-h)}+\left(\dfrac{\lambda+3\mu}{\lambda+\mu}-2t|\xi|\right)e^{-|\xi|h}\right]\\-(\lambda+\mu)^2\left[4(t-h)\left(\Lambda\sinh\left(|\xi|h\right)-te^{-|\xi|h}\right)\xi^2+\left(\dfrac{\lambda+3\mu}{\lambda+\mu}+2(t-h)|\xi|\right)e^{|\xi|h}\right]\\+\dfrac{\tau^s}{2\mu}|\xi|\left\{(\lambda+3\mu)\left[\dfrac{2(\lambda+\mu)(\lambda+3\mu)}{(\lambda+2\mu)}\Lambda|\xi|\cosh\left(\xi(2t-h)\right)+2(\lambda+2\mu)\sinh\left(|\xi|(2t-h)\right)\right]\right.\\-2(\lambda+\mu)\left[2(\lambda+2\mu)(t-h)+\dfrac{(\lambda+3\mu)^2}{\lambda+2\mu}\Lambda\right]|\xi|\cosh\left(\xi h\right)-\dfrac{2(\lambda+\mu)^2(\lambda+3\mu)}{\lambda+2\mu}\Lambda h\xi^2e^{-|\xi|(2t-h)}\\\left.-\dfrac{2(\lambda+\mu)^2}{\lambda+2\mu}\Lambda\xi^2\left[\left((\lambda+3\mu)(t-h)+2(\lambda+\mu)t(t-h)|\xi|\right)e^{|\xi|h}-\left((\lambda+3\mu)t-2(\lambda+\mu)t(t-h)|\xi|\right)e^{-|\xi|h}\right]\right\}\end{array}\right\}\frac{\overline{p}(\xi)}{4(\lambda+2\mu)|\xi|} \tag{A.4}$$

$$E_p=\left\{\begin{array}{l}(\lambda+3\mu)(1+\Lambda|\xi|)\left[\left(1-\dfrac{\lambda+\mu}{\lambda+2\mu}h|\xi|\right)e^{|\xi|(2t+h)}+\left(1+\dfrac{\lambda+\mu}{\lambda+2\mu}h|\xi|\right)e^{|\xi|(2t-h)}\right]+(\lambda+\mu)(1-\Lambda|\xi|)\left[\dfrac{\lambda+3\mu}{\lambda+\mu}-2t|\xi|+\dfrac{\lambda+\mu}{\lambda+2\mu}\left(2t(t+h)|\xi|+h\right)|\xi|\right]e^{-|\xi|h}+\\\left[\dfrac{\lambda^2+4\lambda\mu+7\mu^2}{\lambda+\mu}-(\lambda+3\mu)\left(\dfrac{\lambda+3\mu}{\lambda+2\mu}h+\Lambda\right)|\xi|-(\lambda+\mu)\left(2(1-\Lambda|\xi|)-\dfrac{2(\lambda+3\mu)}{\lambda+2\mu}t|\xi|\right)t|\xi|+\dfrac{(\lambda+\mu)^2}{\lambda+2\mu}\left(2th(1-2|\xi|t)-\Lambda\left(2t(t+h)|\xi|-h\right)\right)\xi^2\right]e^{|\xi|h}\\+\dfrac{\tau^s}{2\mu}|\xi|\left\{(\lambda+3\mu)\left[\left(\dfrac{\lambda+2\mu}{\lambda+\mu}+\dfrac{\lambda+3\mu}{\lambda+2\mu}\Lambda|\xi|\right)\left(1-\dfrac{\lambda+\mu}{\lambda+2\mu}h|\xi|\right)e^{|\xi|(2t+h)}-\left(\dfrac{\lambda+2\mu}{\lambda+\mu}+h|\xi|+\dfrac{\lambda+3\mu}{\lambda+2\mu}\Lambda|\xi|+\dfrac{(\lambda+\mu)^2}{(\lambda+2\mu)^2}\Lambda h\xi^2\right)e^{|\xi|(2t-h)}\right]\right.\\-(\lambda+\mu)\left\{\left[\left(2t(t-h)|\xi|+h\right)|\xi|+\dfrac{\lambda+2\mu}{\lambda+\mu}\left(\dfrac{\lambda+3\mu}{\lambda+\mu}-2t|\xi|\right)-\dfrac{\lambda+3\mu}{\lambda+2\mu}\left(\dfrac{\lambda+3\mu}{\lambda+\mu}-2t|\xi|+\dfrac{\lambda+\mu}{\lambda+2\mu}\left(2t(t-h)|\xi|+h\right)|\xi|\right)\Lambda|\xi|\right]e^{-|\xi|h}-\right.\\\left.\left.\left[\left(2t(t+h)|\xi|-h\right)|\xi|+\dfrac{\lambda+2\mu}{\lambda+\mu}\left(\dfrac{\lambda+3\mu}{\lambda+\mu}-2t|\xi|\right)-\dfrac{\lambda+3\mu}{\lambda+2\mu}\left(\dfrac{\lambda+3\mu}{\lambda+\mu}-2t|\xi|-\dfrac{\lambda+3\mu}{\lambda+2\mu}h|\xi|+\dfrac{2(\lambda+\mu)}{\lambda+2\mu}t^2\xi^2\right)\Lambda|\xi|-\dfrac{2(\lambda+\mu)^2}{(\lambda+2\mu)^2}\left(1-2|\xi|t\right)\Lambda th|\xi|^3\right]e^{|\xi|h}\right\}\right\}\end{array}\right\}\frac{\overline{p}(\xi)}{4\xi^2} \tag{A.5}$$

$$F_p=\left\{\begin{array}{l}(\lambda+\mu)(\lambda+3\mu)\left[\left(1+\Lambda|\xi|\right)e^{|\xi|(2t+h)}+\left(\dfrac{\lambda+3\mu}{\lambda+\mu}+(\Lambda+2h)|\xi|\right)e^{|\xi|(2t-h)}\right]\\+(\lambda+\mu)^2\left[1-\dfrac{\lambda+3\mu}{\lambda+\mu}(\Lambda+2t)|\xi|+\left(2\Lambda(t+h)+4th\right)\xi^2\right]e^{|\xi|h}+(\lambda+\mu)\left(1-\Lambda|\xi|\right)\left[\lambda+3\mu-2(\lambda+\mu)(t-h)|\xi|\right]e^{-|\xi|h}\\+\dfrac{\tau^s}{2\mu}|\xi|\left\{(\lambda+3\mu)\left[\left(\lambda+2\mu+\dfrac{(\lambda+\mu)(\lambda+3\mu)}{\lambda+2\mu}\Lambda|\xi|\right)e^{|\xi|(2t+h)}-\left(\lambda+2\mu+\dfrac{(\lambda+\mu)^2}{\lambda+2\mu}\left(\dfrac{(\lambda+3\mu)}{\lambda+\mu}+2h|\xi|\right)\Lambda|\xi|\right)e^{|\xi|(2t-h)}\right]\right.\\+(\lambda+\mu)\left[\left(\lambda+2\mu\right)\left(\dfrac{\lambda+3\mu}{\lambda+\mu}-2(t+h)|\xi|\right)-\dfrac{\lambda+3\mu}{\lambda+2\mu}\left(\lambda+3\mu-2(\lambda+\mu)t|\xi|\right)\Lambda|\xi|-\dfrac{2(\lambda+\mu)^2}{\lambda+2\mu}\Lambda th|\xi|^3\right]e^{|\xi|h}\\\left.-(\lambda+\mu)\left[\left(\lambda+2\mu\right)\left(\dfrac{\lambda+3\mu}{\lambda+\mu}-2(t-h)|\xi|\right)-\dfrac{\lambda+3\mu}{\lambda+2\mu}\left(\lambda+3\mu-2(\lambda+\mu)(t-h)|\xi|\right)\Lambda|\xi|\right]e^{-|\xi|h}\right\}\end{array}\right\}\frac{\overline{p}(\xi)}{4(\lambda+2\mu)|\xi|} \tag{A.6}$$

$$G_p=\left\{\begin{array}{l}(\lambda+3\mu)(1-\Lambda|\xi|)\left[\left(1+\dfrac{\lambda+\mu}{\lambda+2\mu}h|\xi|\right)e^{-|\xi|(2t+h)}+\left(1-\dfrac{\lambda+\mu}{\lambda+2\mu}h|\xi|\right)e^{-|\xi|(2t-h)}\right]+(\lambda+\mu)(1+\Lambda|\xi|)\left[\dfrac{\lambda+3\mu}{\lambda+\mu}+2t|\xi|+\dfrac{\lambda+\mu}{\lambda+2\mu}\left(2t(t-h)|\xi|-h\right)|\xi|\right]e^{|\xi|h}\\+\left[\dfrac{\lambda^2+4\lambda\mu+7\mu^2}{\lambda+\mu}+(\lambda+3\mu)\left(\dfrac{\lambda+3\mu}{\lambda+2\mu}h+\Lambda\right)|\xi|+(\lambda+\mu)\left(2(1+\Lambda|\xi|)+\dfrac{2(\lambda+3\mu)}{\lambda+2\mu}t|\xi|\right)t|\xi|+\dfrac{(\lambda+\mu)^2}{\lambda+2\mu}\left(2th(1+2|\xi|t)+\Lambda\left(2t(t+h)|\xi|+h\right)\right)\xi^2\right]e^{-|\xi|h}\\+\dfrac{\tau^s}{2\mu}|\xi|\left\{(\lambda+3\mu)\left[\left(\dfrac{\lambda+2\mu}{\lambda+\mu}-h|\xi|-\dfrac{\lambda+3\mu}{\lambda+2\mu}\Lambda|\xi|+\dfrac{(\lambda+\mu)^2}{(\lambda+2\mu)^2}\Lambda h\xi^2\right)e^{-|\xi|(2t-h)}-\left(\dfrac{\lambda+2\mu}{\lambda+\mu}-\dfrac{\lambda+3\mu}{\lambda+2\mu}\Lambda|\xi|\right)\left(1+\dfrac{\lambda+\mu}{\lambda+2\mu}h|\xi|\right)e^{-|\xi|(2t+h)}\right]\right.\\+(\lambda+\mu)\left\{\left[\left(2t(t-h)|\xi|-h\right)|\xi|+\dfrac{\lambda+2\mu}{\lambda+\mu}\left(\dfrac{\lambda+3\mu}{\lambda+\mu}+2t|\xi|\right)+\dfrac{\lambda+3\mu}{\lambda+2\mu}\left(\dfrac{\lambda+3\mu}{\lambda+\mu}+2t|\xi|+\dfrac{\lambda+\mu}{\lambda+2\mu}\left(2t(t-h)|\xi|-h\right)|\xi|\right)\Lambda|\xi|\right]e^{|\xi|h}-\right.\\\left.\left.\left[\left(2t(t+h)|\xi|+h\right)|\xi|+\dfrac{\lambda+2\mu}{\lambda+\mu}\left(\dfrac{\lambda+3\mu}{\lambda+\mu}+2t|\xi|\right)+\dfrac{\lambda+3\mu}{\lambda+2\mu}\left(\dfrac{\lambda+3\mu}{\lambda+\mu}+2t|\xi|+\dfrac{\lambda+3\mu}{\lambda+2\mu}h|\xi|+\dfrac{2(\lambda+\mu)}{\lambda+2\mu}t^2\xi^2\right)\Lambda|\xi|+\dfrac{2(\lambda+\mu)}{(\lambda+2\mu)^2}\left(1+2t|\xi|\right)\Lambda th|\xi|^3\right]e^{-|\xi|h}\right\}\right\}\end{array}\right\}\frac{\overline{p}(\xi)}{4\xi^2} \tag{A.7}$$

$$H_p=\left\{\begin{array}{l}(\lambda+\mu)(\lambda+3\mu)\left[\left(1-\Lambda|\xi|\right)e^{-|\xi|(2t+h)}+\left(\frac{\lambda+3\mu}{\lambda+\mu}-(\Lambda+2h)|\xi|\right)e^{-|\xi|(2t-h)}\right]\\+(\lambda+\mu)(1+\Lambda|\xi|)\left[\lambda+3\mu-2(\lambda+\mu)(t-h)|\xi|\right]e^{|\xi|h}+(\lambda+\mu)^2\left[1+\frac{\lambda+3\mu}{\lambda+\mu}(\Lambda+2t)|\xi|+(2\Lambda(t+h)+4th)\xi^2\right]e^{-|\xi|h}\\-\frac{\tau^s}{2\mu}|\xi|\left\{(\lambda+3\mu)\left[\left(\lambda+2\mu-\frac{(\lambda+\mu)(\lambda+3\mu)}{\lambda+2\mu}\Lambda|\xi|\right)e^{-|\xi|(2t+h)}-\left(\lambda+2\mu-\frac{(\lambda+\mu)^2}{\lambda+2\mu}\left(\frac{\lambda+3\mu}{\lambda+\mu}-2h|\xi|\right)\Lambda|\xi|\right)e^{-|\xi|(2t-h)}\right]\right.\\-(\lambda+\mu)\left[\left(\lambda+2\mu\right)\left(\frac{\lambda+3\mu}{\lambda+\mu}+2(t-h)|\xi|\right)+\frac{\lambda+3\mu}{\lambda+2\mu}\left(\lambda+3\mu+2(\lambda+\mu)(t-h)|\xi|\right)\Lambda|\xi|\right]e^{|\xi|h}\\\left.+(\lambda+\mu)\left[\left(\lambda+2\mu\right)\left(\frac{\lambda+3\mu}{\lambda+\mu}+2(t+h)|\xi|\right)+\frac{\lambda+3\mu}{\lambda+2\mu}\left(\lambda+3\mu+2(\lambda+\mu)t|\xi|\right)\Lambda|\xi|-\frac{2(\lambda+\mu)^2}{\lambda+2\mu}\Lambda th|\xi|^3\right]e^{-|\xi|h}\right\}\end{array}\right\}\frac{-\overline{p}(\xi)}{4(\lambda+2\mu)|\xi|} \tag{A.8}$$

$$A_q=\left\{\begin{array}{l}(\lambda+3\mu)\left[\left(\mu-(\lambda+\mu)\Lambda h\xi^2\right)\cosh\left(\xi(2t-h)\right)+\left(\mu\Lambda-(\lambda+\mu)h\right)\xi\sinh\left(\xi(2t-h)\right)\right]-\\(\lambda+\mu)\left[\left(\frac{\mu(\lambda+3\mu)}{\lambda+\mu}-\mu\Lambda t\xi^2+(\lambda+\mu)\left(t(t-h)-h\Lambda\right)\xi^2\right)\cosh(\xi h)-\left(\mu t-\frac{\mu(\lambda+3\mu)}{\lambda+\mu}\Lambda-(\lambda+\mu)\left(\Lambda t(t-h)\xi^2-h\right)\right)\xi\sinh(\xi h)\right]\\+\frac{\tau^s}{2}|\xi|\left\{(\lambda+3\mu)\left[\left(-\frac{\lambda+2\mu}{\lambda+\mu}+\frac{\lambda+3\mu}{\lambda+2\mu}\Lambda|\xi|\right)\cosh\left(\xi(2t-h)\right)+\frac{\lambda+2\mu}{\mu}h\xi\sinh\left(\xi(2t-h)\right)\right]\right.\\+(\lambda+3\mu)\left[\frac{\lambda+2\mu}{\lambda+\mu}-\frac{\lambda+3\mu}{\lambda+2\mu}\Lambda|\xi|+\frac{2(\lambda+\mu)(\lambda+2\mu)}{\mu(\lambda+3\mu)}t(t-h)\xi^2\right]\cosh(\xi h)\\-(\lambda+2\mu)\left[2t+\frac{\lambda+\mu}{\mu}h-\frac{2(\lambda+\mu)(\lambda+3\mu)}{(\lambda+2\mu)^2}\Lambda t|\xi|\right]\xi\sin(\xi h)+\frac{(\lambda+\mu)^2(\lambda+3\mu)}{2\mu(\lambda+2\mu)}\left(e^{|\xi|(2t-h)}+\frac{\lambda+3\mu}{\lambda+\mu}e^{-|\xi|(2t-h)}\right)\Lambda h\xi^2\\\left.+(\lambda+\mu)\left[\frac{(\lambda+\mu)^2}{\mu(\lambda+2\mu)}t(t-h)|\xi|-\frac{(\lambda+3\mu)^2}{2\mu(\lambda+2\mu)}h\right]\Lambda\xi^2e^{|\xi|h}-\frac{(\lambda+\mu)^2(\lambda+3\mu)}{2\mu(\lambda+2\mu)}\left(t(t-h)|\xi|+h\right)\Lambda\xi^2e^{-|\xi|h}\right\}\end{array}\right\}\frac{\overline{q}(\xi)}{2(\lambda+2\mu)|\xi|\xi} \tag{A.9}$$

$$B_q=\left\{\begin{array}{l}(\lambda+\mu)(\lambda+3\mu)\left[-2\Lambda\xi\sinh\left(\xi(2t-h)\right)+\left(\frac{\lambda+3\mu}{\lambda+\mu}-2h|\xi|\right)e^{|\xi|(2t-h)}-e^{-|\xi|(2t-h)}-\frac{4(\lambda+\mu)}{\lambda+3\mu}\Lambda(t-h)\xi^2\cosh(\xi h)\right.\\+2\Lambda\xi\sinh(\xi h)-\left(\frac{\lambda+3\mu}{\lambda+\mu}-2t|\xi|+\frac{4(\lambda+\mu)}{\lambda+3\mu}t(t-h)\xi^2\right)e^{|\xi|h}+\left.\left(1+\frac{2(\lambda+\mu)}{\lambda+3\mu}(t-h)|\xi|\right)e^{-|\xi|h}\right]\\+\frac{\tau^s}{\mu}|\xi|\left\{(\lambda+3\mu)\left[\left(\lambda+2\mu-\frac{(\lambda+\mu)(\lambda+3\mu)}{\lambda+2\mu}\Lambda|\xi|\right)\left(\cosh\left(\xi(2t-h)\right)-\cosh(\xi h)\right)+\frac{(\lambda+\mu)^2}{\lambda+2\mu}\Lambda h\xi^2e^{|\xi|(2t-h)}\right]\right.\\\left.+2(\lambda+\mu)(\lambda+2\mu)(t-h)\xi\sinh(\xi h)-\frac{(\lambda+\mu)^2(\lambda+3\mu)}{(\lambda+2\mu)}\left[\left(1-\frac{2(\lambda+\mu)}{\lambda+3\mu}(t-h)|\xi|\right)te^{|\xi|h}+(t-h)e^{-|\xi|h}\right]\Lambda\xi^2\right\}\end{array}\right\}\frac{\overline{q}(\xi)}{4(\lambda+2\mu)\xi} \tag{A.10}$$

$$C_q=\left\{\begin{array}{l}(\lambda+3\mu)\left[\left(\mu-(\lambda+\mu)\Lambda h\xi^2\right)\cosh\left(\xi(2t-h)\right)+\left(\mu\Lambda-(\lambda+\mu)h\right)\xi\sinh\left(\xi(2t-h)\right)\right]-(\lambda+\mu)\\\left[\left(\frac{\mu(\lambda+3\mu)}{\lambda+3\mu}-\mu\Lambda t\xi^2-(\lambda+\mu)\left(t(t-h)+h\Lambda\right)\xi^2\right)\cosh(\xi h)-\left(\mu t-\frac{\mu(\lambda+3\mu)}{\lambda+\mu}\Lambda-(\lambda+\mu)\left(\Lambda t(t-h)\xi^2-h\right)\right)\xi\sinh(\xi h)\right]\\+\frac{\tau^s}{2}|\xi|\left\{(\lambda+3\mu)\left[\left(\frac{\lambda+2\mu}{\lambda+\mu}+\frac{\lambda+3\mu}{\lambda+2\mu}\Lambda|\xi|\right)\cosh\left(\xi(2t-h)\right)-\frac{\lambda+2\mu}{\mu}h\xi\sinh\left(\xi(2t-h)\right)\right]\right.\\+(\lambda+3\mu)\left[\frac{\lambda+2\mu}{\lambda+\mu}-\frac{\lambda+3\mu}{\lambda+2\mu}\Lambda|\xi|-\frac{(\lambda+\mu)(\lambda+2\mu)}{\mu(\lambda+3\mu)}h|\xi|\right]\cosh(\xi h)\\-(\lambda+2\mu)\left[2t+\frac{2(\lambda+\mu)}{\mu}t(t-h)|\xi|-\frac{2(\lambda+\mu)(\lambda+3\mu)}{(\lambda+2\mu)^2}\Lambda t|\xi|\right]\xi\sin(\xi h)-\frac{(\lambda+\mu)^2(\lambda+3\mu)}{2\mu(\lambda+2\mu)}\left(\frac{\lambda+3\mu}{\lambda+\mu}e^{|\xi|(2t-h))}-e^{-(|\xi|(2t-h))}\right)\Lambda h\xi^2\\\left.+(\lambda+\mu)\left[\left(\frac{(\lambda+\mu)(\lambda+3\mu)}{\mu(\lambda+2\mu)}t(t-h)|\xi|-\frac{(\lambda+3\mu)^2}{2\mu(\lambda+2\mu)}h\right)e^{|\xi|h}-\left(\frac{(\lambda+3\mu)^2}{2\mu(\lambda+2\mu)}h-\frac{(\lambda+\mu)^2}{\mu(\lambda+2\mu)}t(t-h)|\xi|\right)e^{-|\xi|h}\right]\Lambda\xi^2\right\}\end{array}\right\}\frac{-\overline{q}(\xi)}{2(\lambda+2\mu)|\xi|\xi} \tag{A.11}$$

$$D_q=\left\{\begin{array}{l}(\lambda+\mu)(\lambda+3\mu)\left[-2\Lambda\xi\sinh(\xi(2t-h))-e^{|\xi|(2t-h)}+\left(\frac{\lambda+3\mu}{\lambda+\mu}+2h|\xi|\right)e^{-|\xi|(2t-h)}-\frac{4(\lambda+\mu)}{\lambda+3\mu}\Lambda(t-h)\xi^2\cosh(\xi h)\right.\\ \left.+2\Lambda\xi\sinh(\xi h)+\left(1-\frac{2(\lambda+\mu)}{\lambda+3\mu}(t-h)|\xi|\right)e^{|\xi|h}-\left(\frac{\lambda+3\mu}{\lambda+\mu}+2t|\xi|+\frac{4(\lambda+\mu)}{\lambda+3\mu}t(t-h)\xi^2\right)e^{-|\xi|h}\right]\\ -\frac{\tau^s}{\mu}|\xi|^s\left\{(\lambda+3\mu)\left[\left(\lambda+2\mu+\frac{(\lambda+\mu)(\lambda+3\mu)}{\lambda+2\mu}\Lambda|\xi|\right)(\cosh(\xi(2t-h))-\cosh(\xi h))+\frac{(\lambda+\mu)^2}{\lambda+2\mu}\Lambda h\xi^2e^{-|\xi|(2t-h)}\right]\right.\\ \left.+(\lambda+\mu)\left[2(\lambda+2\mu)(t-h)+\frac{2(\lambda+\mu)(\lambda+3\mu)}{\lambda+2\mu}\Lambda t|\xi|\right]\xi\sinh(\xi h)-\frac{(\lambda+\mu)^3}{\lambda+2\mu}\left(\frac{\lambda+3\mu}{\lambda+\mu}he^{|\xi|h}+2t(t-h)|\xi|e^{-|\xi|h}\right)\Lambda\xi^2\right\}\end{array}\right\}\frac{\bar{q}(\xi)}{4(\lambda+2\mu)\xi} \tag{A.12}$$

$$E_q=\left\{\begin{array}{l}(\lambda+3\mu)(1+\Lambda|\xi|)\left[(\mu+(\lambda+\mu)h|\xi|)e^{|\xi|(2t+h)}-(\mu-(\lambda+\mu)h|\xi|)e^{|\xi|(2t-h)}\right]\\ +\left[\mu(\lambda+3\mu)+(\lambda+\mu)\left((\lambda+\mu)(2t(t-h)|\xi|-h)-2\mu t\right)|\xi|\right](1-\Lambda|\xi|)e^{|\xi|h}+(\lambda+\mu)\left[\frac{\mu(3\lambda^2+12\lambda\mu+13\mu^2)}{(\lambda+\mu)^2}+\right.\\ \left.\frac{\lambda+3\mu}{\lambda+\mu}(\mu\Lambda+(\lambda+3\mu)h)|\xi|+2\mu(1-\Lambda|\xi|)t|\xi|+2(\lambda+3\mu)t^2\xi^2+(\lambda+\mu)\left(\Lambda(2t(t+h)|\xi|+h)+2th(1+2t|\xi|)\right)\xi^2\right]e^{-|\xi|h}\\ +\frac{\tau^s}{2}|\xi|^s\left\{(\lambda+3\mu)\left[\left(\frac{\lambda+2\mu}{\lambda+\mu}+\frac{(\lambda+3\mu)}{\lambda+2\mu}\Lambda|\xi|\right)\left(1+\frac{\lambda+\mu}{\mu}h|\xi|\right)e^{|\xi|(2t+h)}+\left(\frac{\lambda+2\mu}{\lambda+\mu}-\frac{\lambda+2\mu}{\mu}h|\xi|-\frac{\lambda+3\mu}{\lambda+2\mu}\Lambda|\xi|-\frac{(\lambda+\mu)^2}{\mu(\lambda+2\mu)}\Lambda h\xi^2\right)e^{|\xi|(2t-h)}\right]\right.\\ -(\lambda+\mu)(\lambda+2\mu)\left\{\left[\frac{\lambda+3\mu}{(\lambda+\mu)^2}+\frac{2}{\lambda+\mu}t|\xi|+\frac{1}{\mu}(2t(t-h)|\xi|+h)|\xi|-\frac{\lambda+3\mu}{(\lambda+2\mu)^2}\left(\frac{\lambda+3\mu}{\lambda+\mu}+2t|\xi|+\frac{\lambda+\mu}{\mu}(2t(t-h)|\xi|+h)|\xi|\right)\Lambda|\xi|\right]e^{-|\xi|h}+e^{|\xi|h}\right.\\ \left.\left.\left[\frac{\lambda+3\mu}{(\lambda+\mu)^2}+\frac{2}{\lambda+\mu}t|\xi|+\frac{1}{\mu}(2t(t+h)|\xi|-h)|\xi|+\frac{\lambda+3\mu}{(\lambda+2\mu)^2}\left(\frac{\lambda+3\mu}{\lambda+\mu}+2t|\xi|+\frac{\lambda+3\mu}{\mu}h|\xi|+\frac{2(\lambda+\mu)}{\mu}t^2\xi^2-\frac{2(\lambda+\mu)^2}{\mu(\lambda+3\mu)}(1-2t|\xi|)th\xi^2\right)\Lambda|\xi|\right]\right\}\right\}\end{array}\right\}\frac{-\bar{q}(\xi)}{4(\lambda+2\mu)|\xi|\xi} \tag{A.13}$$

$$F_q=\left\{\begin{array}{l}(\lambda+\mu)(\lambda+3\mu)\left[(1+\Lambda|\xi|)e^{|\xi|(2t+h)}+\left(\frac{\lambda+3\mu}{\lambda+\mu}-(\Lambda+2h)|\xi|\right)e^{|\xi|(2t-h)}\right.\\ \left.+\left(\frac{\lambda+\mu}{\lambda+3\mu}(1+4th\xi^2+2(t+h)\Lambda\xi^2)+(\Lambda+2t)|\xi|\right)e^{|\xi|h}+(1-\Lambda|\xi|)\left(1+\frac{2(\lambda+\mu)}{\lambda+3\mu}(t-h)|\xi|\right)e^{-|\xi|h}\right]\\ +\frac{\tau^s}{2\mu}|\xi|^s\left\{(\lambda+3\mu)\left[\left(\lambda+2\mu+\frac{(\lambda+\mu)(\lambda+3\mu)}{\lambda+2\mu}\Lambda|\xi|\right)e^{|\xi|(2t+h)}+\left(\lambda+2\mu-\frac{(\lambda+\mu)(\lambda+3\mu)}{\lambda+2\mu}\Lambda|\xi|+\frac{2(\lambda+\mu)^2}{\lambda+2\mu}\Lambda h\xi^2\right)e^{|\xi|(2t-h)}\right]\right.\\ -(\lambda+\mu)\left[\frac{(\lambda+2\mu)(\lambda+3\mu)}{\lambda+\mu}+2(\lambda+2\mu)(t+h)|\xi|+\frac{(\lambda+3\mu)^2}{\lambda+2\mu}\left(1+\frac{2(\lambda+\mu)}{\lambda+3\mu}t|\xi|+\frac{2(\lambda+\mu)^2}{(\lambda+3\mu)^2}th\xi^2\right)\Lambda|\xi|\right]e^{|\xi|h}\\ \left.-(\lambda+\mu)\left[\frac{(\lambda+2\mu)(\lambda+3\mu)}{\lambda+\mu}+2(\lambda+2\mu)(t-h)|\xi|-\frac{(\lambda+3\mu)^2}{\lambda+2\mu}\left(1+\frac{2(\lambda+\mu)}{\lambda+3\mu}(t-h)|\xi|\right)\Lambda|\xi|\right]e^{-|\xi|h}\right\}\end{array}\right\}\frac{\bar{q}(\xi)}{4(\lambda+2\mu)\xi} \tag{A.14}$$

$$G_q=\left\{\begin{array}{l}(\lambda+3\mu)(1-\Lambda|\xi|)\left[(\mu-(\lambda+\mu)h|\xi|)e^{-|\xi|(2t+h)}-(\mu+(\lambda+\mu)h|\xi|)e^{-|\xi|(2t-h)}\right]\\ +\left[\mu(\lambda+3\mu)+(\lambda+\mu)\left((\lambda+\mu)(2t(t-h)|\xi|-h)-2\mu t\right)|\xi|\right](1+\Lambda|\xi|)e^{|\xi|h}+(\lambda+\mu)\left[\frac{\mu(3\lambda^2+12\lambda\mu+13\mu^2)}{(\lambda+\mu)^2}\right.\\ \left.-\frac{\lambda+3\mu}{\lambda+\mu}(\mu\Lambda+(\lambda+3\mu)h)|\xi|+2\mu(1+\Lambda|\xi|)t|\xi|+2(\lambda+3\mu)t^2\xi^2-(\lambda+\mu)\left(\Lambda(2t(t+h)|\xi|+h)+2th(1+2t|\xi|)\right)\xi^2\right]e^{-|\xi|h}\\ -\frac{\tau^s}{2}|\xi|^s\left\{(\lambda+3\mu)\left[\left(\frac{\lambda+2\mu}{\lambda+\mu}-\frac{(\lambda+3\mu)}{\lambda+2\mu}\Lambda|\xi|\right)\left(1-\frac{\lambda+\mu}{\mu}h|\xi|\right)e^{-|\xi|(2t+h)}+\left(\frac{\lambda+2\mu}{\lambda+\mu}+\frac{\lambda+2\mu}{\mu}h|\xi|+\frac{\lambda+3\mu}{\lambda+2\mu}\Lambda|\xi|-\frac{(\lambda+\mu)^2}{\mu(\lambda+2\mu)}\Lambda h\xi^2\right)e^{-|\xi|(2t-h)}\right]\right.\\ -(\lambda+\mu)(\lambda+2\mu)\left\{\left[\frac{\lambda+3\mu}{(\lambda+\mu)^2}-\frac{2}{\lambda+\mu}t|\xi|+\frac{1}{\mu}(2t(t-h)|\xi|-h)|\xi|+\frac{\lambda+3\mu}{(\lambda+2\mu)^2}\left(\frac{\lambda+3\mu}{\lambda+\mu}-2t|\xi|+\frac{\lambda+\mu}{\mu}(2t(t-h)|\xi|-h)|\xi|\right)\Lambda|\xi|\right]e^{|\xi|h}+e^{-|\xi|h}\right.\\ \left.\left.\left[\frac{\lambda+3\mu}{(\lambda+\mu)^2}-\frac{2}{\lambda+\mu}t|\xi|+\frac{1}{\mu}(2t(t+h)|\xi|+h)|\xi|-\frac{\lambda+3\mu}{(\lambda+2\mu)^2}\left(\frac{\lambda+3\mu}{\lambda+\mu}-2t|\xi|-\frac{\lambda+3\mu}{\mu}h|\xi|+\frac{2(\lambda+\mu)}{\mu}t^2\xi^2-\frac{2(\lambda+\mu)^2}{\mu(\lambda+3\mu)}(1+2t|\xi|)th\xi^2\right)\Lambda|\xi|\right]\right\}\right\}\end{array}\right\}\frac{\bar{q}(\xi)}{4(\lambda+2\mu)|\xi|\xi} \tag{A.15}$$

$$H_q=\left\{\begin{array}{l}(\lambda+\mu)(\lambda+3\mu)\left[(1-\Lambda|\xi|)e^{-|\xi|(2t+h)}+\left(\frac{\lambda+3\mu}{\lambda+\mu}+(\Lambda+2h)|\xi|\right)e^{-|\xi|(2t-h)}\right.\\ \left.+(1+\Lambda|\xi|)\left(1-\frac{2(\lambda+\mu)}{\lambda+3\mu}(t-h)|\xi|\right)e^{|\xi|h}+\left(\frac{\lambda+\mu}{\lambda+3\mu}(1+4th\xi^2+2(t+h)\Lambda\xi^2)-(\Lambda+2t)|\xi|\right)e^{-|\xi|h}\right]\\ -\frac{\tau^s}{2\mu}|\xi|\left\{(\lambda+3\mu)\left[\left(\lambda+2\mu-\frac{(\lambda+\mu)(\lambda+3\mu)}{\lambda+2\mu}\Lambda|\xi|\right)e^{-|\xi|(2t+h)}+\left(\lambda+2\mu+\frac{(\lambda+\mu)(\lambda+3\mu)}{\lambda+2\mu}\Lambda|\xi|+\frac{2(\lambda+\mu)^2}{\lambda+2\mu}\Lambda h\xi^2\right)e^{-|\xi|(2t-h)}\right]\right.\\ -(\lambda+\mu)\left[\frac{(\lambda+2\mu)(\lambda+3\mu)}{\lambda+\mu}-2(\lambda+2\mu)(t-h)|\xi|+\frac{(\lambda+3\mu)^2}{\lambda+2\mu}\left(1-\frac{2(\lambda+\mu)}{\lambda+3\mu}(t-h)|\xi|\right)\Lambda|\xi|\right]e^{|\xi|h}\\ \left.-(\lambda+\mu)\left[\frac{(\lambda+2\mu)(\lambda+3\mu)}{\lambda+\mu}-2(\lambda+2\mu)(t+h)|\xi|-\frac{(\lambda+3\mu)^2}{\lambda+2\mu}\left(1-\frac{2(\lambda+\mu)}{\lambda+3\mu}t|\xi|+\frac{2(\lambda+\mu)^2}{(\lambda+3\mu)^2}th\xi^2\right)\Lambda|\xi|\right]e^{-|\xi|h}\right\}\end{array}\right\}\frac{\bar{q}(\xi)}{4(\lambda+2\mu)\xi} \quad \text{(A.16)}$$

$$\begin{aligned}I=&(\lambda+3\mu)\left[\cosh(2t\xi)+\Lambda\xi\sinh(2t\xi)\right]+2t\xi^2(\lambda+\mu)(\Lambda+t)+\frac{\lambda^2+4\lambda\mu+5\mu^2}{\lambda+\mu}\\ &+\tau^s\left\{(\lambda+3\mu)\left[\frac{(\lambda+3\mu)}{2\mu(\lambda+2\mu)}\Lambda\xi^2\cosh(2t\xi)+\frac{(\lambda+2\mu)}{2\mu(\lambda+\mu)}\xi\sinh(2t\xi)-\frac{(\lambda+3\mu)}{2\mu(\lambda+2\mu)}\Lambda\xi^2\right]-\frac{(\lambda+2\mu)}{\mu}t\xi^2-\frac{(\lambda+\mu)^2}{\mu(\lambda+2\mu)}\Lambda t^2\xi^4\right\}\end{aligned} \quad \text{(A.17)}$$

BIOGRAPHY

The author, Pong-in Intarit, was born in Songkhla, Thailand, on June 2, 1984. He received his Bachelor of Engineering degree in Civil Engineering from Chulalongkorn University in 2006. After graduation, he decided to continue his Doctor of Philosophy degree in Civil Engineering at Chulalongkorn University in the same year under the supervision of Professor Dr.Teerapong Senjuntichai and Associate Professor Dr.Jaroon Rungamornrat with the support from Thailand Research Fund under the Royal Golden Jubilee Ph.D. (RGJ-Ph.D.) Scholarship. He spent the summers of 2010 and 2012 at the Simon Fraser University, Burnaby, Canada, to conduct a research work with Professor Dr.Nimal Rajapakse.

Publications:

Intarit P., Senjuntichai T. and Rajapakse R.K.N.D. 2010. Dislocation and internal loading in a semi-infinite elastic medium with surface stresses. Engineering Fracture Mechanics 77: 3592-3603.

Intarit P., Senjuntichai T., Rungamornrat J. and Rajapakse R.K.N.D. 2011. Surface elasticity and residual stress effect on the elastic field of a nanoscale elastic layer. Interaction and Multiscale Mechanics 4(2): 85-105.